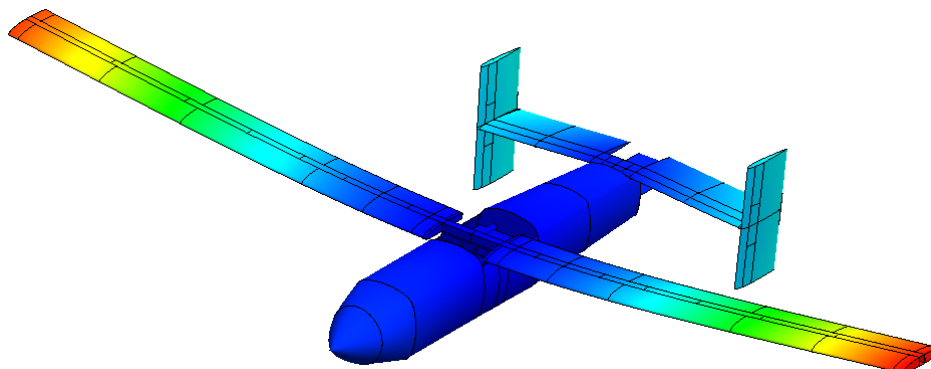




ACADEMIA DA FORÇA AÉREA



Detailed Design of a Class I UAV for Maritime Surveillance

Structure, Propulsion and Systems Integration

João Carlos Marques Correia

AlfAI/EngAer 138081-J

Thesis to obtain the Master of Science Degree in

Military Science - Aeronautical Engineering

Examination Committee

Chairperson: MGEN/ENGAER 076441-J Paulo Manuel Veloso Gonçalves Guerra (DMSA)

Supervisor: MAJ/ENGAER 129905-A Luís Filipe da Silva Félix (AFA)

Supervisor: CAP/ENGAER 131603-G João Vítor Aguiar Vieira Caetano (AFA)

Member of the Committee: Doutor Frederico José Prata Rente Reis Afonso (IST)

Sintra, June of 2018

The Sky is not the Limit,
It is just the Beginning.

Acknowledgments

The production of this thesis was backed by help and support that I must highlight.

I would like to thank my supervisors, MAJ Luís Félix and CAP João Caetano for their guidance, help, and availability throughout this work. Their deep knowledge and intuition certainly contributed to obtain a more consolidated work.

My profound gratitude to my Parents, for their unconditional support through all my life.

I want to thank all my friends and colleagues for helping me to overcome each battle in the last intensive years.

To Mustangs, and especially Franco, for the important partnership and cooperation during these 7 years.

A special mention to Isabel Ferreiro for valuable discussions, tutoring, availability, and precious help during critical moments.

I am grateful to CIAFA Team for the availability and promptness concerning all doubts and for the opportunity to develop a project as interesting as it is important for the Portuguese Air Force.

Resumo

Esta tese destina-se ao design estrutural em materiais compósitos de um Veículo Aéreo Não-Tripulado (VANT) de classe I para vigilância marítima. A intenção de expandir o uso de VANTs pela Força Aérea Portuguesa (FAP), na ampla área de jurisdição portuguesa e nas operações internacionais, motivou a necessidade de desenvolver uma nova plataforma capaz de cumprir todos os requisitos operacionais e tecnológicos. A presente tese começa pela definição dos sistemas a bordo necessários para a aeronave, nomeadamente a carga útil, aviónicos e propulsão. O design estrutural ao nível conceptual e preliminar envolveu o planeamento da disposição geral da aeronave para atingir uma margem estática longitudinal válida e a determinação do envelope de voo com rajada para determinar o factor de carga da aeronave. Este parâmetro vai definir a caracterização das forças aerodinâmicas e inerciais para a manobra crítica de voo. O projecto detalhado da aeronave foi realizado através de modelação em Desenho Assistido por Computador (CAD) com o objetivo de minimizar o peso estrutural. O design foi confirmado por uma análise numérica de tensões através de uma Análise de Elementos Finitos (FEA) e foi alcançada convergência para os valores obtidos de tensão e de deslocamento. O design desenvolvido é capaz de suportar a condição de carga crítica sem falha estrutural. A configuração da aeronave com todos os sistemas a bordo apresenta um peso dentro dos limites para a respectiva classe e uma autonomia de oito horas para operações de vigilância marítima. O design desenvolvido pode apresentar outras configurações, e tem uma autonomia máxima de doze horas.

Palavras-chave: FAP, VANT, Análise de Carga, Compósitos, Design Estrutural, CAD, FEA.

Abstract

This thesis concerns the composite structural design of a class I Unmanned Aerial Vehicle (UAV) for maritime surveillance. The intention to expand the UAV use by Portuguese Air Force (FAP), over the broad area of Portuguese jurisdiction and in international operations, motivated the need to develop a new platform capable to fulfil all the operational and technological requirements. This thesis starts by defining all the necessary onboard systems for the aircraft, namely the payload, avionics and propulsion. The conceptual and preliminary structural design involved planning the general layout to achieve a valid longitudinal static margin and determining the aircraft flight envelope with gust loads to determine the design load. This design driver set the aerodynamic and inertial load characterization of the critical flight manoeuvre. The aircraft detailed design was performed through Computed Aided Design (CAD) modelling with the objective of minimizing the structural weight. The design was endorsed by a numerical stress analysis through a Finite Element Analysis (FEA) and achieved convergence for the stress and displacement results. The developed design withstands the critical load condition without failure of the structure. The aircraft configuration with full payload presents a weight within its class range and an endurance of eight hours for maritime surveillance operations. The implemented design supports other configurations, presenting an endurance up to twelve hours.

Keywords: FAP, UAV, Load Analysis, Composites, Structural Design, CAD modelling, FEA.

Contents

- Acknowledgments v
- Resumo vii
- Abstract ix
- List of Tables xiii
- List of Figures xv
- Nomenclature xvii
- Glossary xix

- 1 Introduction 1**
 - 1.1 Motivation 1
 - 1.2 Topic Overview 2
 - 1.3 Objectives 4
 - 1.4 Thesis Outline 6

- 2 Background 7**
 - 2.1 Theoretical Overview 9
 - 2.1.1 Design 9
 - 2.1.2 Structure Types 11
 - 2.1.3 Material 11
 - 2.2 Method Overview 14
 - 2.2.1 FEA 17

- 3 Conceptual and Preliminary Design 21**
 - 3.1 Systems 21
 - 3.1.1 Payload 22
 - 3.1.2 Avionics and Subsystems 24

3.1.3	Propulsion System	29
3.2	Layout	30
3.3	Longitudinal Static Stability	33
3.4	Load Factor	33
3.4.1	Flight Envelope	34
3.4.2	Design Load	41
3.5	Aircraft Loads Analysis	42
3.5.1	Aerodynamic Loads Characterization	44
3.5.2	Weight and Inertial Loads Characterization	47
3.6	General Considerations	54
4	Detailed Structural Design	57
4.1	CAD modelling	57
4.1.1	Wing	57
4.1.2	Tail	61
4.1.3	Fuselage	64
4.2	Finite Element Analysis	72
4.2.1	Simulations Materials	73
4.2.2	Boundary Conditions	77
5	Results	79
5.1	Configuration	85
6	Conclusions	87
6.1	Future Work	88
	Bibliography	91
	A Technical Requirements	95
	B Material Properties	99
	C External Loads	101

List of Tables

1.1 UAV Requirements.	5
2.1 Decay of Free Vibration.	13
2.2 Aerodynamic Inputs.	15
3.1 Engine Comparison.	30
3.2 Incremental Load Factor for gust.	40
3.3 Weight and Inertial Forces of major components.	49
4.1 Spar Discretization.	60
4.2 Equivalent Diameter for each segment of the aircraft.	72
4.3 Plies Attribution along Spar Surfaces.	74
5.1 Maximum Stress Result for each Mesh applied.	82
B.1 Properties of the CIDIFA's Composite Materials	99

List of Figures

1.1	SAR responsibility area under Portuguese jurisdiction.	1
2.1	Major Topics of Aerospace Engineering.	7
2.2	Configurations of Different UAV.	9
2.3	Unidirectional (U.D.) and Bidirectional (B.D.) fabrics.	12
2.4	Fatigue Behaviour of Materials.	13
2.5	Schematic of the iterative FE process.	17
2.6	Linear Triangular Element and Parabolic Triangular Element.	19
3.1	Layout of the Aircraft.	32
3.2	Components displacements to achieve Static Stability.	34
3.3	Flight Envelope for $V_C = 70knots$	38
3.4	Flight Envelope for $V_C = 90knots$	38
3.5	Model for gust load effect on a aircraft in level flight.	39
3.6	$V - n$ and $V - g$ diagram.	41
3.7	Typical combined flight envelope.	41
3.8	Equivalent set of static conditions for the lower phase of the pull up.	43
3.9	Elliptical, Trapezoidal and Schrenk Lift Distribution for Half Wing	46
3.10	Wing centre of gravity.	50
4.1	Wing Airfoil: Spar Dimensions.	59
4.2	Spar Zones Discretization.	60
4.3	Ribs Planes along Wing Span.	60
4.4	Tail Airfoil Sizing.	62
4.5	Tail Top View.	63
4.6	Standard Bulkhead.	65
4.7	Mold Shape.	65

4.8 Fuselage Exploded View - 3 Sections.	66
4.9 Rear Part of the Fuselage.	66
4.10 Bulkhead 1.	68
4.11 Bulkhead 2.	68
4.12 Central Part of the Fuselage.	69
4.13 Bulkhead 4/5.	69
4.14 Front Part of the Fuselage	71
4.15 Nose Supports.	71
4.16 Lift/Drag ratio for the conceptual and the detailed design.	72
5.1 Finer Mesh Control on Critical Areas	80
5.2 Stress Convergence Analysis for a Mesh refinement.	81
5.3 σ_x Distribution along Wing Span.	82
5.4 Von Mises Stress Distribution on the Aircraft.	83
5.5 Von Mises Stress Distribution on the Aircraft.	83
5.6 Aircraft Resultant Displacement.	84
5.7 Weight distribution per type of elements.	85

Nomenclature

γ	Climb Angle.
\hat{u}	Statistical Gust Velocity.)
λ	Taper Ratio.
μ	Mass Ratio.
ν	Poisson Ratio.
ρ	Density.
σ	Stress.
τ	Shear Stress.
A	Area.
AR	Aspect Ratio.
b	Wing Span.
c	Chord.
e	Oswald Coefficient.
$E1$	dasdsad.
E_1	Tensile Modulus in direction 1.
g	Gravity Acceleration.
K	Gust Alleviation Factor.
L	Lift.

M	Moment.
n	Load Factor.
q	Dynamic Pressure.
S	Area of the Wing.
u	Normal Component of the Gust Velocity.
u, v	Velocity Cartesian components.
V	Velocity.
W	Weight.
C_{D_0}	Base Drag Coefficient.
C_{L_α}	Lift Coefficient Slope.
C_L	Lift Coefficient.

Glossary

AAV	Autonomous Air Vehicle.
AES	Advanced Encryption Standard.
AIS	Automatic Identification System.
AMSL	Above Mean Sea Level.
BRLOS	Beyond Radio Line Of Sight.
C2	Command and Control.
CAD	Computer Aided Design.
CBRN	Chemical Biological Radiological and Nuclear.
CFD	Computational Fluid Dynamics .
CIAFA	Centro de Investigação da Academia da Força Aérea.
EASA	European Aviation Safety Agency.
EMSA	European Maritime Safety Agency.
EO	Electro-Optical.
EPIRB	Emergency Position Indicating Radio Beacon.
EU	European Union.
FAP	Força Aérea Portuguesa.
FEA	Finite Element Analysis.
FI	Fuel Injected.
FRONTEX	European Border and Coast Guard Agency.
GPIO	General Purpose Input Output.
GPS	Global Positioning System.
I/O	Input/Output.

IAS	Indicated Air Speed.
IR	Infra-red.
MDO	Multidisciplinary Optimization.
MS	Margin of Safety.
MTOW	Maximum Take-Off Weight.
NATO	North Atlantic Treaty Organization.
OMIP	Outras Missões de Interesse Público.
PITVANT	Projecto de Investigação Tecnológica em Veículos Aéreos Não Tripulados.
RPA	Remotely Piloted Aircraft.
SAR (Radar)	Synthetic Aperture Radar.
SAR	Search and Rescue.
STANAG	Standardization Agreement.
SatCom	Satellite Communications.
UAS	Unmanned Aerial System.
UAV	Unmanned Aerial Vehicle.
UCAV	Unmanned Combat Aerial Vehicles.
VHF	Very High Frequency.

Chapter 1

Introduction

1.1 Motivation

Portugal presents a maritime jurisdiction area for Search and Rescue (SAR) responsibility over 5 million km^2 (Figure 1.1), which is one of the biggest in the world and the biggest in Europe [1].



Figure 1.1: SAR responsibility area under Portuguese jurisdiction.

This broad operational environment set the need for advanced technological means capable of monitoring and surveillance, which might be accomplished efficiently with Unmanned Aerial Systems (UAS) in integration with manned aircraft.

The development, in Portuguese Air Force (FAP) context of these platforms, started in 2009 with manufacture, tests and mission deployments ever since. Nowadays, the UAS (Antex family) available at CIAFA (Centro de Investigação da Academia da Força

Aérea) present some weaknesses found through some years of operations. A more capable aircraft, with 'high-tech' and up to date systems on board is desired for national and international applications.

Furthermore, FAP won the pole position as a service provider of class I ($\leq 150kg$) UAS for monitoring of maritime pollution, for European Maritime Safety Agency (EMSA). For the CIAFA's fleet be able to accomplish this, it is required to suppress the need of UAS.

Therefore it is required the project, development, production and test of a new class I aircraft capable to fulfil this agency's missions of maritime surveillance and atmospheric pollution monitoring induced by cargo ships, besides satisfying the national interest.

1.2 Topic Overview

History has shown several times that direct needs arising in a war are the despatching factor for creating or improving technologies. The armed forces combine the need, capacity, resources and motivation to discover technical solutions to take advantage over the enemies [2].

The historical accomplishments of unmanned aircraft often supplant a consistent operational pattern, labelled as the three D's, which stand for dangerous, dirty and dull [3] [4]. Dangerous being that someone is trying to bring down the aircraft or the life of the pilot may be at undue risk operationally. Dirty is when the environment may be contaminated by Chemical, Biological, Radiological and Nuclear (CBRN) hazards precluding human exposure [5]. Lastly, dull is when the task requires long hours of manned flight, stressful and exhausting and therefore not desirable. Since the initial developments of unmanned air vehicles in war, the highly dynamic UAS industry continues to improve and at a much faster pace than ever before [6] as a result of the constant advancement of science and technological enablement.

Nowadays the UAS have a wide range of possible missions employments[3]. It is known the military interest for a system capable of simultaneously performing Intelligence, Surveillance, Target Acquisition, Reconnaissance and Neutralization while removing the human risk of the equation. One example of these all capable systems is

the Unmanned Combat Aerial Vehicles (UCAV) already in front-line operations on war zones [2]. With the higher preponderance of UAS in aeronautical defence, the main advantages of the absence of a pilot are the low cost (cheaper aircraft and cheaper cost of operation per mission), reduced risk and the practicality [4].

The worldwide expansion of UAS set the need for proper regulations. The laws applied at the Portuguese unmanned fleet are mostly original from North Atlantic Treaty Organization (NATO), the defence alliance in which Portugal is a historical member [7].

The law evolution of UAS concept in NATO is recent since it only started in 2002. "The NATO UAS Airworthiness standards (2017) represent 15 years of work by NATO military and acquisition experts, based on academic and national UAS platforms experience, to meet the requirement for UAS airworthiness standards" [8]. NATO first Standardization Agreement (STANAG), intended to set the technical requirements for the airworthiness certification of fixed-wing military UAV systems to regularly operate in a non-segregate airspace, was published in 2007 (STANAG 4671 - Edition 1) [9]. This document is an airworthiness code derived from the European Aviation Safety Agency (EASA) CS-23 [10], and safety documents from Eurocontrol, Italy, Australia, United Kingdom, United States of America, among others.

At the present, in the European context, one of the active military operations using UAS is FRONTEX, the European Border and Coast Guard Agency. This entity provides support for European Union (EU) countries and the associated Schengen countries in the management of their external borders, contributing to the harmonization of EU borders controls [11].

Due to the increasing capabilities, the UAS presents some advantages when comparing to some of the others methods of continuous surveillance available for FRONTEX: "They can stay on top of the 'target' for much longer than a satellite, which tracks Earth's movements, and cannot focus on a continuous point for as long as it takes" stated EMSA's director of operations [12]. Also, each UAS deployed by EMSA, working as a service provider for FRONTEX, is equipped to detect the smallest movement at sea, regardless of the visibility conditions, through its state of the art technologies such as cameras, gimbles and radars.

These advantages set the desire of a wide application of UAS to carry border control, maritime surveillance (Mediterranean migration routes) and secure some of EU

sea frontiers. The need of a bigger fleet for EMSA to be able of providing UAS deployments for FRONTEX, foster the creation of a public tender. This 2016 EMSA's public tender attracted most of the giants in the aeronautical industry such as Airbus, Safran and Lufthansa, but the announced winning ticket was eventually drawn by drones made and operated in Portugal. It ranked first in a category which pitched unmanned 150 kg heavy aircraft that could fly up to 10 hours autonomously. This contract signed in March (2017) shows the high level of operational capacities and the successfully evolving technology concerning unmanned air systems in Portugal.

FAP activities and work on UAS date back to 2009, at the start of the Research and Technology Project in Unmanned Autonomous Aerial Vehicles (PITVANT). This project stood out the development of several technological areas such as the design, manufacture and testing, the cooperative control, systems interoperability, advanced vision systems, data fusion and navigation systems, trough the development of three platforms: micro-RPA (Remotely Piloted Aircraft) (1 kilogram and 1 meter of wingspan), ANTEX-X02 (15/25 kilograms and 3 meters of wingspan) and ANTEX-X03 (110 kilograms and 6 meters of wingspan) [13]. Ever since, CIAFA participated in several other projects involving UAS, namely: PERSEUS, SEAGULL, TROANTE AND SUNNY. The main focus of these projects has been the development of operational procedures, capabilities and technologies for Maritime Surveillance missions. Overall, in the last 8 years, FAP has accomplished more than 750 flight hours with UAS operations.

According to FAP's genetic code, it is important to have a three-dimensional perspective for UAS operations: national strictly military, integration with NATO or EU operations and other missions of public interest (OMIP) [2].

In line with this three-way strategic view and EMSA's tender FAP needs a new class I UAV.

1.3 Objectives

The main objective of this dissertation is the (structural) detailed design of an Unmanned Aerial Vehicle (UAV) of class I, based on the CIAFA's requirements of table 1.1. This accomplishment requires a previously conceptual analysis of the flight envelope, design load, structure layout, stability analysis and flight loads characterization.

Table 1.1: UAV Requirements.

<i>Requirement</i>	<i>Value</i>	<i>Requirement</i>	<i>Value</i>
Wingspan	≤ 5 m	Ceiling	4500 m / 15000 ft MSL
MTOW	≤ 150 kg	Take off	Optional
Endurance	20 hours	Maximum T/O altitude	3000 m / 10000 ft AMSL
Range	1000 km	Recovery	Optional
Range (comms)	100 km	Operational temperature	-25° C to +50° C
Cruise speed	45 knots	Anti-icing measures	Heated pitot - static tube
Max level speed	70 knots	Environmental protection	≤ 5mm / hour rain;
<i>Propulsion :</i>			
Fuel Type	Automatic	Engine Type	Internal combustion, FI
Generator	≥ 100 W	Temperature control	Automatic
<i>Payload :</i>			
Transponder	Mode C	Sniffer	by Deimos Engenharia
Vision Payload	≤ 5 kg	SatCom	C2, HD broadcast
Radar SAR	≤ 20 kg		
<i>DataLink :</i>			
Link Rate	~12 Mps	Encryption	128/256 bit AES
Frequency	~2.4 Ghz	Frequency	VHF, capable of C2
<i>FlightSystem :</i>		Autopilot type	Piccolo or UAVision

Further specific requirements of Annex A should be accomplished, if not in contradiction with CIAFA's requirements. To accomplish the structural, mass and operational requirements, the structure's design requires a proactive approach for a optimal sizing of each individual component, balancing three fundamental criteria with associated conditions/restrictions:

- Weight - Minimize the structure's weight;
- Design - Simplify the structure's geometry for the manufacture;
- Material - Use only materials available at CIAFA.

The work carried out to accomplish the main objectives of the design was performed through a Computed Aided Design (CAD) software and endorsed by a stress analysis (FEA). This project has others minor contributions to complete the overall UAV platform such as systems integration, by determining the Payload, Avionics and Propulsion System needed to perform the desired mission.

This aircraft was developed simultaneous and with collaboration with another part

[14], responsible for aerodynamics and flight performance through Computational Fluids Dynamics (CFD).

1.4 Thesis Outline

Seeking the achievement of the stated objectives, this thesis goes from the research process until achieving the contextualized aircraft's results. It is structured as follows:

- Chapter 1: Framework of UAS development, regulations and operations namely at FAP; Thesis motivation and objectives.
- Chapter 2: Market research, theoretical overview of the design, introduction to materials, and theoretical model; Definitions of the Aerodynamic Inputs.
- Chapter 3, Conceptual and Preliminary design including the definition of payload, avionics and propulsion, layout of the aircraft and a longitudinal stability study; Flight envelope, design load and aerodynamic and inertial loads characterization; General considerations about project viability, removable parts, manufacture, approximations and neglected parameters.
- Chapter 4, Aircraft detailed design by CAD modelling of the wing, tail and fuselage; FEA description of assigned materials, mesh assumptions, boundary conditions and static stress study.
- Chapter 5, Stress and Displacement Results and discussion; Aircraft configuration definition.
- Chapter 6, Conclusion and Future work.

Chapter 2

Background

Aircraft design includes four major topics of aerospace engineering: aerodynamics, structures, control and propulsion (Figure 2.1). The main focus of the present thesis is the design of the aircraft structure.

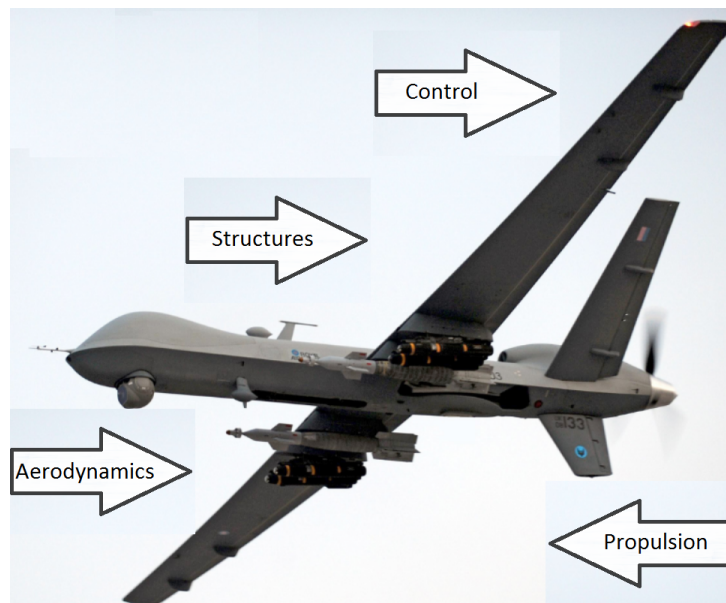


Figure 2.1: Major Topics of Aerospace Engineering.

The starting point for designing a new aircraft is to clearly identify its purpose. Since it is not possible to optimize all of the performance disciplines in an aircraft, defining the ulterior motive leads the way to set the *design drivers* [15]. For a class I UAV targeted for maritime surveillance, they may be further refined into two subcategories, based on specific requirements to accomplish the mission, namely endurance and payload.

The task of the aircraft is primarily to carry the mission payload through a certain route (surveillance), but it also must carry the subsystems necessary for the overall

operation including communications, control equipment, power plant and fuel. The requirement for a high operational endurance (design driver), will determine the fuel load to be carried. From an aerodynamic perspective, to achieve the desired endurance it is needed a maximised performance through an efficient propulsion system and optimum aircraft aerodynamics [3]. Concerning the structural design developed at the present thesis, all the airworthiness airframe requirements for load factors [16] at a specific phase of the flight envelope must be accomplished for the lower weight of the structure as possible. This might not directly mean a decreased fuel consumption, but instead, an increased fuel capacity carried on board since the restricted weight is set for an MTOW of $150kg$, and consequently a higher endurance.

Once the design drivers are set, one can perform a market analysis for systems with similar missions and purposes. The *Israel Aircraft Industries* RQ-2 Pioneer is one of the remarks in UAS surveillance and has flown more than 50 thousand flight hours. It is a twin boom, with a mid-engine pusher configuration powered by a single AR-741 (last upgrade) rotary engine, presenting a five hours endurance for its MTOW of $205kg$ [17].

Following the advancements of this high tech industry, Israel deployed the Aerostar in 2000, and this UAV broke several world records at his class and set unprecedented high standards for reliability, life cycle, operations, endurance, range, payload, cost-effectiveness and ground systems interfaces [18]. It presents an MTOW of $220kg$ and 12 hours of operational endurance, using the Zanzottera 498 engine. Its configuration is similar to the Pioneer with a mid-engine and a twin boom tail [19].

The proven effectiveness of these two widely used aircraft and some other more such as Penguin C, the Shadow family, RQ-5 Hunter, BAE SkyEye and the Bayraktar set the common configuration of a mid pusher propeller with a twin tail boom. The UAVs developed by FAP (ANTEX) to this weight range present the same external characteristics. Overall, this twin tail boom configuration has been the mainstream configuration for this class range ($\approx 150kg$) for the last decades and it has been proven to be effective.

In one hand, considering smaller UAS there are some options with a high endurance and traditional configuration of a push engine at the end of the fuselage. The TEKEVER AR3 and the Boeing ScanEagle both present a MTOW of $22kg$ with a low

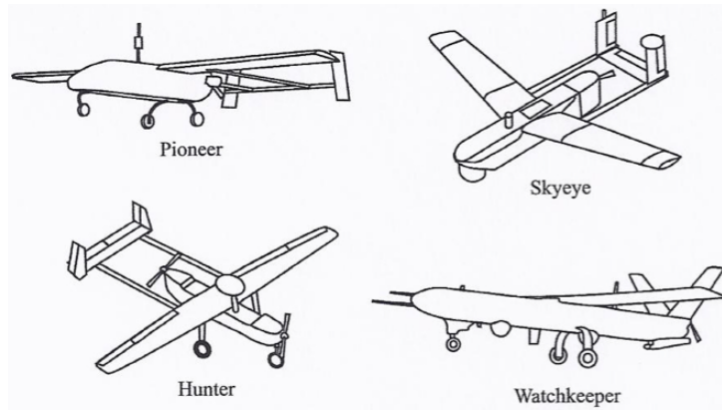


Figure 2.2: Configurations of Different UAV.

weight rear engine. In another side, for an MTOW near $450kg$, there are other options with the same conventional (rear engine placement) configuration such as the Hermes 450 and the WatchKeeper WK450 (Figure 2.2). In this case, the payload of these aircraft is about the same weight ($\approx 150kg$) of the desired UAV, and therefore the impact of having a heavy rear engine can be suppressed.

Through a market research the only different configuration from the main twin boom trend for a $150kg$ class I UAV is the TEKEVER AR5 [20]. This aircraft present a good range endurance from 8 to 12 hours, a length of 3 metres, and a wingspan of only 4,3 metres, being this last specification relatively lower than other similar purpose aircraft. The new configuration, although being fairly distant from the conventional such as the WatchKeeper, set the possibility of designing a medium endurance UAV for surveillance mission without a twin boom tail.

CIAFA, as an investigation centre, craves for innovation when sustained by the necessary theoretical, analytical and experimental results. For this reason, the new configuration without twin boom tail will be the preference if valid results are obtained through the design process.

2.1 Theoretical Overview

2.1.1 Design

Designing a new aircraft comprises three major phases: conceptual, preliminary and detailed design [15]. After the aircraft assembly, there are some more phases includ-

ing the design of modifications during development and subsequent modifications or improvement whilst the system is operational [3].

It all starts by identifying a need or capability for a new aircraft brought about by a perceived market trend and technological advances in Research and Development (R & D). This need will define the mission requirements for a conceptual design.

In this first phase is addressed the general size, configuration and external shape. From theoretical expressions, it is estimated the weight, the aerodynamic characteristics, the total drag, the sizing of the power plant, the static stability and the size of the control surfaces to the desired stage of manoeuvrability [15]. For the structure, it includes the load analysis (design load), material selection and inevitably, the joint analysis of static stability due to the interior systems volume arrangement, needed for placement of mission and flight equipment that inherently affect the stability characteristics.

In the preliminary design, although non-consensual among authors, the original design is refined to achieve the specifications for the mission requirements [3] [21]. In some cases, there may be conflicts between disciplines and one must reach a compromise. However, to obtain a feasible design sound judgement must be exercised considering the implications of the needed modifications or optimization trade-offs to maximize overall performance [22]. This phase also includes a comprehensive definition of the complete system with its interfaces, system specification and aerodynamic fuselage and wing interactions. A three-dimensional layout of the aircraft should be made to provide a better appreciation of how the components will be mounted, the accessibility for maintenance, and define the removable parts if applied. Preliminary design ends with viability considerations about construction and manufacture ('in-house' or external suppliers), maintenance and operations to decide if the project should proceed further [3].

Detailed design involves generating a detailed description of each aircraft component through CAD models, drawings or specifications. In airframe structures analysis, due to the overall aircraft complexity (highly indeterminate structures), numerical methods must be used [23]. This requires a CAD model, material and boundary conditions definition for each component and finally, an FEA. The margin of safety (MS) under design load conditions should be kept close to zero to save structural weight and a

stress check is required for every part of the aircraft to validate the designed structure to the exposed flight loads [21].

2.1.2 Structure Types

A introductory description should be made about the different types of structures present in the aircraft industry. The main body of an aircraft is formed by a fuselage in which wings, tail, engine, landing gear and flight equipment are attached.

Concerning a basic structure for a wing or tail: pressure and shear loads are applied to the skin, transmitted to the ribs and supported by the spar [22] [3]. Wing skins are usually thin, and so the spars are the main load bearing member of the wing. They present a beam shape, running spanwise in the wing or tail, and carry the most part of forces and moments [24] [25].

Now, in respect to the fuselage structure it presents some possibilities such as Frame, Monocoque and Semi-Monocoque structures. In a Frame structure, the frame takes up almost all the loads and it is made up of series of vertical, horizontal, diagonal and longitudinal supports. It is mostly used for light modern aircraft and usually present a skin cover made of composite materials. In a Monocoque structure the skin is the main component, supporting all flight and ground load and providing rigidity for the structure shape. This type of design is inherently heavy and fragile since any damage to skin affect the load carrying capacity. A Semi-Monocoque structure presents shared loads by stringer, skin, longerons and the frame. It has more redundancy then the other option and also a good strength to weight ratio [21] [15] [3].

2.1.3 Material

According to this project requirements, it is intended to manufacture this UAV with composite materials available at CIAFA. A composite material is formed by a combination of at least two non-soluble distinct materials and generally presents a reinforcement (fibre) and a matrix (resin) [26] [27]. The reinforcements available are Carbon, Glass and Kevlar fibre. The matrix at disposal is an Epoxy resin and additionally, there is Airex foam core for sandwich shaped composites.

When manufacturing with composites, one must consider several combinations

such as different fibres, resins, laminating techniques, fabric types and weave patterns. Concerning these patterns, they might be generally divided into unidirectional and bidirectional weaves. The first option of composite layers has a majority of fibres running in one direction such that the maximum strength and stiffness of that material is oriented in that direction. A small amount of fibre (or only resin) may run in other direction to hold the main fibres in position, with a low increase in structural properties [28]. Bidirectional plies have half of its fibres oriented in one direction and the rest oriented perpendicularly to the first direction, as shown in Figure 2.3.

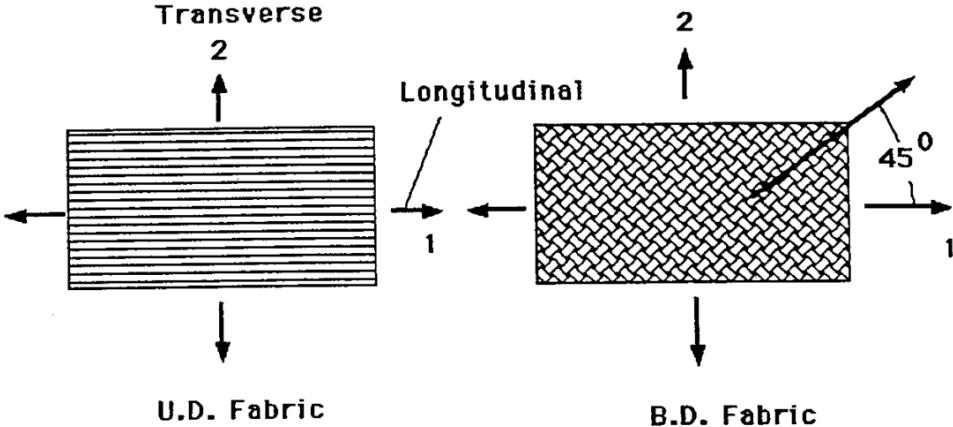


Figure 2.3: Unidirectional (U.D.) and Bidirectional (B.D.) fabrics.

Concerning material selection, the most important factors are cost and weight. The end cost of a structure is comprised of fabrication and tooling cost in addition to material cost. Although the typical cost of graphite/fibreglass is higher than the conventional aluminium, the labour and tooling is cheaper, resulting in a typical 12% less cost [29]. Additionally, composite material present higher strength when comparing to aluminium, resulting in structures with 30% less weight for the same static load resistance [29]. From an aerodynamic perspective, composite structures present a tighter sealing without surface discontinuities, dismissing rivets in the outside surface, reducing the aircraft drag. These advantages set the composites as one of the main aeronautical structures constituent [3].

Composite materials have also a very good behaviour in fatigue when compared to aluminium as shown in the S-N fatigue diagram of Figure 2.4 [29]. In this graph, for a high number of cycles, carbon fibre presents a higher ratio of working stress to ultimate stress that may be used in structural applications until failure. In addition to the good fatigue properties, the vibration damping of composites is superior to steel as shown in

Table 2.1.

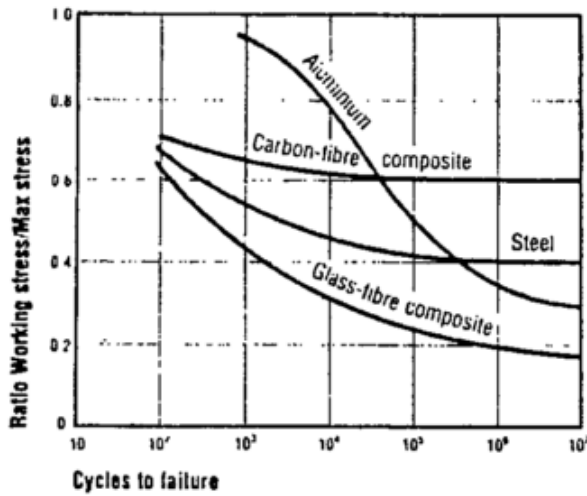


Figure 2.4: Fatigue Behaviour of Materials.

As seen in Figure 2.4 the carbon fibre outstands the glass fibre with a higher ratio between working stress and maximum stress until failure. Moreover, considering two composite materials with the same volume of woven (0° and 90°) fibre (carbon or glass) reinforced with epoxy, the first one presents lower density and a higher tensile, compressive and shear strength. Experimental results show a 110% higher tensile strength per density of woven carbon fibre carbon when comparing to woven glass fibre [30]. Analysing the woven aramid reinforced composite it presents stronger mechanical properties (higher tensile strength per density) than those of glass and carbon fibre reinforcements. Nevertheless, this aramid fibre presents a low shear strength. This mechanical property of woven carbon fibre is 3,34 times higher than that of woven aramid reinforcement.

Overall the carbon fibre presents a low weight, high strength and stiffness [29]. Also, the design team of CIAFA has been using, in every aircraft, this kind of reinforcement as the main composite element. Considering all the benefits and the obtained know-how through years of carbon fibre experience, this composite material will be used as the main element. Additionally, it will be considered both the unidirectional and bidirectional weave patterns and a wet-layup fabric technique.

Concerning the laminate configurations, the most common are the solid laminate and the sandwich. A sandwich structure consists of two thin faces separated by a thick, lightweight core material [31]. Sandwich construction is used to obtain lightweight

Table 2.1: Decay of Free Vibration.

Loss Factor x 10 ⁻⁴	
Stainless Steel	6
Graphite/Epoxy	17
Fiberglass/Epoxy	29
kevlar 49/Epoxy	180

structures with high stiffness. This layout acts like a 'I' beam which is able to handle great loads without bending [26]. Solid laminates offer better resistance to damage, and are more optimized to meet the high-strength loading demands, characteristics of frame structures.

Recently (2017) there were manufactured specimens and some experimental procedures were conducted in accordance with regulations (ASTM). The final mechanical properties were obtained [32] from experimental, statistical and theoretical methods. Material properties are presented in Annex B and will be used as an external input for the present work.

To reduce structural weight, the design should be made to achieve stresses near the yield stress of the material. These specimens experimental tests [32] retrieved a value for the yield and ultimate stress of $508MPa$ for the bidirectional carbon fibre. This value is the minimum of the tensile and compressive tests in both principal directions (0° and 90°). Through a research on known institutions for composite materials specifications, it was found some reports on plain weave carbon cloth by Advanced General Aviation Transport Experiments (AGATE) [33]. This entity states a mean tensile and compressive ultimate stress of approximately $428,2MPa$. This value is valid for a room temperature ($70 \pm 10^\circ F$) dry (RTD) condition which is the closest condition to the flight operation since its temperature is near the mid-range of temperature operation (-13 to $+122^\circ F$). Although the manufacture of the UAV will follow a similar method of the experimental test done in CIAFA in 2017, there is quite a difference in the ultimate load applied to the composite material until failure. One of the possible approaches is to use a mid value between the practical (CIAFA) and the AGATE value that is $\approx 470MPa$. Due to the overall complexity of the project and the high number of components that will be designed, to take into account the needed approximations, a small margin will be used. For the present project, the goal is to achieve a design stress of $450MPa$ on the structure.

2.2 Method Overview

At this stage, it will be described all the steps of the model used to design the UAV. Furthermore, the present work joins conceptual and preliminary design tasks and sort

each task into a 'design chronological order'. The detailed design will be considered to start with the detailed geometric CAD model and the consequently static study to access the design.

Before starting the conceptual and preliminary structural design, there are some important inputs obtained from the aerodynamic conceptual design [14] shown at Table 2.2. Only after having all the presented values it is possible to develop the conceptual structural design.

Table 2.2: Aerodynamic Inputs.

Parameters:			
$\rho(0ft)[kg/m^3]$	1,225	$\rho(8000ft)[kg/m^3]$	0,9631
$W/S[N/m^2]$	450	AR	12
e	0,7060	k	0,0376
$V_{cruise}[m/s]$	36,011	$q_{cruise}[Pa]$	624,489
$C_{D0cruise}$	0,0225	$C_{Lcruise}$	0,71
C_{Lmax}	1,51	$C_{L\alpha}[/rad]$	5,3
$V_{max}[m/s]$	61,733	$q_{max}[Pa]$	1835,233
$\gamma[^\circ]$	10		
Wing:			
$z_{start}[m]$	1,15	$wingweight[kg]$	18,83
$b[m]$	6,26099	$c_{wing}[m]$	0,52175
t/c	0,1	$Airfoil_{wing}$	SG6042
S_f/S_w	0,54	c_f/c	0,3
S_a/S_w	0,36	$z_{AC}[m]$	1,34799
Fuselage:			
$Lenght[m]$	3,00620	d/l	0,1397
$fuselageweight[kg]$	11,62		
Horizontal Tail:			
$z_{start}[m]$	2,62136	$HTweight[kg]$	0,63
$b[m]$	1,53857	$c_{HT}[m]$	0,38464
t/c	0,09	$Airfoil_{tail}$	NACA 0009
$HTweight[kg]$	0,63		
Vertical Tail:			
$b[m]$	2 x 0,75374	$c_{VT}[m]$	0,37687
t/c	0,09	$Airfoil_{tail}$	NACA 0009
$VTweight[kg]$	2,85		
Engine :		$Power_{required}[hp]$	8,23

First, it is necessary to access and define all the system on board. This step includes all the major systems necessary to the aircraft being able to fly, namely the payload, avionics, electrical and propulsion systems. The necessary specifications for

each component include a general description and a verification of accomplishment of the requirements (Appendix A).

Studying all components specifications and having a general exterior dimension for the fuselage, wing and tail (Table 2.2), it is possible to create an overall arrangement layout of the aircraft. This first sketch of the UAV allows for an appreciation about the position of each component, the accessibility for maintenance and the study of removable parts to fulfil the requirements.

Although the theoretical approach defines the stability analysis as a conceptual task and the definition of the systems on board as a preliminary task, that assumption was not made. To perform the needed longitudinal static stability study it is necessary to know every component placement and weight since the inertial load (weight) must be known [3] [21]. This dual area task (stability analysis) was performed simultaneous and with collaboration with the aerodynamic conceptual theory [14]. From this point, the designs followed different paths.

Payload and flight equipment distribution affects the centre of gravity. The precise location of this point is vital to design and achieve a positive static stability, a requirement for an aircraft [34]. Positive stability implies that without control, the nose of the aircraft pitches down. This desirable action prevents an increase in the angle of attack which could lead to stall [15]. The static margin is the normalized difference between the locations of the neutral point and the centre of gravity. To achieve the required positive static margin the centre of gravity must be in front of the neutral point. The aerodynamic design project, agreed with CIAFA in designing the aircraft to obtain a static margin of $\approx 20\%$ at this initial stage. Once a positive longitudinal static stability is achieved, the aircraft design may go further since it now presents a corroborated geometry and equipment placement.

The next step of the selected model is the load factor calculation. It comprises the flight envelope definition for some flight phases considering gust interaction and also, the analysis of the applicable airworthiness to obtain the necessary safety factor. The design load that drives the UAV design is a combination of the safety factors and the maximum expected load of the flight envelope [16].

Succeeding the load factor definition, it must be made an aircraft load analysis to the correspondent flight phase. It encompasses the aerodynamic and inertial load charac-

terization, which represent the boundary conditions that the structure must withstand.

To end the conceptual and preliminary joint design it is necessary an examination review about construction, logistics, maintenance and approximations and neglected subjects of the project, to access the viability of the project.

The subsequent stage is the detailed design which is the focus of this thesis. It must be built and fully described the aircraft CAD model concerning the wing, tail and fuselage, to consequently perform a stress study through FEA. It was chosen a shell analysis since it is adequate for thin parts [35]. The numerical software used was chosen considering the versatility to simultaneously allow construction of complex geometries and also providing the necessary tools for the finite element simulation. Additionally, the author already had an intermediate proficiency in the software, leading to adopt the *Dassault Systems SolidWorks 2017* as CAD and FEA software.

2.2.1 FEA

In airframes structures, the number of redundancies is of the order of thousands resulting in a highly indeterminate structure, where the conventional methods are not feasible [21]. The Finite Element Analysis is a reliable numerical tool for analysing complex engineering design.

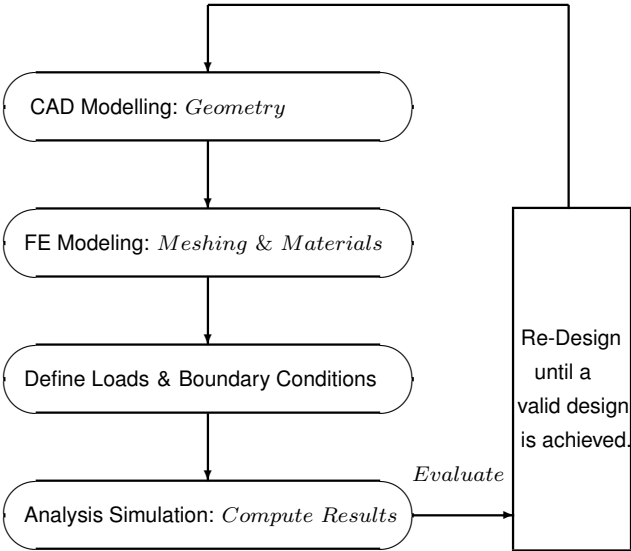


Figure 2.5: Schematic of the iterative FE process.

FEA process ensures the structure performance integrity for the critical load identified with the aircraft flight envelope and the correspondent safety factor. Having the

geometric CAD model (first step), it is necessary to create a Finite Element Model to subdivide the geometric model into discrete elements (meshing) [3]. In this second step, it is also necessary to assign the respective material properties for every surface of the aircraft. A shell model will be created on the CAD software to allow the assignment of each ply individually of the composite material.

The third step is the definition of the analysis conditions, including the applied loads, fixed geometries and contact conditions needed to simulate the critical flight phase.

The last stage is an evaluation of the computed response in respect to the desired structural response (deflection and stress), by comparing the results to the design criteria. The structure maximum stress must be lower than the material yield stress.

If displacement or any of the stress components exceeds the desired value, it will be necessary to re-design the structure and repeat the process until a valid design is achieved. Developing a structural Multidisciplinary Optimization (MDO) tool to each major component would be a valuable option, but concerning the high number of project's variables (geometry, ply orientation, weave patterns, number of plies, thickness variation) it would add complexity to the present work. The schematic illustrated in Fig. 2.5 can represent the finite element iterative process [21].

Next section will describe in further detail some important aspects of the FEA tools of *SolidWorks 2017* as the mesh and static simulation options. At the present stage of the design, the conditions for material assignment and boundary conditions cannot be described since they depend on posterior load analysis.

Mesh

FEA involves a software subdivision of the model into small elements connected at mutual nodes. This "network of discrete interconnected elements" [35] allows the prediction of the behaviour of the entire model.

SolidWorks has an automatic mesh generator which is able to generate a mesh based on global element size, tolerance and local mesh control specifications. Initially, the software estimates a global element size for the model assuming the relation between overall volume, surface area, and other geometric details. Even if, in an early stage of the analysis this default value shall provide a faster solution, for a more accurate solution a convergence analysis must be done, considering some local mesh

control parameters in critical areas.

The multi-tasking software allows CAD and FEA, but it lacks some suitable elements for the analysis. The present 2D shell analysis (adequate for thin parts) is capable of resisting membrane and bending loads, and only presents triangular shell elements, with the 2 options of Figure 2.6.

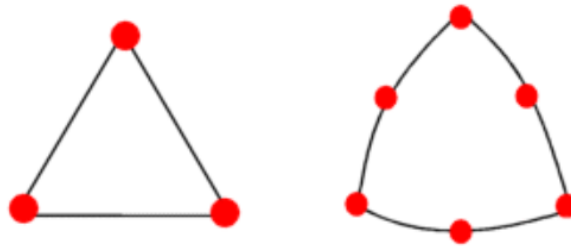


Figure 2.6: Linear Triangular Element and Parabolic Triangular Element.

The first option, by choosing a draft quality mesh, uses linear triangular elements which are defined by three corner nodes with straight edges. The other option uses a high-quality mesh definition with parabolic triangular shell elements presenting three corner nodes, three mid-side nodes, and three parabolic edges. The high-quality mesh is recommended for models with curved geometry and where bending effects are significant [35]. A higher number of nodes offers more degrees of freedom per element implying more accuracy and a lower need for a finer mesh, although using an increased computation time. [36]

Lastly, for the mesh generator definitions, it was chosen the standard mesh which is based on the Voronoi-Delaunay meshing scheme, consisting in a computational method of triangulation [35]. More complex methods are available, being more suitable for high-curvature areas since they create mesh controls (more elements) automatically in this zones. Nevertheless, the expected maximum loads will not be in high curvature areas such as leading or trailing edges, the necessary mesh refinements, after running the simulation will be made manually at the critical surfaces. Therefore the standard mesh generator will be used.

Static Analysis

A static stress study computes displacements, reaction forces, strains and stresses under the effect of applied loads, and the material is considered to fail where stresses

exceed the yield stress. When a load is applied to a body, it will be deformed, and the effect of this load is transmitted throughout the body. This applied external load induces internal forces and reactions through structural elements to render the aircraft into a state of equilibrium [25].

The software used to the analysis makes some static assumptions [35]: Every load is applied slowly and gradually until is reached their entire magnitude, which will stay time-invariant (constant). This presumption allows neglecting the damping forces since no small accelerations and velocities are considered. This case scenario will also dismiss the resonance effect.

Concerning the simulation solver, there are several possibilities available. First, its worth to mention the two classes of solution methods: direct (solver with exact numerical techniques) and iterative (solver with approximations in each iteration). Both must be compared and the results discussed.

Chapter 3

Conceptual and Preliminary Design

Once the aerodynamic conceptual design is done [14], the wings, tail sections and fuselage have been designed, representing the majority of the external shape of the aircraft. The present chapter deals with all the necessary calculations required to design the internal structure of the UAV in order to withstand all the loads during flight. First, all the systems (avionics, payload and propulsion) needed to perform the mission must be defined to study a general layout and the stability of the aircraft. Then it is necessary to draw the flight envelope taking into account theoretical manoeuvres to obtain the design load, which is used to analyse the aircraft aerodynamic and inertia loads. This chapter ends with some general considerations about the viability of the project and some limitations and approximations.

3.1 Systems

All the systems on board should accomplish CIAFA requirements of Table 1.1, if not in contradiction with Appendix A requirements. When in conflict, at least the less restrictive one has to be achieved. All sensors should be able to operate in adverse environmental conditions with strong and turbulent weather, including crosswind of $27knots$, light precipitation of $1mm$ and temperature range from $-25^{\circ}C$ to $+50^{\circ}C$, at a flight altitude up to $15000ft$ above mean sea level (AMSL).

3.1.1 Payload

The main task of the aircraft is to carry the mission payload (sensors) through a certain route (surveillance). The following section describes the most important parameters of the necessary components to perform the required mission, even though the aircraft is able to fly without them.

Vision Payload: Gimble

The vision payload is one of the most important and advanced features of the aircraft to accomplish the mission, specifically for monitoring operations. Requirements demand that the gimble must weight less than $5kg$ and include all the following sensors in synchronisation:

- A day and night gyroscope fully stabilised and steerable in all directions for Target Tracking, Electronic Stabilization and Moving Target Indicator;
- An Electro-Optical (EO) sensor capable of:
 - Field view of $\geq 40degrees$;
 - Optical zoom $\geq 10times$;
 - $\geq 1000pixels$ in one dimension.
- An (short, medium or long wave) Infra-Red (IR) sensor capable of:
 - Field view of $\geq 30degrees$;
 - Optical zoom $\geq 10times$;
 - $\geq 600pixels$ in one dimension;
 - Noise equivalent temperature resolution better than $0,1K$;
 - Temperature range from $0^{\circ}C$ to $+2000^{\circ}C$.
- An Laser Illuminator in the IR capable of:
 - Field view of $\geq 60degrees$;
 - $\geq 1000pixels$ in one dimension;

- Noise equivalent temperature resolution better than $0,1K$.

After a market analysis, it was identified the Gimble Epsilon 140 Octopus that fulfils the technical requirements. This equipment has the following characteristics:

- Weight of $1570g$;
- Power (peak) consumption of $40W$;
- Base dimensions of $140x140mm$ with a length of $189mm$. Volume required inside the fuselage is $960400mm^3$, which corresponds to a length of $49mm$.

Radar SAR

CIAFA's specific requirements of Appendix A recommended, for the UAV's radar, the utilization of the Synthetic Aperture Radar (SAR): RASAR developed by *srcinc*. This system is a lightweight, self-contained radar designed for installation under the wing or fuselage of an aircraft. For project considerations the radar presents the following characteristics:

- Weight of $11340g$;
- Power (peak) consumption of $150W$;
- Exterior placement, with no interior volume occupied.
- This item maximum operational altitude is restricted to $8000ft$, lower than the maximum ceiling altitude of the aircraft which is set to $15000ft$.

AIS

As required by CIAFA's design team (Appendix A), the aircraft should have the SR161 Automatic Identification System (AIS) receiver with capabilities to relay the data. This component specifications are:

- Weight of $400g$;
- Power (peak) consumption of $1,5W$ ($+9V$ to $+15V$);
- Dimensions of $115x75x28mm$ which corresponds to a volume of $241500mm^3$.

Air Pollution Monitoring Payload

As imposed by CIAFA, the Air Pollution Monitoring Payload is a sniffer developed by *Deimos Engenharia* capable of collecting samples, analysing, and broadcast the results in near-real time. This equipment has the following characteristics:

- Weight of $2000g$;
- Power consumption unknown;
- Dimensions of $170x140x100mm$, corresponding to a volume of $2380000mm^3$.

Distress Sensor

The distress sensor is a receptor capable of receiving the $406MHz$ satellite Emergency Position Indicating Radio Beacon (EPIRB) signal from surrounding ships, and relay the information to a desired control centre. CIAFA's design team will apply to this aircraft an already in use sensor, which the given specifications are described next:

- Weight of $600g$;
- Power consumption unknown;
- Dimensions of $100x100x100mm$ which corresponds to a volume of $1000000mm^3$.

3.1.2 Avionics and Subsystems

This section describes all the systems required for the aircraft to fly. It involves avionics, subsystems and electrical components.

Autopilot

CIAFA has experience in operating UAS with *Piccolo* and *UAVISION* autopilots. However, EMSA does not accept the *UAVISION* autopilot. Therefore, it was identified the following possibilities:

- **Piccolo Nano:** This compact modular flight management is designed to meet the requirements of the smallest UAVs. The *Piccolo Nano* series provides small,

lightweight, flexible architecture to support small hand launched or uniquely configured UAS systems. Although it is the newest addition to the Cloud Cap Piccolo family, it is also the smallest one and therefore it does not support Integrated Radio Frequency Data Link options, GPS, Waypoint Navigation, Inertial Sensors and several others peripherals like transponders, Iridium SatCom and Gimbals. Due to lack of software this model is not a valid option.

- Piccolo II:
 - Weight of 200g;
 - Power (peak) consumption of 4W (+8V to +20V);
 - Additional I/O support (16 configurable GPIO lines);
 - Dimensions of 142x46x62mm which corresponds to a volume of 404984mm³.
- Piccolo SL:
 - Weight of 110g;
 - Power (peak) consumption of 4W (+4V to +28V);
 - Additional I/O support (14 configurable GPIO lines);
 - Dimensions of 131x57x19mm which corresponds to a volume of 141873mm³.

Both the Piccolo SL and II versions accomplish all the requirements to perform the mission and have almost the same specifications. The Piccolo II with over a decade in the field has become the UAS industry standard flight management system offering more reliability [37], but in terms of features only adds two more configurable General Purpose Input Output (GPIO) lines than the Piccolo SL. Regarding the specifications, the SL version's inertial sensors only admit accelerations up to 6g instead of the 10g limit on the II version. According to the expected mission envelope for surveillance operations, 6g should be enough so both autopilots are acceptable in this aspect.

Another difference is the pressure measurement. Piccolo SL measures a pressure differential up to 6kPa, corresponding to a maximum Indicated Air Speed (IAS) of 192knots, while Piccolo II is limited to a pressure differential of 4kPa for a Maximum IAS of 155knots. Concerning design requirements of Appendix A the maximum velocity is set to 120knots, therefore both options are valid. The two components present the same power consumption, but the newer version (Piccolo SL) has its weight reduced by 45% and its volume also reduced by 65%. Overall, the Piccolo II offers more two GPIO lines and a better reliability based on a higher value of flight hours. Nevertheless, the better geometry, lower volume and weight, of Piccolo SL balance these advancements of Piccolo II. Concerning the reliability and robustness, since Piccolo SL is an upgrade

of the older one, it should be a reliable choice as well, thereby it will be used on the UAV.

SatCom

As required by CIAFA (Appendix A) the UAV's SatCom must be the *NAL Research Corporation* A3LA-RS model. This system is a low-cost data-only Iridium satellite modem. This equipment has the following characteristics:

- Weight of 122g;
- Power (peak) consumption of 1,75W (+3,5V to +5,4V);
- Operating temperature between $-30^{\circ}C$ and $+70^{\circ}C$;
- Dimensions of $92 \times 48 \times 23 \text{mm}$, corresponding to a volume of 101568mm^3 .

Transponder

As described in Appendix A it is required the Mode S and ADS-B version of the *Sagetech* MX Transponder. Its specification are presented next:

- Weight of 150g;
- Power (peak) consumption of 15W ;
- Dimensions of $83,8 \times 63,5 \times 19,1 \text{mm}$, which represent a volume of 101637mm^3 .

Pilot Cam

It is required a pilot cam placed at the rear back of the aircraft (on top of vertical tail) to provide an above view of the UAV to the ground operator. Due to the lack of information on this subject, it was considered same specifications as the *GoPro* Hero 5 black series:

- Weight of 118g;
- Power (peak) consumption of 5,4W;
- Dimensions of $61,7 \times 44,4 \times 24(\text{deep}) \text{mm}$, having all its volume outside the fuselage.

Energy Converter Box

The component responsible to provide power supply to the remaining systems is the power distribution box, developed at CIAFA, presenting an estimated weight of 4000g.

Onboard Computation

Onboard computation is capable of processing sensor data and broadcasting through selected data link. Requirements of Appendix A recommend two specific *ConnectTech* equipments (Rosie and Rudi), which specification are described next:

- Rosie Embedded System:
 - Weight of 1430g;
 - Power input: (+9V to +36V);
 - Operating temperature between $-20^{\circ}C$ and $+80^{\circ}C$;
 - Dimensions of 163,6x108x96,3mm, corresponding to a volume of $1698385mm^3$.
- Rudi Embedded System:
 - Weight of 703g;
 - Power input: (+12V);
 - Operating temperature between $-20^{\circ}C$ and $+80^{\circ}C$;
 - Dimensions of 135x50x105mm, corresponding to a volume of $708750mm^3$.

Data Link

According to requirements of Appendix A, the data link component should be the Air-link, a Digital IP Data Link from *Octopus*, with the following characteristics:

- Weight of 108g;
- Power (peak) consumption of 5W (+10V to +16V);
- Operating temperature between $-20^{\circ}C$ and $+80^{\circ}C$;
- Dimensions of 100x52x19,7mm which corresponds to a volume of $102440mm^3$.

This component has an additional tracking antenna option available for a range further than 100km, that must be used to fulfil the 300km Beyond Radio Line of Sight (BRLOS) requirement.

Servo-actuators

This component was defined by the CIAFA's design team to be the same as the previously developed UAVs, the CBS-15 *CAN* Brushless Servo. The operational requirements specific crave for redundancy in all control surfaces. In this aircraft there are 6 control surfaces. For safety, duplicated actuators means 12 servo-actuators. The overall group of 12 components have the following specifications:

- Total weight of 1296g (108g each);
- Overall maximum power allocated of 20W;
- Operating temperature between $-20^{\circ}C$ and $+80^{\circ}C$;
- Small exterior dimensions and placement on wings and tail.

Power Supply

The power supply is granted by an onboard generator when the engine is working. CIAFA's design team recommended the utilization of the same generator as the previous UAVs (Antex) of CIAFA, having an estimated weight of 2000g for $\approx 150W$ of output power. Although the peak power of all the considered elements is almost 243W it is not expected to have peaks of all the systems at the same time. In case of engine failure, there are backup batteries on board, namely:

- Backup batteries capable of 2 hours of main systems (autopilot, servos and transponder) made of Lithium ($\approx 1600g$).
- Sensor backup batteries capable of 20 minutes of full operation (Radar SAR and Gimble) made of Iron ($\approx 4000g$);

Others

At this point, all the required components by CIAFA were define, besides the propulsion system. Nevertheless, there are some extra items needed for the aircraft to be operational [14] [34]. The assigned weight will be taken into account for the overall inertial distribution:

- The Air Data System with an estimation of 1361g;
- The GPS antenna with an estimation of 454g;
- The Inertial Navigation System with an estimation of 1361g;
- The Strobe lights with an estimation of 1000g;
- The Environmental Control System with an estimation of 2995g;
- The wiring system with an estimation of 4512g.

3.1.3 Propulsion System

Engine

Concerning the propulsion system, the CIAFA's design team recommended applying to this aircraft the *Wankel* AR 741 engine already used in ANTEX-M x03, although accepting other engines with a justified increased performance. Its reliability comes from several years powering similar aircraft such as the RQ-2 Pioneer (205kg) and the RQ-7 Shadow (170kg). According to the aerodynamic conceptual design of Table 2.2, the 38hp power delivered by this engine is enough to attain the desired flight performance. Statistical data collected from CIAFA flights with ANTEX-M X03 ($\approx 150kg$, equipped with this engine (fuel injected with oil mix), showed an expected consumption of fuel (98 octanes) of 5l/h and oil of 0,8l/h.

According to theory, two-strokes engines tend to produce twice the power per unit of time compared to a four-stroke engine at the same rotational speed [3]. Therefore a four stroke engine option will be dismissed.

After a market research, two engines were identified for the same applications and with similar performance. Manufacturer's specifications are presented in Table 3.1.

The *Zanzottera* 498 two-stroke boxer engine is used by the Israeli Aerostar. Although it presents more power, its power to weight ratio is lower than the rivals. Comparing the AR 741 with the 3W engine, it is heavier, presents more maximum power, has a higher worldwide UAV use and an important *know-how* of its maintenance at CIAFA. Therefore it was decided to use the AR 741 engine, even though the 3W-342i is also a valid choice if the interest of investing in a new engine arises.

Table 3.1: Engine Comparison.

	AR-741	Zanzottera 498H	3W-342i B2 TS CS
Maximum Power [hp]	38	44	35,8
SFC at Max.Power [lb/hp/hr]/[l/hr]	0,570 / 4,97	0,572 / 4,30	/
Weight [kg]	10,700	16,300	8,820
Price [€]	/	/	4 732,90

Additionally to the engine's mass, it is added a 1200g factor to take into account the installation, a no fire protection and damping shockers, and also a 1325g factor for the propeller [14] [34].

Fuel Tanks

An endurance of 8 hours is a mandatory requirement with a full set of sensors. From operational data presented previously, an operational fuel consumption of 5l/h implies a minimum gas tank capacity of 40 litres. Using the same approach, it is required at least a 6,4l oil tank. Since the aircraft will not have its full payload in every flight, it will be mounted on the aircraft an equivalent tank of 60l in total, divided into 2 fuel tanks and 2 oil tanks. Therefore a longer endurance above 8 hours can be achieved for example if the RADAR SAR ($\approx 11kg$) is not on board. It was estimated 2400g of empty weight for the tanks.

3.2 Layout

Figure 3.1 shows a possible modular layout of the aircraft. It shows a lateral view of the fuselage. This modular construction allows a easy access to all components. Furthermore, it is used the frame type structure for the fuselage, which means that the main loads are shared by the internal frame compound by bulkheads, longerons, and other longitudinal supports connecting bulkheads. This approach represents a low thickness skin on its majority, to allow panels access to components and maintenance without impact on the strength of the structure.

Firstly, it must me stated the used axis for the present project. As shown in Figure 3.1, the z axis represents the longitudinal axis of the aircraft, while the x axis is the

spanwise axis of the aircraft. y axis represents the vertical axis of the aircraft. The origin is at the nose of the UAV.

According to requirements of Appendix A, every component must be capable of transportation within $3m$. Since the aircraft wingspan is higher than $6m$ (Table 2.2) that should imply a division in at least 3 parts. An experimental analysis of the logistics (transports), revealed that the limitation length was indeed $3,20m$. Considering this maximum logistic dimension the wingspan should be at least divided into two pieces. At this stage, for manufacturing and operational simplicity, the wing will be divided into 2 half-wings that will be attached to one central piece at the fuselage. These lifting surfaces modules are detachable by disconnecting the electrical connections and the structural joints.

Since the engine module is placed at the rear end of the fuselage and does not have any surface cover, it has easy access for inspection and maintenance. Inside the fuselage, and still linked to this module, supported by the fuselage there will be the generator powered by a shaft from the engine.

The aerodynamic inputs of Table 2.2 present the length and the diameter of the aircraft obtained by the fineness ratio (d/l). The aerodynamic design provides the centre of lift for wing and tail. Furthermore, the configuration analysis [14] set a 'H' configuration for the tail. Since the tail is placed further back as possible it is possible to estimate the desired distance between both centres of lift and calculated the position of the wing in the aircraft [14]. The wing placement is stated at Table 2.2 and allow a sketch of the fuselage. Wing and landing gear must be supported by a structure with high stiffness.

Observing the layout of the aircraft there will be several payload/components in the aircraft nose. The access might be done via a removable cover, for example with a structural connection involving quick acting pins [3]. This cover would give free access to the electronic bay station, which could then be removed as an entire piece for bench testing or avionics replacement. An electrical connection should be made by joining suitable switches, instead of individual connections.

The market research of Chapter 2 stated that the main problem with this innovative configuration would be the weight distribution. The rear end pusher engine demands that avionics must create the necessary positive impact on the longitudinal stability, to

place the overall centre of gravity in front of the neutral point [15]. The power supply equipment (batteries and energy converter box) will be placed in the first nose compartment due to its considerable high weight in order to create a greater positive impact on the longitudinal balance. Also, its closeness to the payload bay is beneficial to reduce cable length. Additionally, the forward-looking camera (gimble) is mounted at the nose to have a free frontal view and the RADAR SAR is placed under the fuselage supported by a local reinforcement of the airframe structure.

An initial sketch of the fuselage structure must be known to allow the project development. To provide the necessary support for the components, the bulkheads of the aircraft are placed carefully to allow its storage (Figure 3.1). At this stage, it was estimated for the UAV to present two bulkheads in the nose section. The first at $250mm$ from the nose is set to support the batteries and the attachment for the nose gear. The second at $z = 500mm$, provide support for the payload bay and the Radar SAR. The wing will be mounted in the visible top skin cut between two bulkheads at $z = 1148,5mm$ and $z = 1673,25mm$, which represent the wing chord longitudinal length. Furthermore, there is a main double bulkhead near mid-section of the wing responsible for the wing and main gear attachment. At the rear part, the last bulkhead houses the tail and power plant, and it is connected to the main bulkheads through 4 cylindrical longerons. A further accurate design will be made in the present thesis.

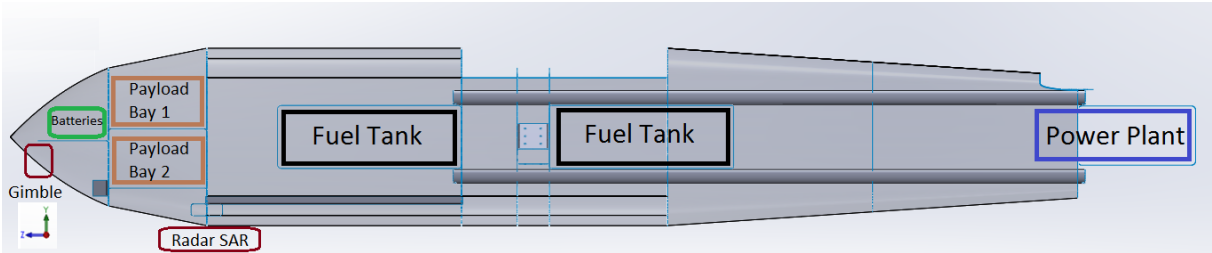


Figure 3.1: Layout of the Aircraft.

The high mass of fuel required for the medium endurance operations must be carried near the aircraft centre of mass, but in this case, the wing and landing gear fixations do not allow it. The solution is to divide into 2 different tanks, in which each position is at the same distance to the centre of mass.

3.3 Longitudinal Static Stability

As previously explained the longitudinal static stability study is essential to validate the present design. It also provides vital information for the load analysis of the structure, since the tail lift loading is one of the outputs. This study depends on several variables, such as tail sizing, weight distribution, distances between centres of lift (wing and tail), and others. At this stage, the structure weight is not known but it must be estimated. A possible approach is through historical coefficients [15].

The aerodynamic conceptual design [14] at this initial stage aimed a positive static stability of $\approx 20\%$. This corresponds to a centre of gravity at $1,47m$ from the nose and a necessary tail lift of $\approx -115N$. The structural weights estimations impact greatly this results. The design process will refine the weights and therefore a new tail lift value will be obtained. This implies a new design since different loads will require different material thickness to resist them. Different material assignments will again modify the weight. This iterative loop will continue until a stable geometry is achieved and a 'near-final weight' is achieved for each structure. To prevent this extensive detailed process, some analysis were made starting with the estimated structural weights of Table 2.2.

These estimations revealed to be greater than the necessary and after some initial iterations, it was obtained new weight estimations to a static margin of $\approx 18,51\%$. The correspondent components positions and weights are shown in Figure 3.2 in respect to the nose position at $z = 0$. For this configuration, the centre of mass is at $\approx 1,253m$ from the nose while the wing centre of lift is at $\approx 1,348m$. This lead to a necessary $-87,77N$ of lift produced by the tail for level flight. [14]

These analytical results were obtained by the method described in the aerodynamic part of this project [14]. For every other option of components configuration, the exchangeable payload must be balanced by an equivalent mass moment about the aircraft centre of gravity [3].

3.4 Load Factor

The design of the structure is based on a load limit, which is the largest expected load. During manoeuvres, significantly high load factors can occur. Since these set the limit

Load Type	Weight (kg)	Magnitude (N)	z_start (m)	z_end (m)
Fuel & Oil before wing	19,016	186,54696	0,9	1,1
Fuel & Oil after wing	19,016	186,54696	1,4	1,6
Radar SAR	11,34	111,2454	0,4	0,6
Gimble	1,57	15,4017	0	0,2
Payload (sniffer , AIS, distress)	3	29,43	0,3	0,4
Fus. Structure+paint	20,84725825	204,5116035	0	3,015629
Engine	14	137,34	2,6156285	3,015629
Propeller	1,325006456	12,99831333	3,0156285	3,015629
Wing Structure	15,016	147,30696	1,15	1,672015
Horizontal Tail (sw)	1,25	12,2625	2,62	3,004937
Vertical Tail (sw)	1,25	12,2625	2,62	2,997159
Twin Boom	0	0	0	0
Main Gear	12,67607029	124,3522496	1,29161	1,37361
Nose Gear	3,085404547	30,2678186	0,2	0,3
Wiring	4,5122	44,264682	0,1	1,672015
Actuators _ wing + stroblight	1,864	18,28584	1,15	1,672015
Actuators _ tail	0,55	5,3955	2,62	3,004937
Batteries & energy converter box	9,6	94,176	0,1	0,2
Fixed Equipment	8,793372654	86,26298574	0,25	0,4
Total	148,7113122	1458,857973		
Tail Lift required (N)	-87,77426866		2,62	3,004937

Figure 3.2: Components displacements to achieve Static Stability.

of the internal structure, it is mandatory to determine the maximum load factor of the aircraft.

3.4.1 Flight Envelope

The flight envelope of an aircraft refers to the capabilities of the aircraft structure and depends on the velocity and load factors to a certain altitude. It is a graphical representation of the allowable load factors that an aircraft must handle in flight, as a function of the airspeed. It sets the boundaries for the structural design [15].

One of the possible approaches is based on the MTOW of the aircraft and encompasses actual flight phases such as intercept, instantaneous and sustained turns, climb, as well as limiting condition set by the highest angle of attack flight and dive

conditions [15]. All the manoeuvres are analysed for a configuration without flaps, and in addition, the added load factor resulting from wind gusts is calculated.

Intercept

The intercept flight phase minimizes the drag to weight ratio and thereby maximizes the excess power. This acceleration phase is considered to occur at cruise speed ($70knots$) and altitude ($8000ft$) [15], and using inputs from the aerodynamic conceptual design of table 2.2:

$$n = \frac{q}{W/S} \sqrt{\frac{C_{D_0}}{k}} = 1,073. \quad (3.1)$$

Instantaneous Turn Rate

The load factor corresponding to the instantaneous turn rate is based on conditions that might be representative of manoeuvres occurring at cruise speed ($70knots$) and altitude ($8000ft$) [15]. Using inputs from the aerodynamic conceptual design of table 2.2 it is possible to estimate the instantaneous turn rate:

$$\frac{W}{S} = \frac{qC_{L_{max}}}{\sqrt{\left(\frac{\dot{\psi}V}{g}\right)^2 + 1}}. \quad (3.2)$$

Trough the previously analytical equation a instantaneous turn rate of $0,503$ degrees per second is obtained. As expected, this is low value, since the design do not include combat, and so, wing loading was optimized to other low manoeuvrability flight phases. Using this value the load factor is obtained:

$$n = \sqrt{\left(\frac{\dot{\psi}_{inst}V}{g}\right)^2 + 1} = 2,098. \quad (3.3)$$

Sustained Turn Rate

In a sustained turn, the speed and altitude are kept constant meaning that the thrust equals the drag, and the load factor is constant. Since the maximum sustained turn rate is lower then the instantaneous turn rate [15], and the analytical expressions are

similar:

$$n = \sqrt{\left(\frac{\dot{\psi}_{sust} V}{g}\right)^2 + 1} \leq 2,098. \quad (3.4)$$

This flight phase presents a lower load factor and so it will not be the largest expected load.

Climb

The climb phase is based in a unflapped configuration [15], and from the inputs of table 2.2 it is possible to obtain the climb gradient:

$$G = \frac{(T - D)}{W} = \sin\gamma = 0,174. \quad (3.5)$$

The load factor (equation 3.7) requires a condition on the thrust to weight ratio, to the value inside the radical to be positive. The minimum required value T/W_{min} , must be calculated:

$$\frac{T}{W} \geq G + 2\sqrt{\frac{C_{D0}}{\pi Ae}} = 0,232. \quad (3.6)$$

Considering a 10% value above the minimum thrust to weight ratio, it will result in two different values for the plus and minus operations:

$$n = \frac{(T/W - G) \pm [(T/W - G)^2 - (4C_{D0}/\pi Ae)]^{0.5}}{2C_{D0}/C_L} = \begin{cases} n^+ = 1,636 \\ n^- = 1,179 \end{cases}. \quad (3.7)$$

The load factors for the plus and minus operations of Equation 3.7 are denoted n^+ and n^- . When the actual thrust to weight ratio equals the minimum ratio the load factors will present the same value.

High Angle of Attack

This manoeuvre happens at cruise conditions, and can result from an instantaneous change in the angle of attack during level flight. The resulting load factor [15], using the maximum lift coefficient without flaps and the inputs from table 2.2:

$$n = \frac{qC_{Lmax}}{W/S} = 2,098. \quad (3.8)$$

Dive

The load factor corresponding to the maximum dynamic pressure is produced in a dive condition, based at the highest flight velocity that is 1.5 times [15] the cruise velocity (105knots). But, due to the requirement of maximum velocity of 120knots , the load factor will be calculated for this speed since a greater speed will present a consequently greater dynamic pressure. This was taken at the cruise altitude for a cruise lift coefficient according the standard equation for the load factor [15]:

$$n = \frac{qC_{L_{cruise}}}{W/S} = 2,893. \quad (3.9)$$

V-n Diagram

A V-n diagram shows the flight load factors that are used for the structural design as a function of the airspeed. These represent the maximum expected loads that the aircraft will experience. It varies from all reasonable combinations of altitude, speed, weight and payload configuration, and so several assumptions must be made. The flight envelope is designed for the MTOW of the aircraft at the cruise altitude (surveillance operations), with a clean configuration (no high lift devices-flaps) and assuming a symmetric flight without movement in roll or yaw axis. Through the previous manoeuvres analysis the maximum expected load factor for a cruise velocity of 70knots at an altitude of 8000feet is 2,893.

Since this design is aimed for manufacture and consequently certification for international operations, from NATO AEP-83 [16], applied to UAS, it is required for the aircraft airworthiness: " A symmetric limit manoeuvring load factor ≥ 3.8 (...) and a symmetric negative limit manoeuvring load factor ≤ -1.5 should be established". The expected maximum load is lower than the required value, so the design and the flight envelope will admit these highest positive and negative load factors.

The V-n diagram, showing the flight envelope of load factor for the assumptions above, is presented in Figure 3.3. The curve from the origin at $n = 0$ to point A represents the maximum normal component load produced by a high angle of attack flight given by equation 3.9. The maximum value ($3.8g$) is determined by airworthiness requirements for this specific aircraft (UAS), corresponding to the horizontal line from point A to D. Point D occurs at the highest velocity (dive), required by CIAFA to be

120knots. The dashed black line represents the desired cruise velocity of 70 knots. At cruise, $n = 1$, and the intersection of the O-A curve with this value represents the stall velocity $V_S (\approx 25m/s)$, which is the minimum speed at the aircraft can maintain level flight, for the specified configuration. The line from point H to F represents the maximum negative load for this aircraft (NATO's UAS requirements). The curve from the origin to point H is also obtained by equation 3.9, but considering a $C_{L_{min}}$ for the lowest angle of attack. Point F corresponds to the intersection of the negative load limit and the design cruise velocity. The negative load factor envelope is closed by a linear joint of the point F to the dive velocity for $n = 0$ [15].

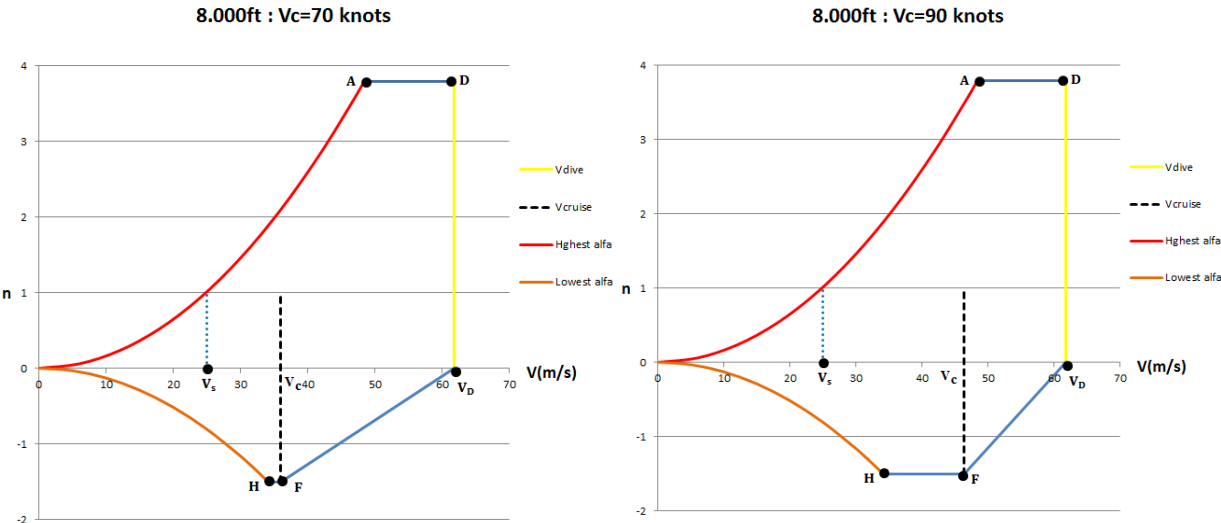


Figure 3.3: Flight Envelope for $V_C = 70knots$. Figure 3.4: Flight Envelope for $V_C = 90knots$.

For the preliminary aerodynamic design, it was studied an alteration of the required cruise velocity of 90knots. It was proven that the aircraft perform a more efficient [14] flight for a cruise velocity of 70knots and this value was accepted by the CIAFA's design team. Nevertheless, due to operational requirements, the aircraft could have to perform some mission at a cruise velocity of 90knots. Its flight envelope was determined to this new condition and presented in figure 3.4 For cruise velocity of 90knots, the manoeuvre for maximum load factor is the highest angle of attack presenting a 3,469g. This case, is also lower than the required for airworthiness, will present the same maximum positive and negative load factors. The increased cruise velocity allows a greater manoeuvrability at negative load factors and a higher margin of positive load factor that can be applied to the aircraft at cruise velocity. Thus, for a cruise velocity of 70knots (below V_A , the maximum loads which can be applied to the aircraft are governed by

$C_{L_{max}}$, meaning a relatively small area before stalling the aircraft. Overall, the aircraft with $90knots$ cruise velocity has a better all-around performance and is safer for a flight plan linked to a more dynamic mission (an example of flight tests), not usual at the typical steady surveillance mission. All these calculations were made for clean configuration. If it is assumed the highest angle of attack for take-off with high lift devices, the lift coefficient increases to $C_{L_{max}} = 2,45$. In this case, it is obtained the stall velocity of $V_S \approx 20m/s$.

Gust Loads

Operationally, gust interaction should be considered since the environment of 'near-shore' maritime surveillance mission favours atmosphere turbulence. Technically, the UAV is assumed to be subjected to symmetrical vertical and lateral gust in level flight, and the resulting limit load factors should be determined for a positive and negative gust values [16]. This chapter only takes into account the vertical gust. Lateral gust will be studied later in this project.

The previous flight envelope considered aircraft's loads resulting from prescribed manoeuvres in the longitudinal plane of symmetry. Other types of in-flight loads are caused by air turbulence and gusts subjecting the aircraft to a sudden increase or decrease in the angle of attack and consequently in the wing lift, $\Delta n = \pm\Delta L/W$ [25].

In Figure 3.5 it is shown the effect of a gust on an aircraft in level flight. The turbulent gust produces small velocity components, v and u . For analytical simplification it is assumed that these components are much lower than the flight speed, therefore $V + v \simeq V$, and so, $\Delta\alpha \simeq u/V$ [15].

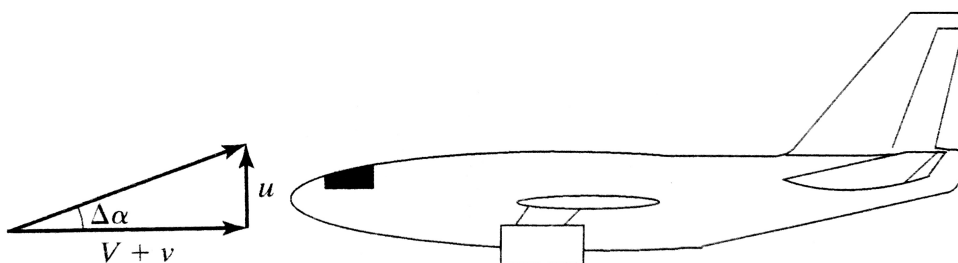


Figure 3.5: Model for gust load effect on a aircraft in level flight.

To determine the incremental load factor of Equation 3.10a, it is first required to analyse some parameters. The normal component of the gust velocity, u , is a product

of statistical [15] average of values from flight data, \hat{u} , and the response coefficient, K presented in Equation 3.10b. This statistical input varies for different flight phases and is shown in table 3.2. The attenuation factor, K , defined for subsonic flight on equation 3.10c requires a previous calculation of the mass ratio μ , in equation 3.10d, governing the frequency response of the atmospheric turbulence.

$$\Delta n = \frac{\rho u V C_{L\alpha}}{2W/S}, \quad (3.10a)$$

$$u = K \hat{u}, \quad (3.10b)$$

$$K = \frac{0.88\mu}{5.3 + \mu} \approx 0,762. \quad (3.10c)$$

$$\mu = \frac{2W/S}{\rho g \bar{c} C_{L\alpha}} \approx 34,212, \quad (3.10d)$$

Using the inputs parameters of Table 2.2, the peak load factor is calculated, for 3 different manoeuvres such as cruise, dive and high angle of attack, resulting in different values of incremental load factors [25]. Therefore, the total load factor including gust loading is: $n_{peak} = 1 + \Delta n$, presented in table 3.2.

Table 3.2: Incremental Load Factor for gust.

Flight Condition	$\hat{u}[m/s]$	Δn	n_{peak}
Dive Condition	7,5	2,01	3,01
Cruise Flight	15,25	2,39	3,39
High Angle of Attack	20	3,13	4,13

According to theoretical gust values [15], the combined flight envelope for the UAV results from the superposition of the manoeuvre $V - n$ diagram with the gust loads ($V - g$ diagram), and it is shown in Figure 3.6.

A typically combined flight envelope is presented in Figure 3.7. Several intersections occurs between the curves of additive gust loads with the $V - n$ diagram, which allow the determination of the impact in the maximum load factor.

Analysing the graph superposition for the UAV of the present project, at standard conditions of $8000ft$ and cruise velocity of $70knots$, it is possible to see some differences. The literature values for gust [15] [25], results in large values of incremental load factor (for cruise and high angle of attack conditions) that surpass the manoeu-

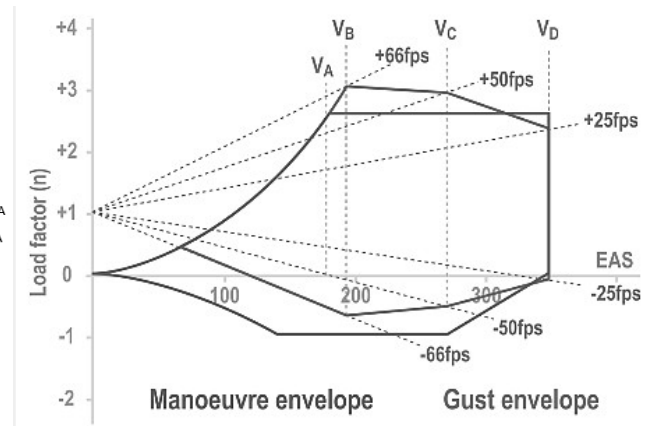
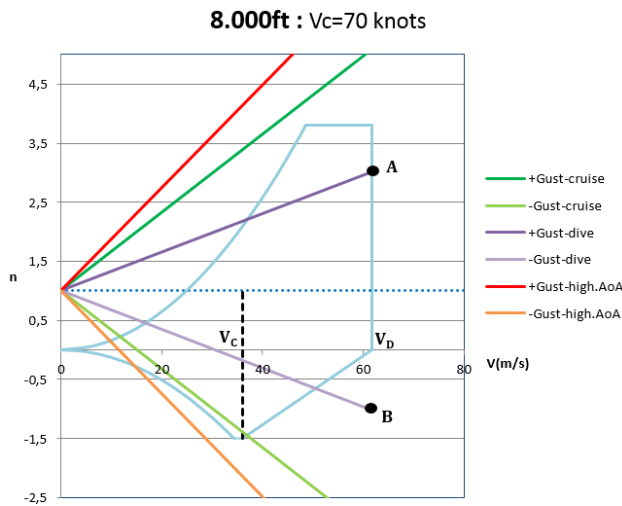


Figure 3.6: $V - n$ and $V - g$ diagram. Figure 3.7: Typical combined flight envelope.

ving envelope, resulting in a preclusion of combination of both diagrams. Nevertheless, it provides information concerning the dive condition, in which point A (Figure 3.6) refers to the load factor at the dive velocity for a condition of positive gust, and point B corresponds to the addition of loads from negative gust in dive conditions.

All the previous method present the required analysis of gust effect for standard aircraft [15] [25]. Closely analysing the project requirements of Appendix A it is required for the UAV to be able of operating in a condition of turbulent gusts up to $27knots$ ($\approx 13,9m/s$). This value is lower than the theoretical $20m/s$, and remaking the calculations it would result in a peak load factor for high angle of attack of only $3,19g$ instead of $4,13$.

Through the previous manoeuvres analysis, the gust will increase the maximum expected load factor for a cruise velocity of $70knots$ at an altitude of $8000ft$ from $2,893g$ to $3,18g$. Proceeding the same analysis for the $90knots$ cruise velocity, the maximum load factor for gust conditions increase from $3,469g$ to $3,80g$. Overall, this atmospheric turbulence will not impact the design load since none of the maximum loads, exceeds the $3.8g$ load factor required for airworthiness.

3.4.2 Design Load

To ensure general minimum standards of strength and safety, airworthiness regulators present several factors which the primary structure must satisfy. The maximum load that the aircraft is expected to experience in normal operation ($3,8g$), is the limit load. The proof factor [25] of 1.25 creates the proof load ($4,75g$) meaning that the UAV's

structure must withstand this acceleration without detrimental distortion. Lastly, the ultimate load, as know as the product of the limit load and the safety factor (1.5), is the lowest load at which the structure could achieve structural failure. This standard safety factor used in aeronautical industry accounts for uncertainties in design, variation in structural strength, structural deterioration over time and operator usage [21].

NATO regulation for light ($\leq 150kg$) unmanned aircraft systems [16], also defines that a rationale positive margin beyond the maximum operating envelope must be used: " an ultimate safety factor ≥ 1.5 for structures whose failure would lead to a Hazardous or more serious failure condition." Also, as stated in paragraph 23.303 of FAR Part 23, the safety factor of 1.5 must be used for all structures.

NATO AEP-83 refers that the integrity of the structure must be ensured, applying a further special factor in the cases where the failure of a component would result in the loss of the structural integrity of the aircraft. "The guaranteed minimum design mechanical properties ('A' values - value above which at least 99% of the population of values is expected to fall with a confidence of 95%) should be met" [16]. In this case of "in-house" manufacture of composite materials, the designer is unable to provide satisfactory statistical justification for A values. So an additional factor ≥ 1.2 , for a tested specimen with well-established manufacturing and quality control [32], should be applied to ensure that A values are met.

The design load factor is then defined as the product of the limit load and the safety factors:

$$n_{design} = SF_{load} \cdot SF_{composite} \cdot n_{limit} = 1.5 \cdot 1.2 \cdot 3.8 = 6.84 . \quad (3.11)$$

3.5 Aircraft Loads Analysis

It is now considered the analysis of the flight condition, within the boundary of the flight envelope, which represent the most critical manoeuvre for the structure to withstand. It is also required a load characterization of all forces acting on the aircraft.

Concerning air loads, these can be divided into surface forces (acting on the surfaces of the structure: aerodynamic and hydrostatic pressure) and body forces (acting upon the volumes of the structure: gravitational and inertial effects) [25].

As described in section 3.4.1, after applying the safety margin factor to the critical

load the design load of $6.84g$ is obtained. For the aircraft main mission of surveillance, the correspondent manoeuvre could be for example a rapid pull up (at the bottom position) from a dive condition.

To analyse this symmetric manoeuvre it is needed to replace the dynamics conditions of the accelerated motion by an equivalent set of static conditions in which the applied loads are in equilibrium with the inertial forces (Figure 3.8).

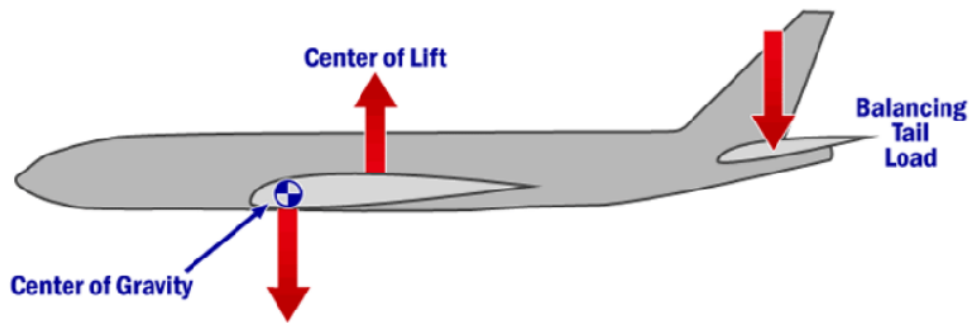


Figure 3.8: Equivalent set of static conditions for the lower phase of the pull up.

To design a structure of an aircraft, different directions of forces should be studied in separately analysis. Therefore, this UAV project will be designed to withstand the (vertical) critical resultant force and no others resultant forces (horizontal) will be considered to the structural analysis [38].

This approach is made since: "pressure loads are generally of a much greater magnitude than aerodynamic loads which are caused by shear" [24]. Therefore, Lift is much greater than Drag. Also, the wing structure is inherently strong in the drag component direction, since the relevant resistive length for the resultant bending moment is the wing chord, which is large compared to the wing thickness ($t_{max}/c = 0.1$). Hence, the principal bending of the wing occurs in the lift component direction. The design of the internal structure of the wing is then primarily driven by the need to counter the wing-thickness bending moments [15].

On that account, some considerations about horizontal equilibrium must be made. In equilibrium, the thrust is considered to remain constant in magnitude and equal to the appropriate value of all body's drag contributions before the manoeuvre began: $T \approx D$. Furthermore, the thrust is considered to act parallel to the direction of flight in order to simplify the analytical calculations [25].

The critical loading occurs perpendicular to the longitudinal axis of the aircraft, and for a static condition, the acting forces are the Wing Lift (L), Tail Lift (P), Weight and

Inertial Forces (nW). To achieve in flight equilibrium, the tail creates a (negative) downward force of $87,774N$ as shown in section 3.3. The vertical equilibrium of the aircraft, considered at the lowest point of the pull-out, is:

$$L - P - nW = 0 \quad \wedge \quad \begin{cases} nW = n_{design} \cdot g \cdot W = 10065,06N \\ P = n_{design} \cdot L_{tail} = 600,374N \end{cases} \Leftrightarrow L = 10665,434N . \quad (3.12)$$

Further description of these forces characteristics is referred next.

3.5.1 Aerodynamic Loads Characterization

Wing

At the design of an aircraft, one of the most important tasks is to calculate the strength of the wing in bending, to carry out the sizing of the main spar and wing attachments. The wing bending loads are caused by vertical loads, generated by wing lift and wing weight.

Concerning the spanwise lift distribution, and since no CFD software was used, it was chosen to apply the semi-empirical method of Schrenk's approximation. Before ploughing in this method's prepositions, some thoughts must be given to verify the applicability to this project's structure. The Schrenk distribution method provides satisfactory and useful results [39] if applied to a monoplane's cantilever untwisted and unswept wing with a general trapezoidal planform shape, without flap deployment and changes in aerofoil section. The wing geometry satisfies all these requirements.

"As a result of the finite aspect ratio of the wing, the lift distribution varies along the span, from a maximum lift at the root to a minimum lift at the tip" [15]. The Schrenk's approximation assumes that the spanwise lift distribution on a non-elliptical wing is the average of the actual planform shape and the elliptic shape of the same span and area, as shown in Equation 3.13a.

$$\bar{L}(x) = \frac{1}{2}[L^T(x) + L^E(x)] . \quad (3.13a)$$

$$L^E(x) = \frac{4L}{\pi b} \sqrt{1 - \left(\frac{2x}{b}\right)^2} . \quad (3.13b)$$

$$L^T(x) = \frac{2L}{b(1+\lambda)} \left[1 - \frac{2x}{b}(1-\lambda) \right]. \quad (3.13c)$$

where $L^E(x)$, shown in Equation 3.13b, represent the total lift generated by an elliptical half wing. The spanwise coordinate, at $x = 0$ corresponds to the wing root, and $x = b/2$ corresponds to the wing tip. Since the docking zone of each half wing has $200mm$ of width, it will be taken a conservative approach and assume that all the half lift is applied at half wing. $L^T(x)$ represents the total lift for the trapezoidal lift distribution (Equation 3.13c), and for the present rectangular wing ($\lambda = 1$): $L^T(x) = L/b$, which is the correct lift per span [15].

According to Equation 3.13a and inputs from Table 2.2, the approximated spanwise lift distribution is then the local average of the two different distributions:

$$\bar{L}(x) \approx 851,3020 + 1083,9130\sqrt{1 - 0.1019x^2}. \quad (3.14)$$

The lift distribution according to Schrenk's method is presented in Figure 3.9, as well as the lift distribution for an elliptical and a trapezoidal wing. The approximation for the rectangular wing takes into account the real flow effects, meaning a lift reduction towards the wing tip as a consequence of spanwise flow [15]. All the lift distribution methods presented have the same total lift (area under the lift equation) $L = 10665,434N$.

Once the lift distribution is known, it must be found the pressure centre, where the total lift must be placed to get an equivalent representation. The span position of the lift distribution can be found by:

$$\bar{x} = \frac{\int x \cdot f(x)dx}{\int f(x)dx}. \quad (3.15)$$

The denominator represents the graph area (lift), and the numerator must be integrated between zero and the half-span. Applying this analytical formulation to determine the centroid of the Schrenk distribution of equation (3.14):

$$\bar{x} = \frac{\int_0^{b/2} x \cdot \bar{L}(x)dx}{A} \approx 1,447m. \quad (3.16)$$

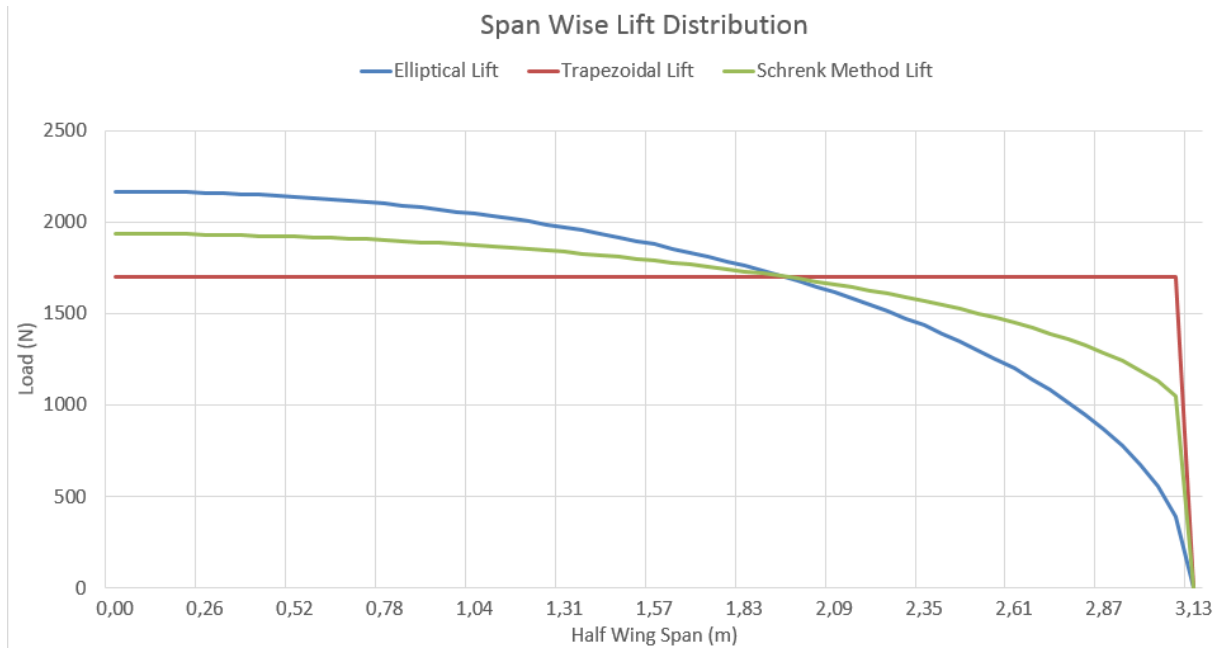


Figure 3.9: Elliptical, Trapezoidal and Schrenk Lift Distribution for Half Wing .

With the total lift and the pressure centre (centroid), it is possible to calculate the bending moment at the wing root:

$$M_{half-wing-root} = \bar{x} \cdot L_{half-wing} \approx 7716,442 N.m . \quad (3.17)$$

This moment will be applied, as suction load, at the imaginary axis of the chord (the line between the leading and trailing edge of the airfoil) at the root. To compare the model used, an assumption of a linear lift distribution on the rectangular wing would increase by 8% the resultant moment at the wing root.

Tail

For longitudinal equilibrium, the horizontal stabilizer should create a downward lift force. The demonstration at 3.12 showed that $L_{tail} \approx -600,374 N$.

The general geometry of the tail is more complex than the wing and consequently, the model for lift distribution will be different. Due to the installation of the propulsion system, the tail zone will be one of the most critical areas as a consequence of the significant large loads and vibrations (engine) applied at the tail joint to the fuselage. Because of the position of the engine and stability surfaces (horizontal and vertical stabilizers), the aircraft tail will be subject to large bending moments, in respect to

the aircraft centre of gravity. Therefore, a conservative approach, when designing this highly dynamic, area should be used.

The tail in *H* shape presents the vertical stabilizer at the wing tip of the horizontal stabilizer, which will decrease the spanwise flow, acting as a winglet. Therefore, assuming a near-elliptical flow would not be a precise approximation, and so it will be considered a linear distribution. This approach will create a higher bending moment at the tail docking zone, leading to a stiffer design.

Concerning the wind gust component, CIAFA (Appendix A) requires UAV operation in wind conditions up to $\approx 13,9m/s$. The NATO airworthiness requirements define that the UAV should be subjected to lateral gust with a positive and negative gusts values of $15,2m/s$ [16]. According Corke[15] approach of designing the aircraft it is recommended a intensity of $20m/s$ for the gust for a manoeuvre of high angle of attack. Since the tail is a critical component of the aircraft, it is a good procedure to apply a conservative approach. Therefore it will be considered a $20m/s$ wind intensity.

It is assumed that the horizontal lateral gust is perpendicular to the vertical stabilizer surface. As a conservative approximation, the vertical stabilizer is considered to be a flat plane. Consequently, wind gust creates a pressure on the respective perpendicular area. In this case, the load force can be calculated by Equation 3.18. This analysis will be made for the maximum design load, and thereby for an altitude of $8000ft$. The vertical area of each stabilizer is $\approx 0,568m^2$.

$$F_{wind-gust} = 1/2\rho v^2 A \approx 54,7N . \quad (3.18)$$

This value will be applied in the same direction in each one of the vertical tails. By default option, it will be applied from the left side to the right. For example, this results in a compressive force on the left vertical tail.

3.5.2 Weight and Inertial Loads Characterization

The weight of a body is obtained through a product of its mass and the Earth's gravity acceleration ($g = 9,81m/s$). For the critical flight manoeuvre of Figure 3.8, the inertial force is a consequence of centrifugal force. At the equilibrium position, the inertial forces and weight have the same direction for its vertical component.

The overall design ($n_{design} = 6,84$) is made for the MTOW of the aircraft of $150kg$. Equation 3.12 refers to a joint term for body forces representing the sum of the aircraft weight and the inertial load applies on the aircraft:

$$\begin{cases} W_{aircraft} = g \cdot m_{aircraft} \\ F_{inertial_{aircraft}} = (n - 1) \cdot g \cdot m_{aircraft} \end{cases} \Leftrightarrow BF_{aircraft} = n_{design} \cdot W_{aircraft} = 10065,06N . \quad (3.19)$$

The aircraft body force is applied at the centre of gravity [25]. But this approximation does not represent the weight or inertial forces distribution on the aircraft. Taking the example of the wing, its structure can be considered as a cantilever beam, which is rigidly supported at the wing root. The resultant force and bending moment take into account the lift and weight distribution, including structural components and equipment.

If the overall weight of the aircraft is considered to be at the centre of gravity (fuselage), an important component of the wing (body force) load will be neglected, resulting in a bending moment different from reality. Therefore the overall weight of the components will be applied separately at each part, such as wing, tail, fuselage, engine, and avionics. Most of them will be considered distributed loads, but they can be treated as a concentrated load in the correspondent centre of gravity.

As explained in Section 3.3 the initial weight estimation and the consequently further iteration present at this point a structural weight estimation for each component. The body forces resulting of weight and inertial loads for each component are presented in Table 3.3.

The wing, tail, main and nose gear, present an estimated weight [14]. To the fuselage component, is added the paint's mass. Other payload refers to the sniffer, AIS and distress sensor. Fixed Equipment joins the mass of autopilot, onboard computation, air data system, GPS antenna, inertial navigation system, data link, SatCom, transponder and environmental control system.

In the following sections, it is presented a detailed description of the body loads applied. They are gathered for zones of application.

Table 3.3: Weight and Inertial Forces of major components.

<i>Component</i>	<i>m[kg]</i>	<i>nW[N]</i>	
<i>Structure:</i>			
Wing	15,016	1006,553	
Tail	2,500	167,58	
Fuselage and others	20,846	1398,775	
Main Gear	12,677	850,565	
Nose Gear	3,086	207,032	
<i>Motion:</i>			
Propulsion System	15,325	1028,314	
Fuel system	38,032	2549,361	
<i>Avionics:</i>			
Radar SAR	11,340	760,143	
Gimble	1,572	105,363	
Other payload	3,000	201,096	
Fixed equipment	8,794	589,451	
<i>Others:</i>			
Wiring	4,513	302,495	
Servos and stroblight (wing)	1,864	124,948	
Servos (tail)	0,550	36,868	
Batteries and Energy box	9,600	643,507	
<i>Total:</i>			
Aircraft	150,000*	10065,06	Distributed

Wing

As explained at the beginning of this chapter, the load analysis of the wing is primary driven by the need to counter the wing thickness bending moment. For this reason, the torsion at the wing root, due to the wing pitching moment [24] will be dismissed. The loads will be considered homogeneously distributed chordwise.

The body loads applied on each wing (separately) will be the half wing's weight, strobe lights and the necessary servo-actuators for the control surfaces. From the CAD model, after defining the composite layup for the critical load (iterative process), it is possible to obtain the mass of a component. Each wing is estimated to weight 6,508kg.

Since the number of plies changes drastically from the wing root to the wing tip, to

resist the increasing bending moment, the wing structure is far from being symmetric in weight. Considering spanwise direction (x axis), the centre of gravity is located at $1369mm$ from the middle point of the fuselage as seen in Figure 3.10. This means that the distance from the wing root is $1169mm$, since the docking zone is $200mm$ wide per side.

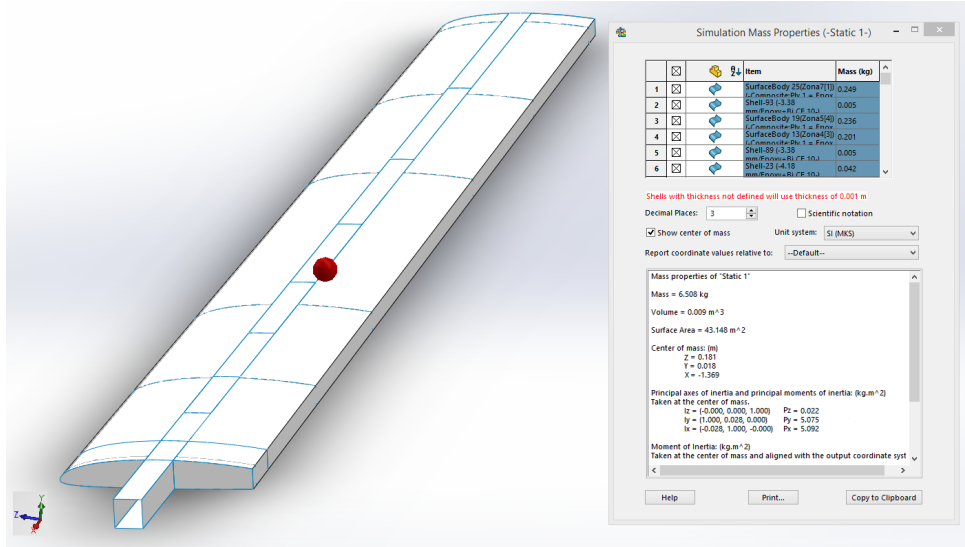


Figure 3.10: Wing centre of gravity.

To the weight of this component, it must be added the estimated weight of the flaps and aileron, since they were neglected for the structural simulation due to the applied conservative approach. For the total of 4 control surfaces (two flaps and two ailerons) for each side, it was estimated $1kg$. According to Table 3.3, the servo-actuators and the strobe lights have a mass of $0,932kg$ for each wing. Joining these two components with the control surfaces it is obtained a mass of $1,932kg$, which shall be considered to be applied at the geometrical centre of the wing (half wing). The global wing body force equilibrium is:

$$W_{half\,wing} \cdot X_{CG} = (W_{controlsurfaces} + W_{servos+strobe\,light}) \cdot b/4 + W_{structure} \cdot X_{CG\,structure} \cdot (3.20)$$

Knowing that: $W_{half\,wing} = 566,327N$, the correspondent centre of mass for all the wing components is: $X_{CG} = 1236,815mm$, referring to the wing root. This represents the point where the body load is applied, creating a moment:

$$M_{half-wing-root} = 700,442N/m$$

Tail

The definition of the body loads for the tail follows the same assumptions as for the wing. This requires to divide the tail in half, to consider the bending moment created by each half of the tail at the fuselage joint, the servo-actuators and the pilot camera. Using the centre of gravity for the entire tail, this moment would be neglected, since the central part is fixed to the fuselage.

From the geometric model, after the necessary iterative process to define the composite layup, it was estimated a weight of $1,250kg$ for each structure of half tail. Considering spanwise direction (x axis), the centre of gravity is located at $520mm$ from the tail's root.

To complete weight estimation, it is necessary to consider the mass of two servo-actuators, one for the elevator and other for the rudder and also the pilot camera. Each servo has a mass of $0,108kg$ of mass and the pilot camera presents an estimated mass of $0,118kg$. The elevator's actuator is considered to be applied at the geometrical centre of the horizontal tail. The actuator for the rudder and the pilot camera are placed at the end of the horizontal wing tip, at the vertical stabilizer. The tail load equilibrium is:

$$W_{half_{tail}} \cdot X_{CG} = (W_{servo} + W_{pilot.cam}) \cdot b/2 + W_{servo} \cdot b/4 + W_{structure} \cdot X_{CG_{structure}} \quad (3.21)$$

Knowing that: $W_{half_{tail}} = 106,287N$, the correspondent centre of mass for the half tail is: $X_{CG} = 546,338mm$, with reference to the tail root. This is the point where the body load should be applied to compute the resultant moment at the fuselage joint.

For consistency, this vertical and negative (direction) force has to be applied as a distributed load along the chord at the specified coordinates (X_{CG}). To simplify the load application, it will be calculated an equivalent load to be applied at the vertical stabilizer (top rib):

$$W_{half_{tail}} \cdot X_{CG} = W_{equi} \cdot b/2 \quad (3.22)$$

Through equation 3.22 the equivalent load to be applied at the right vertical stabilizer to simulate the tail body load is $W_{Rtail} = 75,483N$. For the left stabilizer, without the camera, the equivalent load of $W_{Ltail} = 67,566N$ should be applied.

Fuselage

The aircraft's fuselage, act as an essential structural component, being responsible for the overall geometry and stiffness. For simulating its weight and the inertial forces, it is applied an analytical estimated distributed (negative) load through all surfaces from nose to the end of the fuselage: $W_{fuselage} = 1398,775N$.

Components Loads on First Bulkhead

As shown in the layout description of the aircraft (Figure 3.1), the first bulkhead (at $0,25m$ from the nose) of the UAV, must have the necessary stiffness to support the shear and moments created by the body loads of the nose gear, gimble, batteries and the energy converter box.

From the fig 3.2, the batteries and the energy converter box present a combined mass of $9,6kg$ and will be centred at $0,15m$ from the nose. The gimble will be placed in front of the nose gear to have a clear vision and therefore its centre of gravity is at $z = 0,10m$, presenting a mass of $1,570kg$. Joining these components body forces:

$$W_{energy+gimble} \cdot z_{CG} = W_{gimble} \cdot z_{CGgimble} + W_{energy} \cdot z_{CGenergy} \quad (3.23)$$

Knowing that: $W_{energy+gimble} = 749,511N$, the correspondent centre of mass is: $X_{CG} = 142,949mm$, referring to the nose. This represents the point where the body force load should be applied (downward).

Lastly, the nose gear represents a load of $W_{nose.gear} = 207,032N$ which is directly attached to the first bulkhead, to provide more resistance to impact.

Components Loads on Second Bulkhead

Between the first ($0,25m$) and second bulkhead ($0,50m$), it is intended to have a multi-layer dedicated shelf for avionics systems. This zone shelters the fixed equipment ($W_{fixed} = 589,451N$) at $z_{fixed} = 325mm$ and some other payload ($W_{payload} = 201,096N$) at $x_{payload} = 350mm$, according to Table 3.3 and Figure 3.2.

Joining these components body loads:

$$W_{multi-layer} \cdot z_{CG} = W_{fixed} \cdot z_{CGfixed} + W_{payload} \cdot z_{CGpayload} \quad (3.24)$$

Knowing that the combined weight is $W_{multi-layer} = 790,547N$, the correspondent centre of mass can be calculated, presented a value of $z_{CG} = 331,709mm$. This represents the point where the body force load should be applied (downward).

Lastly, the Radar SAR with a weight of $W_{SAR} = 760,143N$ has its centre of support on the second bulkhead.

Main Gear

The main landing gear is placed at its docking zone in the central bulkhead. This component has an estimated weight of $W_{main-gear} = 850,565N$, which shall be divided in half and applied at each insertion zone for the main gear support.

Propulsion system

The propulsion system presents a mass of $15,325kg$ and accounts for the engine, generator, propeller and the installation supports as well as a no fire protection and dumping shockers if necessary. This conservative factor is important since any weight variation in the rear part of the fuselage has a great impact on the overall stability of the aircraft.

All the weight of this system will be applied as a vertical (negative) distributed force of $W_{prop} = 1028,314N$ at the engine part (designed in the CAD software).

Fuel system

The fuel system includes the fuel and oil tank filled with the necessary quantity to satisfy the mission proposed. For this design, it is required a overall fuel moisture of $46,400litres$, which is possible will the aircraft all loaded up. Knowing that the fuel weights $\approx 0,75kg/l$ its $40litres$ weights $30kg$. The amount of oil required is $6,4litres$, and the used oil weights $\approx 0,88kg/l$ resulting in a total of $5,632kg$.

Since a longer endurance is a key advantage of the system, it is mounted on board a double tank with a total 60 litres of volume, which can be filled in case of absence of some payload. At each CAD model of the tank will be applied a load of $W_{fuel} = 1274,68N$.

The front fuel tank is placed at the bulkhead at $z = 1148,5mm$ and at $104,58mm$ in front of the CG. The rear fuel tank is placed at bulkhead at $z = 1372,11mm$ and at $119,03mm$ back from the CG. The longitudinal static stability study imposed that the fuel tanks should present the same distance to the centre of gravity. In this design solution there is a $14,5mm$ difference that should be corrected when attaching the fuel tanks to the structure. One of the possible solutions is to place a backstop with the necessary thickness ($14,5mm$) between the front fuel tank and the bulkhead where it is attached.

3.6 General Considerations

At this stage of the project, the aircraft already presents a general layout. Before the detailed design it is necessary some general ending considerations to assess the viability of the design, and mention some approximations of the project.

The new configuration of this UAV presents several differences when comparing to the previous CIAFA aircraft. In respect to the conceptual design of stability study, this geometry is a valid option for flight operations since it has a valid margin of safety for longitudinal static stability.

Due to logistics requirements, it is necessary to have removable parts. The highest dimension of a single component is $\approx 3,20m$ which means a little bigger than half-span, allowing a single division of the wing in two.

From a manufacturer perspective, all the ideas and design parts represent a possible option of construction and the operational and maintenance applications of the aircraft are within the limits of the 'know-how' of the design team, achieved with the previous UAV of CIAFA.

The aim of the project is the complete design of the aircraft structure and definition of its main components, such as avionics, payload and propulsion system. The wide range of areas comprehended in the project leads to some uncovered areas of the design and also some necessary approximations, which are described next.

One of the dismissed areas is the internal routing of electrical connections (wiring) for every electronic equipment. Also, the fixations of the servo-actuators responsible for the deflection of control surfaces will not be considered for the structural design. Never-

theless, the weight of electrical cables and the servo-actuators were accounted for the weight estimation and distribution, and therefore for the determination of the structural loads. Some avionics systems such as the GPS antenna and others real-time data transmission systems may jam each other. The electromagnetic interferences were not considered while placing the avionics. The radio interference of graphite/carbon fibre [29] were also dismissed.

Another neglected subject is the inclusion of holes on the structure either for bolting purposes or to allow routing of cables. For example, some bulkheads and ribs will mandatory present some kind of circular holes on its geometry. Recently (2017) a project developed in coordination with CIAFA studied the effect of holes and the consequent delamination [32]. This study presented some reinforcement solutions, that could be used. There are several other methods to prevent cutouts impacts such as bonded repair or restrain lateral deformation [31].

The pusher engine placed at the ending bulkhead of the aircraft will, due to its nature, generate vibration depending on its rotation modes. The effects of these vibrations to the tail and the transmission through the longerons will not be studied on this thesis, where only a structural static study will be applied at the designed aircraft.

Chapter 4

Detailed Structural Design

4.1 CAD modelling

In this chapter, it is described the shaping and sizing of each component of the UAV. The aircraft CAD model concerning the wing, tail and fuselage must be built to consequently perform a stress study through FEA. The software version was previously defined as well as the axis of reference (section 3.2).

4.1.1 Wing

Spar

An essential step to this practical project aimed to be built and operated by the Portuguese Air Force is to consider the experience achieved from years of operating, manufacturing and maintaining RPA. The previous aircraft of the CIAFA fleet had a removable spar, which was the attachment element between the wing and the fuselage. Firstly, the manufacture of such a short margin gap between surfaces requires a very high precision, difficult to achieve. Secondly, due to transportation constraints, the recurrent process of mounting the wing leads to a loosen fixation and consequently an unwanted divergent relative movement between the wings and the fuselage. One of the solutions is to design a non-removable spar for the wing.

To start, it is necessary to know the relative spar localization on the wing. To the spar first geometry, it is recommended a 10% cross area of the complete wing airfoil [29]. Also, it would be positive to increase spar dimensions since the stress is inversely

proportional to the second moment of inertia [25]. A growth in dimensions of the spar will mean more material far away from its centroid and so a bigger second moment of inertia to the section. This step would decrease the stresses along the spar (see Equation 4.1). To achieve this maximized moment of inertia, the design solution is to place the main spar where the airfoil thickness is highest. For the chosen profile, SG-6042, the maximum thickness is found at 34,25% of the chord, which will be the centre of the spar.

$$\sigma = \frac{M \cdot y}{I} [Pa]. \quad (4.1)$$

In respect to the spar's geometry, since the height (web) of the spar is restricted by the airfoil dimensions, the only variables will be the width (cap) and the thickness of each component. Before it can be performed a finite element analysis, it must be defined the spar's width in order to create the finite element model. Based on a practical approach [29] it is assumed the width of the spar of $40mm$ in order to obtain for the cross area of the spar the recommended 10% of the airfoil area ($18835, 10mm^2$). This initial geometry showed that even with a high number of plies of composite material it was very difficult to do not exceed the ultimate tensile strength of the material. The outcome of having almost 100 plies of carbon fibre and small dimensions in a complex geometry would make this spar almost impossible to build. Since the spar is perfectly joint to the skin, every added layer of composite material will be placed in the inside, therefore each layer will have a lower impact in the spar second moment of area and, consequently, a lower impact in stress reduction. Simplifying the manufacturing process is also a goal of this project, and it is a better choice to increase spar's width in spite of increasing the layers of the laminate.

Knowing that the spar caps will have the airfoil shape, it is important to have an almost steady rectangular shape. Studying the area of the airfoil around its maximum thickness there is an approximate horizontal set of coordinates from 30% to 40% of the cord, where the thickness only changes up to 0,04% of the chord. Estimating a spar width of approximately 9,5% of the chord, centred at airfoil maximum thickness (34,25%) would mean a spar from 29,75% to 39,25% of the chord with 49,57mm of width, as shown in figure 4.1. The presented spar has a cross area of $2580,87mm^2$, corresponding to 13,7% of the airfoil cross area.

Moreover, for the present configuration, through aerodynamic design [14], knowing that the wing leading edge starts at $\approx z = 1,150m$, it is calculated that the wing centre of pressure is placed at $\approx z = 1,348m$ (Table 2.2). This value corresponds to a neutral point placed at $\approx 37,94\%$ of the chord. Since this value is at the width range of the designed spar, the previously stated dismiss of the resultant pitching moment (torsion) is maintained.

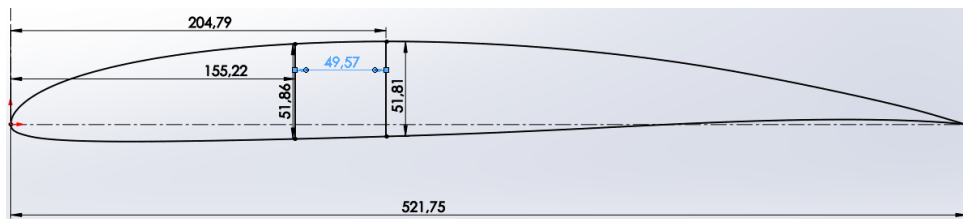


Figure 4.1: Wing Airfoil: Spar Dimensions.

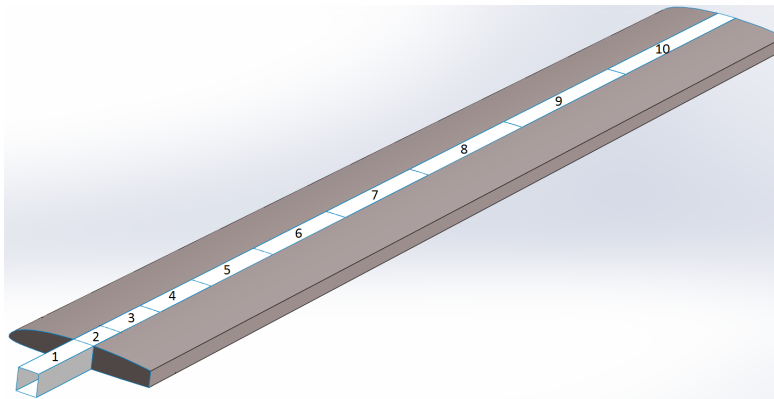
The used approach of a Frame structure implies a thin skin design where the majority of the loads are carried by the spar. According to the lift distribution (equation 3.14), the shear force near the wing tip is almost neglectable relatively to the wing root. Therefore a constant thickness spar would create an oversize and overweight structure [29].

Since the work done on the CAD model is the basis to the finite element analysis, some options must be taken. The spar has to be divided (spanwise) into small sections to be able to set different laminates along the spar. Considering only half span, the docking zone (Zone 1 of Figure 4.2) of the spar is set from the longitudinal axis ($x = 0$) until the start of the wing ($x = 200mm$). The main wing spar will be divided into nine zones, with an increasing length alongside the span (Table 4.1). This division is not homogeneous since at the wing root the stresses are higher and a greater number of sections allows a more smooth transition of material thickness. This sectioning is made for the spar caps and webs and is shown in figure 4.2. This discretization of the spar results in forty different surfaces with decremental thickness.

Ribs and Control Surfaces

Besides maintaining the shape of the wing cross section, the ribs are also important to sustain the control surfaces insertions, and this is the driven parameter to rule their positions. Overall, there are eight ribs per half-wing placed at the equivalent plane num-

Table 4.1: Spar Discretization.



Spar Zone Divisions [mm]	
Zone 1	0 to 200
Zone 2	200 to 300
Zone 3	300 to 450
Zone 4	450 to 650
Zone 5	650 to 900
Zone 6	900 to 1206
Zone 7	1206 to 1575
Zone 8	1575 to 2015
Zone 9	2015 to 2535
Zone 10	2535 to 3130,5

Figure 4.2: Spar Zones Discretization.

ber (see Figure 4.3). The control surfaces at the wing are the flaps and the ailerons, responsible for an increase in lift and drag in take-off and landing operations, and for manoeuvrability in the roll axis of the aircraft, respectively.

The trailing edge pain flap was initially estimated to be , through to the aerodynamic conceptual analysis, $1690,461mm$ long ($S_f/S_w \approx 54\%$) per half-wing, with $156,525mm$ of chord ($c_f/c_w \approx 30\%$). These inputs combined with the requirement of redundant control surfaces, result in two flaps per side with $845,230mm$. For the ailerons, the analytical results present a span of $1126,974mm$ ($S_a/S_w \approx 36\%$) per half wing and the same chordwise length of the flaps. Each wing has have 2 ailerons of $563,487mm$. This values will be the starting point for the ribs location.

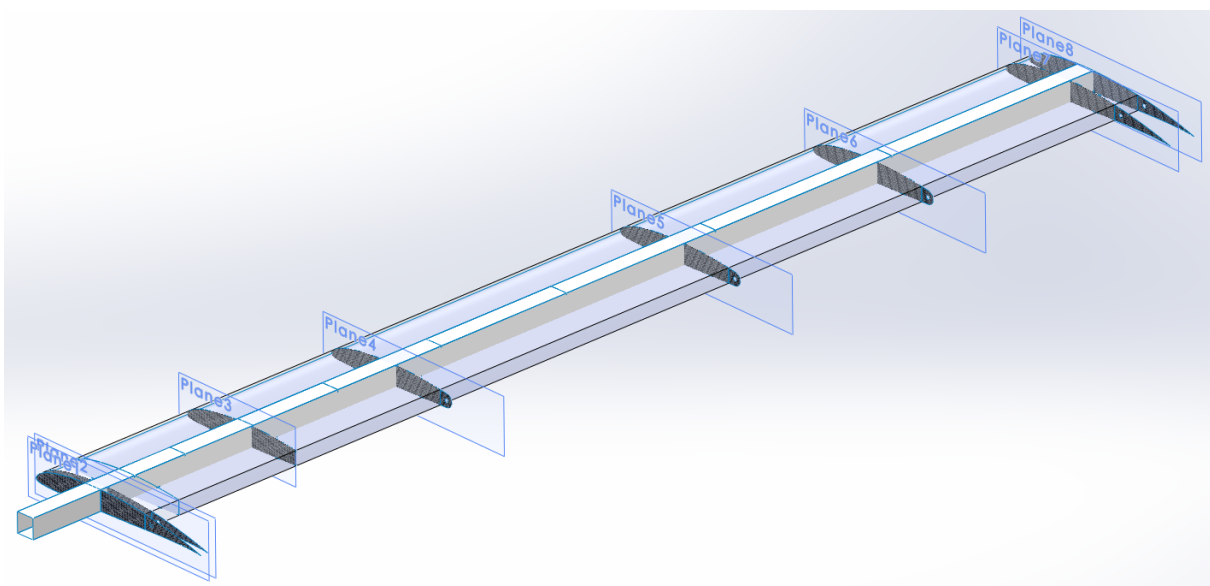


Figure 4.3: Ribs Planes along Wing Span.

For the figure 4.3, the rib 1 is at the plane 1, and the rib 2 is at the plane 2, and the same for all the remaining ribs. The wing root starts at rib 1 ($x = 0$) and has a full chordwise surface until rib 2 ($x = 20mm$). According to the previous information, the first flap is placed between the rib 2 ($x = 20mm$) and 4 ($x = 871,230mm$). Since the shear stresses and this area are higher, due to the bending moment, this first flap has a reinforced mid-span rib place at plane 3 ($x = 445,615mm$). This rib's localization is also the better option for a future need of payload placement at the wing.

The second flap is placed between the rib 4 and 5 ($x = 1722,460mm$). Using the same approach, ailerons are between the rib 5 and 6 ($x = 2291,947mm$), and the rib 6 and 7 ($x = 2861,434mm$). From rib 7 to 8 ($x = 2930,5$) the wing presents a full surface from the leading edge to the trailing edge.

Ribs 1,2,7 and 8 have the full airfoil geometry. Ribs 4,5 and 6 have a trailing edge cut off, replaced with a small surface for the shaft bearing. Rib 3 has only the geometry of the wing to be tested structurally, neglecting control surfaces. Every surface that present relative movement to the wing (rotation of control surfaces) will have $3mm$ gap. For example, between the end of the second flap and the rib 5, and from the rib 5 to the start of the first aileron, there will be a gap for both cases.

Concerning the control surfaces, each one will present three ribs, one for each tip and other for the mid-span where the servo actuator will be connected to.

4.1.2 Tail

The tail of the aircraft will be manufactured as a whole piece and designed to be attachable due to transportation constraints. The requirements allow the tail to be permanently linked to the fuselage, but it is not possible since the maximum width for transport equals the ANTEX-M tail width. The present project presents a wider tail ($1884,42mm$) with approximately more $395mm$ than the already in use UAV.

As shown in section 3.5.1, the aerodynamic loads on the tail are much lower than the ones on the wing (94,4% lower). Therefore, the preponderance of a design made for resisting bending moments decreases. Since the tail, the engine and the generator are mostly supported by only one bulkhead, the complexity of this segment increases, and the design driver will be the geometry, associated with good structural components joints. Before starting the tail design some conditions must be made.

From Table 2.2, the horizontal tail has the NACA 0009 airfoil with a chord of $384,64\text{mm}$ and a maximum thickness of 9% . The aircraft fuselage, as result of the aerodynamic conceptual design, presents a length of $3006,200\text{mm}$. Due to the importance to have the tail far apart from the wing as possible, the horizontal tail should start at $z = 2621,36\text{mm}$ (longitudinal coordinate). The AR741 engine is approximately 350mm long, meaning that the further back possible position of the engine support (last bulkhead of the aircraft) is at 2717mm from the nose tip. Analysing the relative positions, this aircraft rear bulkhead is placed at $24,86\%$ of the chord of the horizontal tail. In this case, both geometries are fixed since this last bulkhead and the tail shall not change its positions.

Also, "For symmetric airfoils in subsonic flight the aerodynamic centre is located approximately at 25% of the chord from the leading edge of the airfoil. Thus the aerodynamic centre does not change with variation in angle of attack" [34]. The present value can be accepted as a good chordwise position for the main spar of the tail and the correspondent fixation to the aircraft since it is approximately at the aerodynamic centre and is also close to the profile maximum thickness at 28% .

From a lateral view, sketched in Figure 4.4, the bulkhead position will be at $95,80\text{mm}$ from the leading edge of the horizontal stabilizer. To decrease torsional moments applied to the bulkhead, the fixation should be centred at this point. First, the spar caps of the horizontal stabilizer will be 80mm long, 40mm for each side. At the centre of each half-spar, at 20mm in front and back from the aerodynamic centre, it is considered to be a screw. The connection between the tail and the bulkhead is made through two 'L' shaped supports placed in each half under spar cap.

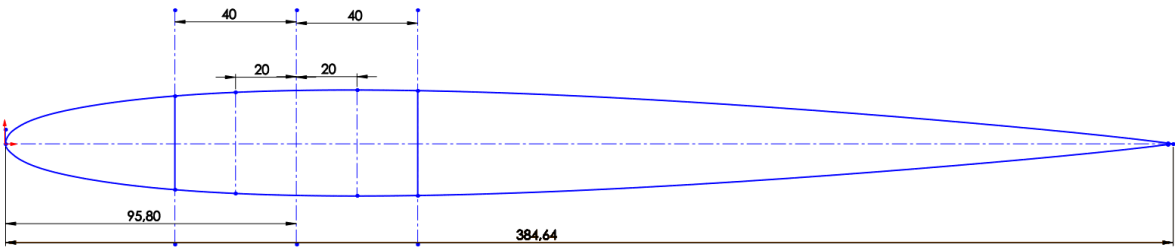


Figure 4.4: Tail Airfoil Sizing.

From top view (Figure 4.5, there are several sections of the geometry to describe:

First, there is a central part made for the attachment with the fuselage. This zone presents a back cut out of the airfoil and the correspondent surface, to allow the engine placement, and the air intake. Considering only half tail, this central zone starts at the

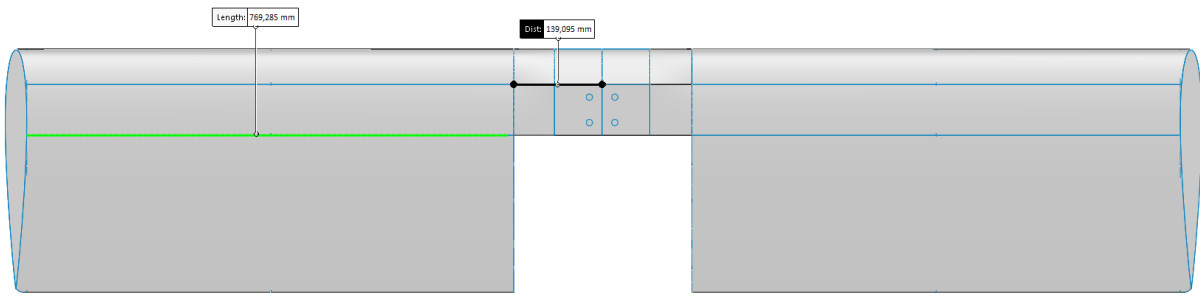


Figure 4.5: Tail Top View.

longitudinal axis ($x = 0$) and it is divided into 2 further sections until the start of the horizontal tail root at $x = 139,095mm$. The first sector goes up to $x = 75mm$ and, the lower cap is straight to allow a clear fixation to its support. Figure 4.5 shows the multiple screw attachment. The chordwise details were previously presented. From a spanwise context, the holes are estimated to be at $20mm$ from the longitudinal axis of the aircraft. The second mid-sector is a lofted design surface with a complicated shape, as a result of its boundaries. The inner part presents a horizontal segment, while the outer part (horizontal tail root) present the designed airfoil. This curved connection surface allow a perfect joint of these two different shaped geometries.

Concerning the internal structure of this central part, the spar cap is complemented with the spar web until the tail root at $x = 139,095mm$. Additionally, accounting for the compressive load of screw attachment there are ribs at the end of the first section ($x = 75mm$) and at the tail root.

At this docking zone, without full airfoil and with its surfaces in an inner position of the fuselage, it will be neglected the creation of lift. Therefore the surface area of the horizontal stabilizer is assumed to start at $x = 139,095mm$ with a $769,285mm$ of span per side. The spar caps are designed with a constant thickness because of the assumed rectangular lift distribution and the loads applied by the vertical stabilizer. There is no application of spar webs on the tail, in behalf of the relatively low loads applied. The shape and integrity of the horizontal tail are sustained with three ribs presented at the tail root, tip, and at mid-span, acting also as a support for the elevator's shaft and consequently to its servo-actuators.

About the vertical tail, it has the NACA 0009 airfoil with a chord of $376,87mm$ and a maximum thickness of 9% . In respect to the 'H' configuration tail, each vertical stabilizer will have a span of $753,740mm$, linked to the horizontal tip at its halfway point.

As presented in Table 2.2, this results obtained by the aerodynamic conceptual design, estimated different chords to the vertical and the horizontal stabilizer. First, since the vertical tail has a lower chord, both stabilizers will be aligned and fixed at the aerodynamic centre. This design assumption assumes that the same reinforced area of each spar cap is perfectly connected, in the interest of an easier manufacture and a smoother stress distribution through these surfaces.

In respect to relative placement position, the vertical tail will be tangent to the tip of the horizontal stabilizer. Physically it means that the airfoil surface of the vertical tip only touches the horizontal tip rib at one point, at the maximum thickness. Thus, the vertical chord will be placed at $\approx 17,27mm$ (half of the maximum thickness) from the horizontal tip. Concerning the internal structure, the vertical tail has three ribs (equally spaced) without spar webs. The spar caps are equally divided into three surfaces, to be able of defining a decreasing spar thickness along the span.

4.1.3 Fuselage

The fuselage will provide structural integrity for the wing and tail coupling and will shed all the payload and fixed components during flight.

One of the first steps when designing the fuselage of an aircraft is to choose its general exterior shape. For example, it can be obtained by the fineness ratio, a geometrical parameter. It represents the ratio between the equivalent diameter of the cross area and the length of the aircraft [15]. From Table 2.2 the design ratio is $d/l \approx 0,1397$ meaning an equivalent diameter of $420mm$ and a overall length of $3006,20mm$. This length ruled the UAV development. However, an equivalent diameter is difficult to set. A fuselage presents a wide range of variation of its cross area along its length, since zero at the nose, a maximum value in the middle section, and a certain value at the rear end. During design, this variations must be taken into account while trying to match the equivalent diameter. After the design, an analytical calculation must be made to confirm the theoretical value or study the impact of the results obtained on the Lift/Drag ratio if it was obtained a different equivalent diameter for the fuselage.

Before starting the fuselage development along its longitudinal axis, it is needed to find the standard cross area shape for the bulkheads and the fuselage skin. Respecting the airframe requirements for construction, the fuselage should be made of flat shapes

or with a low depth shape to allow 'in-house' manufacture. From a structural point of view, for future finite 2D element analysis, sharp corners are a problematic issue that should be avoided.

Firstly, it is assumed an exterior square with 450mm per side and an internal square with 370mm per side. The designed bulkhead will have the minor square vertexes, in which each edge will be replaced by an ellipse that is tangent to the exterior square at the midpoint of each edge as seen in Figure 4.6. To present a smoother transition, each inner corner presents a rounded fillet with a 80mm radius, resulting in an interior edge reduction to 360mm . To manufacture the skin at this cross area shape, it is needed a single mould (Figure 4.7) with 45mm of dept and $\approx 360\text{mm}$ of width. Four identical parts joint together result in a 360 geometry for a specific area of the aircraft.

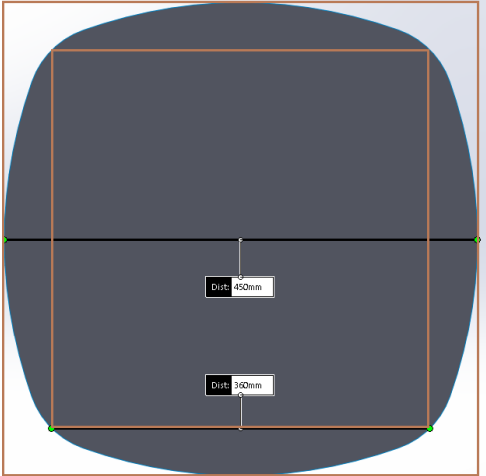


Figure 4.6: Standard Bulkhead.

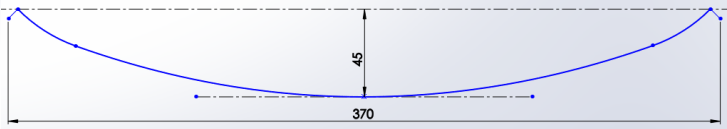


Figure 4.7: Mold Shape.

Concerning the components of the fuselage (Figure 3.1) they can be divided into 3 sections, as shown in Figure 4.8. The main part is the central one, with the same longitudinal length as the wing chord (from $z = 1148,50\text{mm}$ to $z = 1673,25\text{mm}$), which will accommodate the wing, the main landing gear, and the other two fuselage sections: the nose supporting the avionics and the payload, and the rear attachment to the tail and the propulsion system.

From this point of the dissertation, to present a clear identification, the designed bulkheads will be enumerated from back to the nose, from 1 to 8. This means that the rear part of the aircraft will have the bulkhead 1 and 2. The central part will have the bulkhead 3 where the rear part will be attached. Then it has the double main bulkhead (4 and 5) where the wing and the landing gear will be fixed. Lastly, the

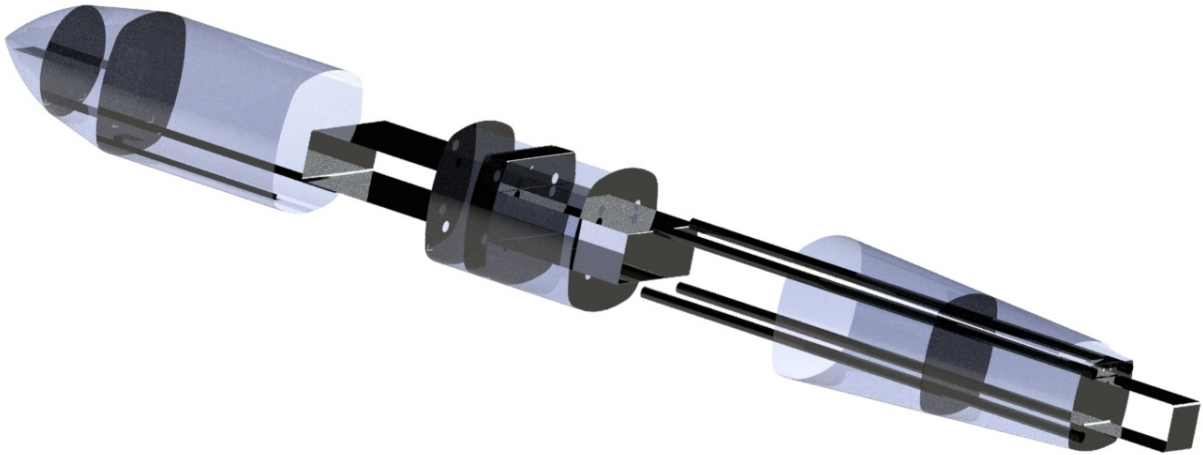


Figure 4.8: Fuselage Exploded View - 3 Sections.

bulkhead 6 will allow the connection of the front part (nose) to this central section. The nose part presents at its structure the bulkhead 7 and 8. A detailed description of each of these 3 major sections is presented next.

Rear Fuselage

This rear section of the aircraft starts in the first bulkhead at $z = 2717,00mm$ and goes up to the trailing edge of the wing at $z = 1673,25mm$. The location for the bulkhead 1 has been chosen knowing the length of the engine and the respective length of the aircraft. The process for designing this structural bulkhead was based on the dimensions of the engine. The goal was to present at this location, a cross area of the fuselage approximately the same as the engine, to decrease the induced drag created by this non-fuselage component.

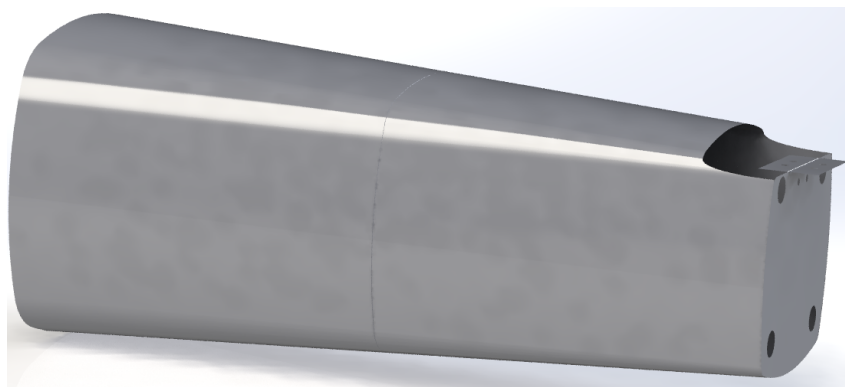


Figure 4.9: Rear Part of the Fuselage.

To build the bulkhead 1, it was used the same approach of the standard bulkhead

of Figure 4.6, but this time using the dimensions for the outer square of 310mm and for the inner one of 270mm . The round fillet of the corners has 20mm of radius. Furthermore, as seen in Figure 4.9, due to the tail fixation, this bulkhead will not have all the cross area in this section. It was made a cut in the top of the bulkhead with the vertical dimension of the maximum thickness of the horizontal stabilizer ($34,62\text{mm}$). This action would create a sharp corner, which was avoided by applying a rounded fillet of 15mm . This cut out and the 2 'L' supports allow the tail attachment and a smoother flow transition. These supports will be centred at mid-section and will have a $40 \times 40\text{mm}$ cross-section with a 75mm width. Each screw hole is at $x = 20\text{mm}$ from the longitudinal axis, and they will be at 20mm also from the top edge of the bulkhead 1 (Figure 4.10).

Lastly, the bulkhead 1 presents 4 holes with a radius of 35mm for the cylindrical longerons. Each hole is at 100mm from the x and y axis origin at the midpoint of the cross area. These dimensions for the longerons will be the same for every bulkhead of the aircraft. Since the skin cross area changes considerably, in spite of a skin reinforced with longerons, it was used an approach where the longerons will remain horizontal and aligned with the longitudinal axis to simplify the manufacturing process. This option also takes into account the Frame structure approach described in the conceptual design. A skin without stringers or longerons can easily be removed and replaced by an access panel or other possibilities. Thus, a more versatile structure is designed. This values for the relative position of the longerons were achieved by assuming an approximate margin of 20mm from the outer radius of the hole cut to the bulkhead edges, at the smaller bulkhead (1). This approach aimed for a wider longerons placement, resulting in a higher moment of inertia, and a stiffer structure, helpful to resist the tail loads.

The skin on this section is a perfect lofted homogeneous surface between the edges of bulkhead 1 at $z = 2717,00\text{mm}$ (without the $34,62\text{mm}$ upper cut) and bulkhead 3 (standard bulkhead) at $z = 1673,25\text{mm}$. The skin at the top rear end will present the airfoil cut to allow the tail insertion.

Since these bulkheads are $1043,75\text{mm}$ apart from each other there is a high bending moment. Bulkhead 2 is set at the approximate mid-position ($z = 2195\text{mm}$) between bulkhead 1 and 3, and offer extra stiffness for the structure, helping to maintain the skin shape. The geometry of bulkhead 2 is restrained by the skin shape at this coordinate,

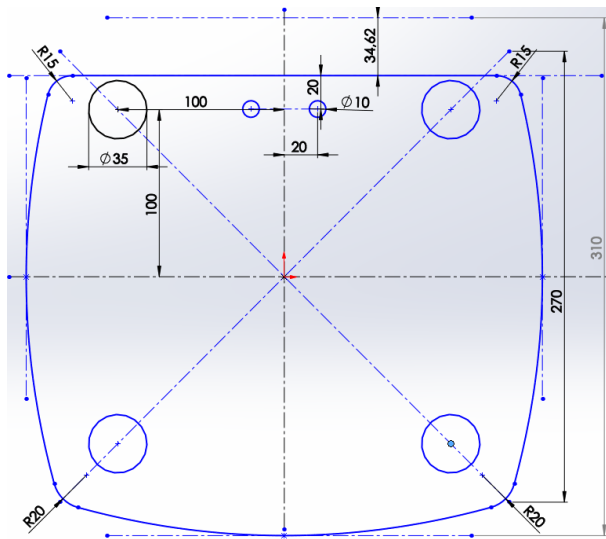


Figure 4.10: Bulkhead 1.

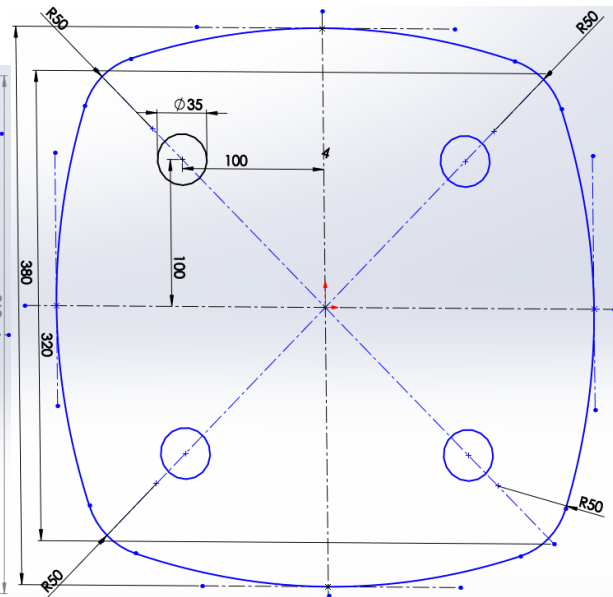


Figure 4.11: Bulkhead 2.

and its values are presented in Figure 4.11. As previously established, the longerons docking zone are at 100mm from the x and y axis at the midpoint of the cross area.

Central Fuselage

The design of the central section of the fuselage is constrained by the wing geometry. The skin will present the standard shape, with a cut with the height of approximately the wing maximum thickness (50mm) and the length of the wing chord $c = 521,75\text{mm}$, to allow the wing attachment. It means that the upper surface of the wing in the docking zone will be almost aligned with the skin before the leading edge, to create a smoother flow transition.

As shown in Figure 4.12, the docking zone is placed between the bulkhead 3 at $z = 1673,25\text{mm}$ and the bulkhead 6 at $z = 1148,5\text{mm}$, both presenting the full cross area section of the standard bulkhead previous described (Figure 4.6). Additionally, the bulkhead 3 will present a cut off in its section as a result of the fuel tank placement, with a cross area of $400 \times 160\text{mm}$.

One of the main structural parts of this aircraft is the double central bulkhead. Bulkhead 4 is placed at $z = 1372,11\text{mm}$, 82mm away from bulkhead 5 at $z = 1290,11\text{mm}$. Both of them present the same geometric shape, and they accommodate the attachment supports for the wing and the landing gear. Its detailed shape is presented in Figure 4.13. It can be seen the top 50mm cut over a lateral length of 400mm to allow

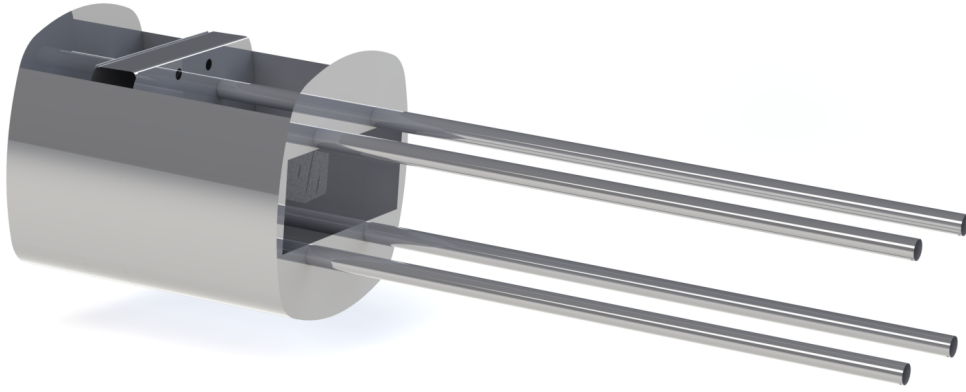


Figure 4.12: Central Part of the Fuselage.

the attachment of the wing surface. The wing support is between both bulkheads and its screw holes are shown in Figure 4.13. The wing support will thereby present the same relative height of these bulkheads as seen in Figure 4.12. This upper face of the support, to match perfectly with the wing, was designed with the airfoil geometric shape at the corresponding chord position.

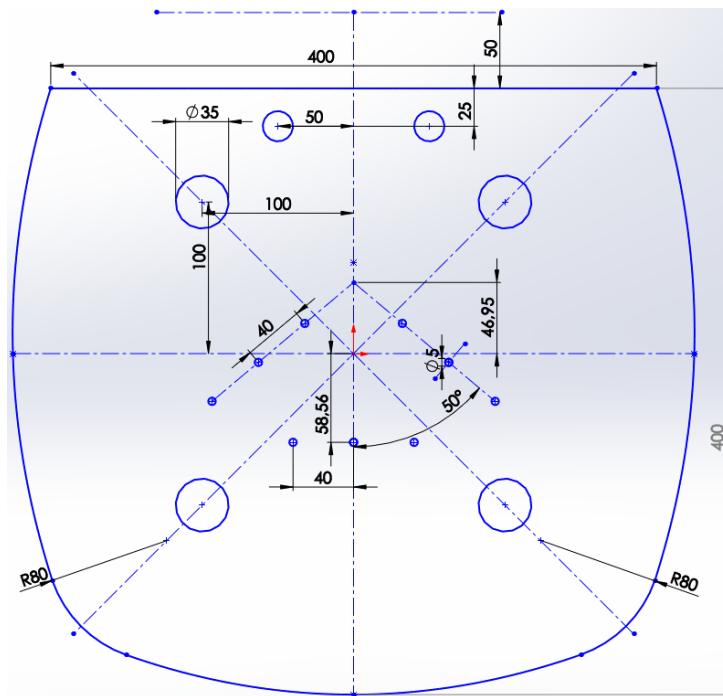


Figure 4.13: Bulkhead 4/5.

Concerning the landing gear design for the present UAV, in 2016 CIAFA conducted a study for sizing, shaping, manufacturing and experimental testing of a new landing gear [40]. The objective of this project was to increase the ground clearance to allow the installation of a radar (under fuselage) and to upgrade the overall quality. Therefore,

since the premises are the same to the present project and the experimental data retrieved for CIAFA fulfil the desired need, it is used the same type of landing gear. For a visual representation, on bulkhead 4/5 of Figure 4.13 it can be seen the triangular shaped supports, each one presenting three screws, and the two top edges are 50° from the vertical axis of the aircraft.

Lastly on this section, bulkhead 3, 4, 5 and 6 present the four longerons docking zone with a diameter of $35mm$ at $100mm$ from the x and y axis at the midpoint of the cross area.

Front Fuselage

As sketched in Figure 4.8 the frontal section of the fuselage will be attached to the bulkhead 6 at $z = 1148,5mm$. From this point until bulkhead 7 at $z = 500mm$, the skin presents the standard shape of Figure 4.6. A support between these two elements is set to provide structural stiffness and to accommodate the frontal fuel tank. The demanding longitudinal static margin requires that the heavy ($\approx 11kg$) under-fuselage Radar, must have all of its weight applied at the bulkhead 7. It can be seen at Figure 4.14, in which is also represented a sketch of the possible configuration of the nose gear and Radar. Through Figure 4.14 and 4.15 it is possible to see a close up of the solution of a double fixation supports to provide a more stable support than a single point connection to the Radar. This support presents a cross area (lateral view) of $40 * 30mm$ and a length of $60mm$. Between bulkhead 7 and bulkhead 8 ($z = 250mm$) there is a double fixed support for the avionics systems bay. Both these platforms present a cross area (lateral view) of $250 * 30mm$ and a length of $120mm$.

The design of the frontal bulkhead (8) shape was achieved through a maximization of the longitudinal cross area at $250mm$ from the nose tip. Since there are no inputs for the nose shape, some empirical data must be used. At this coordinates, there is the goal to go from a single point at the nose tip to the standard skin shape at $z = 500mm$. These lofted surfaces should allow all the systems placement inside, and also present a smooth shape that reduces as much as possible the drag. The drag analysis is not a goal of the present work, and therefore it was assumed a certain balanced geometry to the project.

It was assumed a complete circular shape for the bulkhead 8 with a diameter of

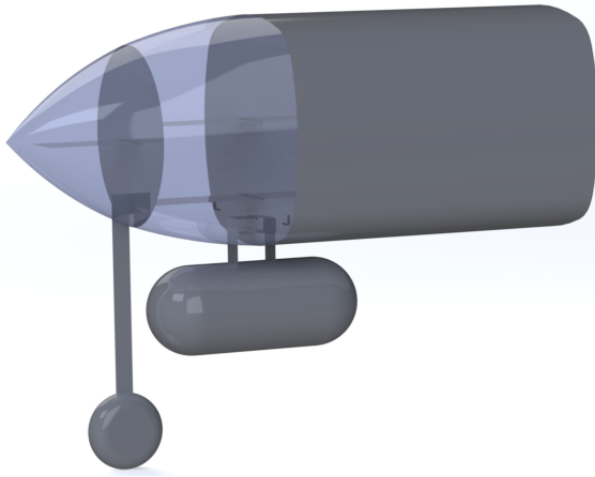


Figure 4.14: Front Part of the Fuselage

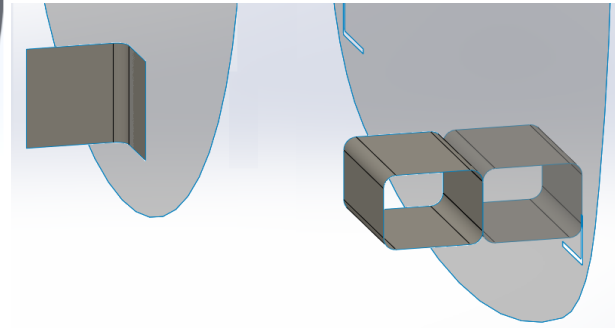


Figure 4.15: Nose Supports.

350mm, to create a smoother transition from the nose single point to the quadrangular geometry of bulkhead 7. The skin from the bulkhead 8 to the 7 follows some design details. First, from a lateral view, the slope gradient smoothly decreases until matching zero at the intersection with bulkhead 7. This gradient is not constant since the geometry changes from a circular cross area to a quadrangular section. The bulkhead 8 presents a nose landing gear support with an 'L' shape as shown in Figure 4.15 with a vertical cross section of 40 * 30mm and 40mm of length.

Overall

As described before, the design ratio should result in an equivalent diameter of 420mm and an overall length of 3006,20mm . This length ruled the UAV development, but along the fuselage, the diameter presents a wide range of variations. At this point having the general shape, it is needed to confirm the real equivalent diameter of the platform. The CAD software performs an area calculation on each of the bulkheads cross areas. Having these values and the length of each section it is possible to determine the equivalent diameter per each segment and consequently calculate the final result of the aircraft:

$$A_o = \pi r^2 \quad \Leftrightarrow \quad d_{equivalent} = 2 \left(\frac{A_{cross.area}}{\pi} \right)^{1/2} . \quad (4.2)$$

The results of Equation 4.2 are presented at Table 4.2 for each segment of the aircraft.

The equivalent diameter for each segment is multiplied by its relative length per-

Table 4.2: Equivalent Diameter for each segment of the aircraft.

$Length[mm]$	0 – 500	500 – 1673,25	1673,25 – 2717	2717 – 3006,20
$d_{equivalent}[mm]$	350	473,06	403,20	333,26

centage, resulting in an equivalent diameter of $\approx 414,9mm$ (detailed design) for the aircraft.

The difference from the original value of $420mm$ (conceptual design) will have an impact on the Lift/Drag ratio since it presents a different fineness ratio. Using the conceptual design estimations for the drag and lift theoretical analysis, it is possible to compare the results obtained for this two different equivalent diameters. Figure 4.16 show the curve variation of the Lift/Drag ratio in function of the fineness ratio maintaining these diameters constants [14].

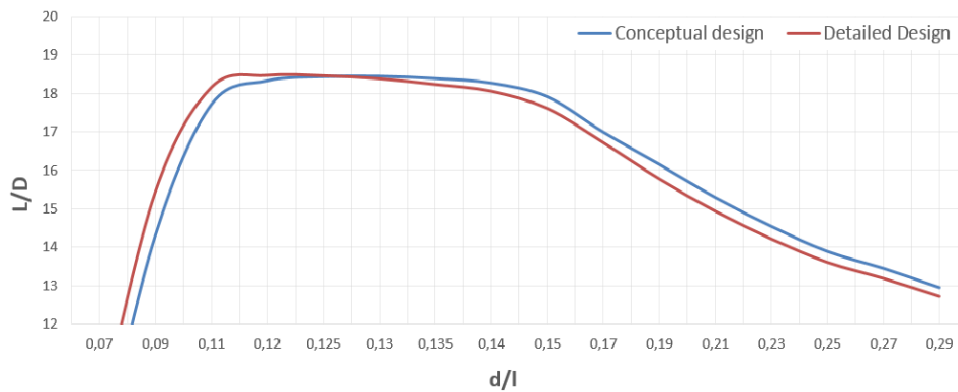


Figure 4.16: Lift/Drag ratio for the conceptual and the detailed design.

As shown, both designs present similar curves, and the specific values for each configuration are $L/D \approx 18,095$ for the conceptual design and $L/D \approx 18,134$ for the detailed design obtained by the CAD software. Since the inputs used to the analytical calculations were based on the conceptual design, the results obtained can be used only as a comparison between configurations, in spite of an absolute value.

4.2 Finite Element Analysis

Until this point of the project, it was discussed all the main areas needed to design an aircraft. To verify the UAV design it is needed to perform a stress study, where the proposed design must handle the design load without failure. Therefore, following

the CAD modelling, the same software will be used to perform an FEA, which all the conditions of this analysis must be stated.

4.2.1 Simulations Materials

Before running a finite element analysis it is necessary to assign the material to each surface of the structure. Since one of the requirements of this project is to use only materials that are available at CIAFA, it must be defined new custom materials in the FEA software. As stated in Appendix B it was created a Unidirectional and Bidirectional Carbon Fibre (orthotropic material) and an Airex (isotropic material) foam core [32].

The material is simulated as an orthotropic material, which properties are calculated from the laminate data. It is possible to input laminates with up to 50 plies of different materials and orientation angles. This allows the definition of monolithic or sandwich laminates.

As previously described, the iterative process requires a full definition of all the conditions of the aircraft to obtain results. These values will, therefore, drive the necessary changes to be made to the geometry, material thickness, until the desired range of stress values is achieved. To this specific design of Section 4.1 it was made an initial guess of composite thickness per surface which was insufficient and the static study revealed several areas where the stress was larger than the design stress of 450MPa . A dual analysis should be made for every simulation, also evaluating the overall displacement that for the wing should be near 5% of wingspan.

As shown in Figure 2.5, the finite element process presents an iterative behaviour with multidisciplinary areas. For the case of a small discrepancy between the maximum stress and the desired value, it is not necessary to redefine the geometry, while a new ply sequence should be enough [29]. Therefore, it is necessary to review the composite laminate definition of the different structural components until a feasible result is obtained. In the following sections are presented the final results for the wing, tail and fuselage structures.

Wing

One of the objectives of the present work is to minimize the structural weight. Therefore the materials properties must be used correctly for the design. This means that in zones whereas the stress distribution is aligned in the main direction, the unidirectional carbon fibre should be used. It offers more than the double of the ultimate tensile and compressive strength comparing to the bidirectional fibre, as well as almost the double of the elastic modulus (Appendix B).

For a rectangular wing, the spar presents the highest stresses aligned with the spanwise direction [3]. Thus, the overall bending moment will be resisted by the spar caps that shall have in their constitution the unidirectional carbon fibre with a ply angle of zero degrees collinear with the x axis of the aircraft. According to the Figure 4.2 the plies used for each surface are described in Table 4.3. Since the software does not allow more than 50 plies per laminate, when necessary, the unidirectional ply thickness is adapted to represent the total amount of material desired. For example, for section 1, the 58 unidirectional plies were represented by 48 plies of $0.2683mm$ of thickness. The bidirectional fibre presents a thickness of $\approx 0,19mm$, while the unidirectional fibre presents a thickness of $\approx 0,222mm$.

Table 4.3: Plies Attribution along Spar Surfaces.

#	<i>TopSparCap</i>	<i>UnderSparCap</i>	<i>SparWebs</i>
1	$2 * Bi + 58 * Uni$	$2 * Bi + 80 * Uni$	$25 * Bi$
2	$2 * Bi + 56 * Uni$	$2 * Bi + 80 * Uni$	$22 * Bi$
3	$2 * Bi + 55 * Uni$	$2 * Bi + 62 * Uni$	$22 * Bi$
4	$2 * Bi + 54 * Uni$	$2 * Bi + 57 * Uni$	$22 * Bi$
5	$2 * Bi + 48 * Uni$	$2 * Bi + 55 * Uni$	$15 * Bi$
6	$2 * Bi + 45 * Uni$	$2 * Bi + 52 * Uni$	$13 * Bi$
7	$2 * Bi + 41 * Uni$	$2 * Bi + 44 * Uni$	$9 * Bi$
8	$2 * Bi + 35 * Uni$	$2 * Bi + 38 * Uni$	$8 * Bi$
9	$2 * Bi + 29 * Uni$	$2 * Bi + 32 * Uni$	$7 * Bi$
10	$2 * Bi + 23 * Uni$	$2 * Bi + 26 * Uni$	$6 * Bi$

The bidirectional fibres were placed at spar caps to ease the manufacture and to smooth the shear stresses transmitted by the skin and the spar webs. All the skin on the wing presents a sandwich composite with a single bidirectional carbon fibre ply per side and a $3mm$ width of the Airex foam $[C_1^{0^\circ}/A_1/C_1^{0^\circ}]$. All the 8 ribs of Figure 4.3

present the same composite laminate of the skin.

Tail

Following the wing approach, the spar caps of the tail should present unidirectional carbon fibres collinear with the spanwise direction of the aircraft x axis. The tail geometry is shown at 4.5, and the material distribution is symmetric with regard to the aircraft fuselage.

Concerning the middle section: the four top horizontal spar caps and the two wider in the under section present 20 plies of 0, 222mm of unidirectional carbon fibre. The 2 under central spar caps presents 25 plies of the same material. This increase is due to the high compressive forces to this attaching zone, resulting from the downward bending moment. The spar webs were designed as a sandwich of 5 plies of bidirectional carbon fibre per side and an Airex foam of 3mm $[C_5^{0^\circ}/A_1/C_5^{0^\circ}]$. The 2 ribs on this central section (not at the horizontal tail root) present the same plies as the spar webs. Lastly, the leading edge of the central section, composed of 4 surfaces, was assigned with the following sandwich laminate: $[C_2^{0^\circ}/A_1/C_2^{0^\circ}]$.

The geometry of the horizontal tail does not have spar webs, and each under spar cap presents a sandwich form with unidirectional carbon fibre: $[uC_5^{0^\circ}/A_1/uC_5^{0^\circ}]$. The upper spar cap has a 7 plies sandwich of the same laminate composition. The complete rib at the horizontal root is constituted by $[C_5^{0^\circ}/A_1/5_1^{0^\circ}]$. The remaining 2 ribs have also a sandwich shape, but with only 1 ply of fibre. The remaining skin in the tail present the following laminate: $[C_2^{0^\circ}/A_1/C_2^{0^\circ}]$. This skin presents a thicker composite surface due to its complicated geometry at the intersection corners of the tail root with the central section. The manufacturer should perform a round joint on this zone to avoid critical stresses concentration.

The vertical spar cap is divided into 3 equally divided sections. The mid-section which will be attached to the horizontal stabilizer, presents a composition of $[C_3^{0^\circ}/A_1/C_3^{0^\circ}]$. The outer 2 section has also a sandwich laminate, but only with 2 plies of fibre. The three ribs and the skin of the vertical stabilizer are defined as: $[C_1^{0^\circ}/A_1/C_1^{0^\circ}]$.

Fuselage

At this section, it is described all the components that were not until this point. At the bulkhead 1, it is attached the double support responsible to handle all the loads from the tail. These crucial elements present 45 plies of bidirectional carbon fibre. The bulkheads from 1 to 8 have a sandwich shaped composite with 8 plies of bidirectional carbon fibre as follows: $[C_8^{0^\circ}/A_1/C_8^{0^\circ}]$. The longitudinal structural elements mainly responsible to resist the fuselage bending, the longerons, were designed to be manufactured as solid laminates with 20 plies of bidirectional carbon fibre.

The middle section constituted of the double bulkhead (4 and 5) will be connected by the triangularly shaped landing gear supports ($[C_{20}^{0^\circ}]$) and the wing attachment support ($[C_{50}^{0^\circ}]$).

Concerning the fuselage's skin, it presents a thicker surface than at the wing. While the wing present mostly bending moment in respect to the longitudinal (z) axis of the aircraft, the rear fuselage will handle more moments along other axis since the tail besides vertical loads also handle lateral loads due to the wind gust. This results in a moment along the vertical(y) and the spanwise (x) axis of the UAV. This increase in the degrees of freedom leads to a more loose structure at the rear of the aircraft creating more shear moments along its skin. Although the main resistive structure is the longitudinal longerons, the skin will suffer some high stresses due to the imposed displacement.

Thus, the rear skin of the fuselage will present a sandwich with 2 plies of bidirectional carbon fibre $[C_2^{0^\circ}/A_1/C_2^{0^\circ}]$. Due to the lack of structural components in the front part of the fuselage, the skin between bulkhead 6 and 7 will present the same reinforcement. The remaining skin in front of the bulkhead 7 will present a single bidirectional ply of carbon fibre in a sandwich configuration: $[C_1^{0^\circ}/A_1/C_1^{0^\circ}]$. The central skin between the bulkhead 3 and 6 will present an increased number of plies (3) to increase the overall stiffness of this critical attachment area. The 'L' shaped supports between bulkhead 6 and 7 present 10 plies of bidirectional carbon fibre, while the avionics and batteries support at the nose will both present a composite structure of 20 plies of the same material.

4.2.2 Boundary Conditions

Loads and restraints are necessary to define the structural simulation. The result of the analysis directly depends on the specified geometric entities where these boundary conditions are applied.

Concerning all the load analysis, that were done in the previous chapter it is presented in Appendix C all the 17 external loads applied to the aircraft. Some of the inertial loads were joint to the aerodynamic loads since they are applied to the same body.

These boundaries conditions simulate the set of static conditions in which the aerodynamic loads are in equilibrium with the inertial forces. In reality, the overall load distribution results in a small resultant load due to the approximations. Therefore, a fixed geometry is required to run the FEA simulation. To that end, the degrees of freedom of the three supports of the landing gear were fixed. This assumption allows the design of the central bulkheads, but some more test must be made to design the respective supports.

In this project is not addressed the problem of fastened and bonded joints. For the finite element simulation, it must be set one of multiples component contact options. The contact settings describe the interaction between part surfaces that are initially in contact or come into contact during loading [35]. According to CIAFA design team, the usual manufacture option is the industrial glue, which can be approximated as a 'bonded surfaces' input for the software simulation analysis.

Chapter 5

Results

FEA solvers

Concerning the solver used for the simulation, it was made some experimental tests. For a mesh with a general element size of $15mm$ and with a mesh control on critical areas (wing and tail attachments) of $12mm$ the FEA was performed for every solver available at the software. For the given conditions, all the direct methods (large problem direct sparse, direct sparse and intel direct sparse) presented results within $0,02\%$ from each other for every component of the stress. With this value, it can be approximated that all the direct methods available present the same simulation results. Concerning the iterative solver, it granted results within $0,2\%$ of the mean value of the direct methods. In addition, since the direct methods use exact numerical techniques, they are furthermore demanding in terms of RAM memory and needing multiple CPU.

For a case of a mesh element size of $15mm$ and with a mesh control on critical areas of $6mm$, as iterative method, the mesh present approximately 208 thousand finite elements, in which each one present 6 nodes and every node has 6 degrees of freedom, 3 for rotation and 3 for translation [35]. Since the least demanding direct method requires 1 GB per every 200 thousand degrees of freedom (other direct methods require 2 million), it means that it would be necessary almost 40 GB of RAM memory, which were not available for the present simulations. For this reason, and since the previous tests presented good results for the iterative method, this method was considered acceptable.

Convergence

Through the iterative process of trial and error it was achieved the geometry and material thickness specifications previous described. Applying the boundaries conditions and computing the finite element analysis simulation it was achieved acceptable results for the design of the default mesh generator. For a mesh with $18mm$ of maximum dimension for the parabolic triangular element, the computed results show a maximum stress along the x component of $\sigma_x = 374,3MPa$ on the lower part of the wing attachment to the fuselage. This zone was expected to have the maximum effect under load action, since the bending moment on the wing present the highest value for the aircraft.

To verify this results of the software, first, it is necessary a convergence study. Thus, several meshes were created to assess the results variations for each finer mesh. First, maintaining a constant element size for all the aircraft this size was reduced to $1mm$ per simulation until reaching the $15mm$ for element size. From this last iteration it was set a local mesh refinement for the areas that presented higher values of stress, namely, the central zone of the wing attachment until $b = 300mm$ on each half-wing, the complete horizontal tail spar, the two tail supports linked to the bulkhead 1, and the skin on the horizontal tail (between the spar an the trailing edge) due to corners conflicts and interactions with the vertical tail. An example of this mesh control areas is shown in Figure 5.1. On this figure is possible to see the different element size between the central wing spar and the front fuselage. In the rear of the zone, the tail spar and rear skin present also a smaller element size than the fuselage skin and bulkhead.

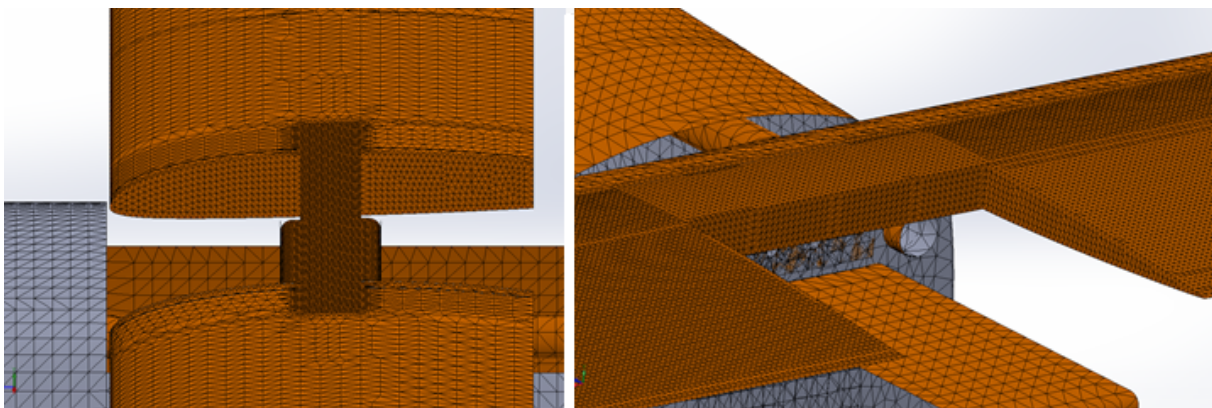


Figure 5.1: Finer Mesh Control on Critical Areas .

The mesh convergence study showed that the *SolidWorks* mesh generator presented some difficulties for certain finite element sizes. For example, it was unable

to run a mesh control simulation for element size of $11mm$ and $8mm$. This may have been caused by high curvature (beyond limits) mesh elements, a zero Jacobian for some elements or the presence of singularities [35].

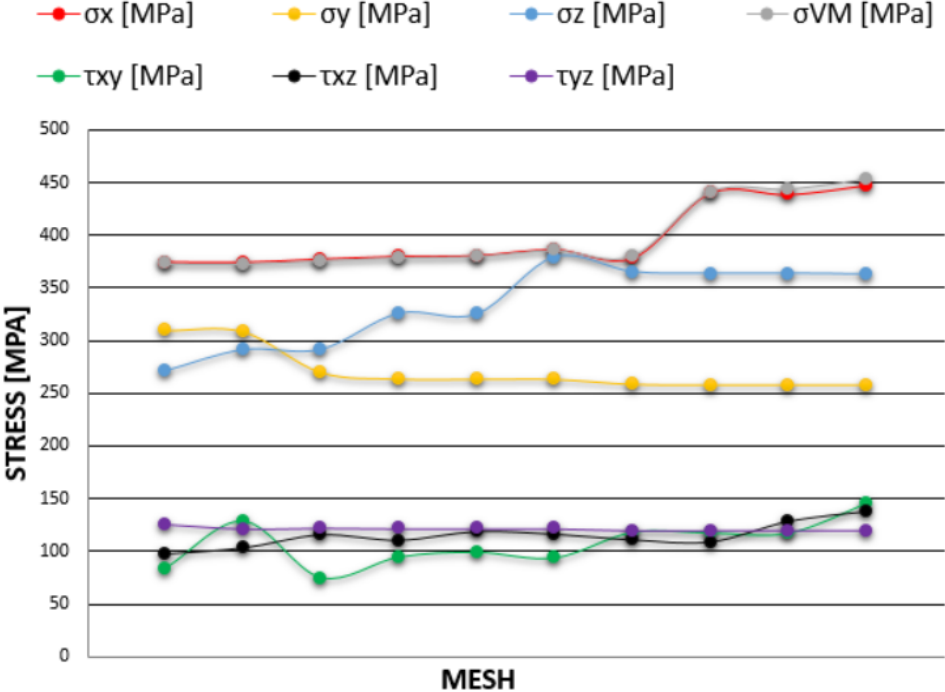


Figure 5.2: Stress Convergence Analysis for a Mesh refinement.

At Figure 5.2 is shown the convergence study, wherein the x axis is presented a finer mesh for each point. It can be seen that decreasing the finite element size, there are some oscillations in the stress value until it finally converges to an acceptable variation between each component. Detailed results are shown in Table 5.1. Mesh convergence was considered to be achieved for the last mesh control of $15mm$ for general element size with a finer $6mm$ element in critical areas. This mesh results presented a maximum difference, when comparing to the two previous results, for the principal stress (σ_x) component of 2%.

When analysing the shear stress value of τ_{xz} through the mesh refinement it presented a continuously increasing value. The maximum value for this component was always detected at the tail corner between the rib at the horizontal stabilizer root and the spar web of the central section. This value will be considered to be a consequence of a geometry conflict instead of a critical loading condition.

For further clarification, a mesh of $5mm$ for the global aircraft was not able to run in the used machine. Even though, performing a structural analysis for independent wing

and tail, they both presented slightly lower stress for a mesh of $5mm$ than for the global results of the final mesh ($15 + 6mm$).

For the displacement analysis, it was achieved convergence since the first mesh. As expected, the displacement converges sooner than the stress.

Table 5.1: Maximum Stress Result for each Mesh applied.

FE Size	$\sigma_x[SI]$	$\sigma_y[SI]$	$\sigma_z[SI]$	$\sigma_{VM}[SI]$	$\tau_{xy}[SI]$	$\tau_{xz}[SI]$	$\tau_{yz}[SI]$
18mm	374,3	309,5	271,1	373,2	95,3	97,04	119,6
17mm	373,8	308,4	291,1	372,9	104,0	102,9	119,6
16mm	376,9	269,5	291,5	376,2	99,9	115,6	119,6
15mm	379,5	263,3	325,6	379,0	106,5	110,4	119,6
15 + 13mm	380,3	263,1	325,0	380,2	108,3	118,8	119,6
15 + 12mm	386,0	263,0	379,2	385,9	105,6	116,2	119,6
15 + 10mm	377,8	258,2	365,1	380,5	118,1	110,8	119,7
15 + 9mm	440,3	257,6	363,7	441,0	117,5	108,9	119,8
15 + 7mm	438,5	257,6	363,7	443,5	117,3	128,7	119,9
15 + 6mm	447,4	257,7	362,9	452,9	116,9	138,3	119,9

Results

Each mesh definitions, including the mesh element size, the finer mesh control size and the correspondent stresses components are presented in Table 5.1.

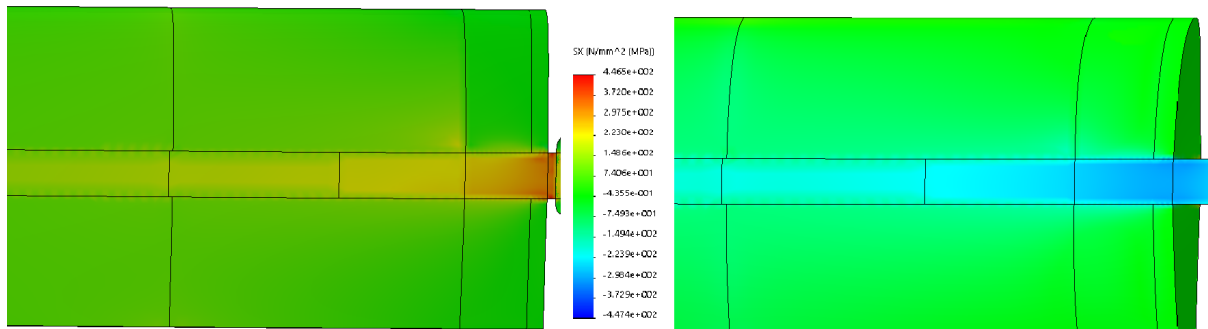


Figure 5.3: σ_x Distribution along Wing Span.

The maximum stress along the spanwise (x) axis is found at the wing root. The left image of Figure 5.3 represents the under section of the wing which is under tensile loading and has a maximum σ_x of $446,5MPa$. The right image represents the upper section of the wing which is under compressive loading and has a maximum σ_x intensity of $447,4MPa$. Both cases present almost the same magnitude for the upper and under

section. The different number of plies was studied until achieving very close results in both upper and under section. This way, there is a minimization of the structural weight, since there is no excess of material on the upper section. Additionally, both values are very close to the design stress for the structure of $450MPa$.

Once the maximum stress zone was identified for the aircraft, it is also important to analyse the stress distribution for the remaining geometry. It will be considered the Von Mises Stress distribution since it represents a compound stress, and therefore offers more information for a visual analysis than a simple component would do. Figure 5.4 shows this stress component distribution for a lateral view of the UAV. First, it is represented a deformed preview which is not at the real scale. Second, it is possible to see the influence of all the equipment's weight placed at the nose of the aircraft, favouring a bending (nose down) moment of the fuselage in respect to the spanwise axis. Consequently, there are some mensurable skin stresses near the stiffer central area.

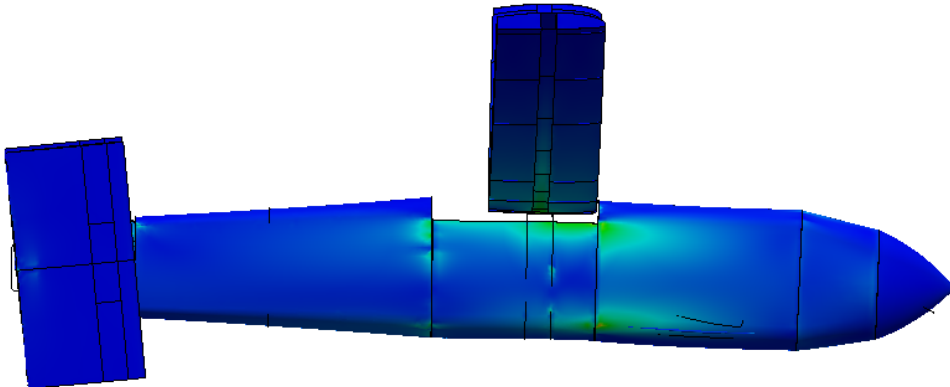


Figure 5.4: Von Mises Stress Distribution on the Aircraft.

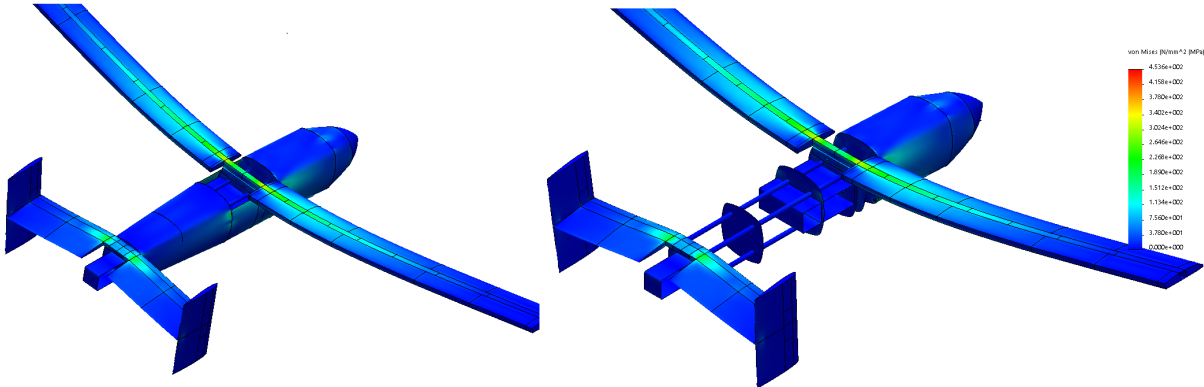


Figure 5.5: Von Mises Stress Distribution on the Aircraft.

Figure 5.5 presents a top view of the aircraft showing the Von Mises stress distribution. It can be seen the wing stress slowly decreasing from the wing root to the wing tip, presenting as expected, greater loads for the spar than for the skin. The horizontal tail presents the same distribution but with lower intensity. If the tail was designed to present higher stresses it would also mean higher displacements and a highly unstable geometry. One of the images has the rear skin suppressed. Therefore, it is possible to see the stresses of the bulkheads and the longerons. Once again, to provide the necessary stiffness, these structural components should present a very low displacement and consequently must not have high stresses. Analysing Figure 5.6 it is seen the near-zero displacements for the fuselage, even though the high value of the load factor.

The displacement is shown in Figure 5.6 presenting a maximum resultant displacement at the wing tip of $307,6mm$ for the design load of $6,84g$. This corresponds to a wing tip deflection of $\approx 4,9\%$ of the wingspan. Concerning the tail, the horizontal stabilizer tip presents approximately $80mm$ of displacement while the vertical stabilizers reach almost $90mm$.

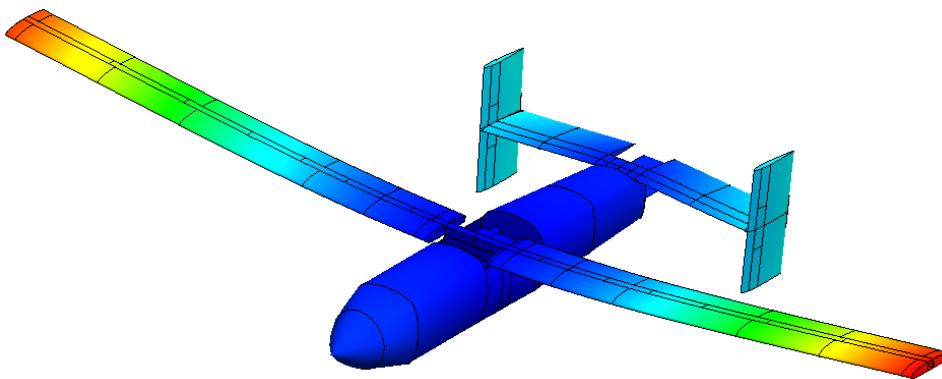


Figure 5.6: Aircraft Resultant Displacement.

In respect to the fixed geometries, some more tests have to be made to size all components of the aircraft. All the previous values were obtained assuming that the degrees of freedom of the three supports of the landing gear were fixed. Some other simulations were performed considered as fixed fixtures, the bulkhead 4 and 5, and the wing. These two options presented lower maximum stresses along the aircraft structure.

5.1 Configuration

For the UAV with a full set of systems on board, the aircraft is theoretically capable of achieving an endurance of 8 hours with an MTOW of $\approx 148,7kg$ as specified in Figure 3.2. The weight distribution per type of major elements is shown at Figure 5.7.

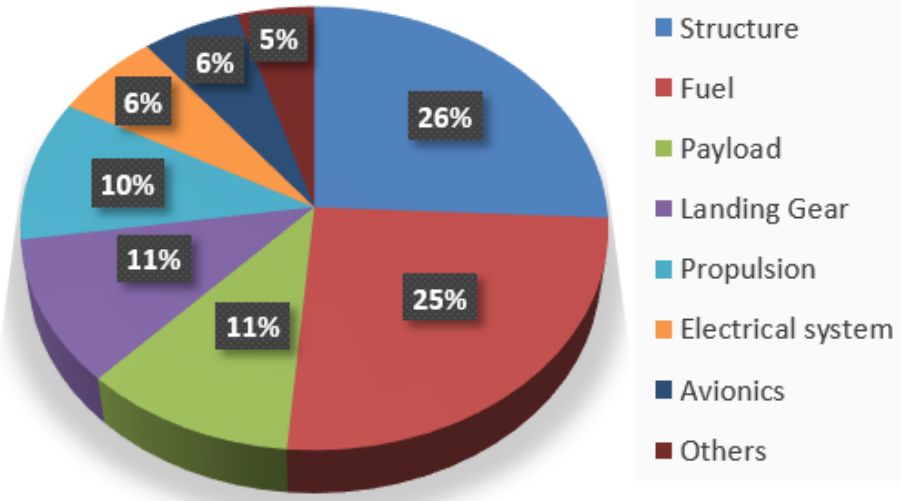


Figure 5.7: Weight distribution per type of elements.

The structure, fully designed with composite materials, weights $\approx 26\%$ of the overall weight and is capable of handling an operational flight up to the design load of $6,84g$, without failure.

As stated in section 2.1.3 the goal was to achieve a design stress of $\approx 450MPa$, which was verified by the FEA. The wing tip displacement for the design load is approximately 5% of the wingspan, while the tail presents almost 2% at the vertical stabilizer.

The wide range of possible missions applications for this UAV will sometimes lead to a configuration without some of its payloads. For example, if the aircraft is set to take off without the Radar SAR and the Sniffer it is capable of taking on board fuel up to 60 litres. This option is only available if the overall weight distribution remains equivalent to the one presented in Figure 3.2, with the position for the centre of gravity at: $\approx 1,253m$.

Chapter 6

Conclusions

Motivated by FAP's need of a more capable aircraft for maritime surveillance and the intention to provide monitoring services to EMSA, the main goal of this dissertation was to develop the structural design of a new class I UAV, according to specific requirements.

This thesis starts by defining all the necessary onboard systems for the UAV to meet the given mission requirements. It included the payload, avionics, electrical and propulsion systems. Once each component was known, it was defined an innovative design for the aircraft and some decisions were taken about accessibility and maintenance, and the attachable wing was assumed to be symmetrically divided into two parts.

The proposed method enforced the objective to achieve a longitudinal positive static margin of 20%. According to the performed weight distribution, the centre of gravity of the UAV is at $1,253m$ from the origin at the nose, representing a valid static margin of 18,51%. This value allowed the project to move forward.

The flight envelope considering gust interaction, for the correspondent cruise velocity and altitude, was determined. Its graphical demonstration showed a low manoeuvrability envelope, and a stall velocity close to the cruise velocity. An additional flight envelope was determined for an increased cruise velocity of $90knots$, which presented a better all-around performance and a safer behaviour in flight.

The applicable airworthiness regulations for the class I UAV required two safety factors for the designed composite structure. Combining the safety factor with the critical manoeuvring load, it was obtained the design load of $6,84g$. Hence, an aircraft

load analysis was made for the correspondent flight condition. All the aerodynamic and inertial loads were characterized (magnitude and point of applications), representing the set of equivalent boundary conditions that the structure must withstand without failure.

Afterwards, the overall aircraft was modelled using a CAD software (*SolidWorks* 2017), in which each component was sized in detail. After composite material assignment and mesh definition, the FEA solvers presented stress and displacement solutions for the simulation condition. It was followed by the iterative process of re-design until a valid design was achieved, for the minimized structural weight. Comparisons between different solvers were made proving that it is possible to achieve similar results with the low-time consuming methods (iterative).

The verification procedures of mesh convergence, showed a maximum stress of $447,4MPa$ along x component, in the wing attachment to the fuselage, which is close to the desired maximum stress $450MPa$. The low difference showed that the excessive structural weight at zones of maximum stress is low. According to the approximations stated on the project, the aircraft configuration for the full set of payload presents a weight of $\approx 148,7kg$ and is capable of performing a maritime surveillance mission for 8 hours of endurance.

This versatile UAV may present an increased endurance in case of absence of some of the payload. The high capacity fuel tanks allow operation up to $12hours$, which is a key advantage of the system. Nevertheless, the centre of gravity should be kept constant in any of the possible configurations, to not affect the control dynamics of the aircraft.

6.1 Future Work

To further explore some of the presented solutions in this thesis it is suggested to:

- Study of the vibration impact of the engine regime in the structure, to prove if the damping shockers are effective;
- Evaluation of the interference and jam effect between all systems onboard, to apply a favourable component's location if necessary. Access the carbon fibre (removable panel) interference with radio frequency transmissions;

- Analyse, test and define the precise wiring routes to avoid excessive weight;
- Perform a analysis to study the impact of the necessary holes in the structure;
- Take into account the fire protection sealing necessary to the structural support of the propulsion system.

Bibliography

- [1] J. P. Morgado. Centro De Investigação Da Academia Da Força Aérea: Atividades de Investigação, Desenvolvimento & Inovação na área dos Sistemas Aéreos Autónomos Não-Tripulados. *Cidadania e Defesa*, 53:16–21, 2015.
- [2] M. D. D. Nacional. Visão Estratégica Para Sistemas de Aeronaves Não Tripuladas. *MFA 500-12*, 2013.
- [3] R. Austin. *Unmanned Aircraft Systems: UAVS Design, Development and Deployment*. WILEY, 1st edition, 2010. ISBN 9780123745187. doi: 10.1016/B978-0-12-374518-7.00016-X.
- [4] R. K. Barnhart, S. B. Hottman, D. M. Marshall, and E. Shappee. *Introduction to unmanned aircraft systems*. CRC Press, 1st edition, 2012. ISBN:978-0387303031.
- [5] NATO. Chemical , Biological , Radiological, and Nuclear Response. *Joint Publication 3-41*, (September 2016), 2016. URL http://www.dtic.mil/doctrine/new_pubs/jp3_41.pdf.
- [6] D. O. *UAV: Info, History, Timeline*, 2017 (Retrieved March 22, 2018). URL <http://www.theflightbay.com/uav/>.
- [7] N. Teixeira. Portugal e a NATO: 1949-1999. *Nação e Defesa*, 89(2):15–41, 1999. ISSN 0870-757X.
- [8] J. E. Mayer. State of the Art of Airworthiness Certification. *NATO STO-MP-AVT-273*, 4(27):1305–1335, 2017. ISSN 9782858730117.
- [9] NATO. UAV Systems Airworthiness Requirements (USAR) for North Atlantic Treaty Organization (NATO) Military UAV Systems. *STANAG 4671-Edition 1*, 2007.

- [10] E. A. S. Agency. Certification Specifications for Normal, Utility, Aerobatic, and Commuter Category Aeroplanes: CS-23. (2), 2003.
- [11] E. Border and C. G. Agency. *Mission and Tasks*, 2016 (Retrieved March 15, 2018). URL <https://frontex.europa.eu/about-frontex/mission-tasks/>.
- [12] P. Pena. *EU shops for drones to survey migration routes*, 2017 (Retrieved March 21, 2018). URL <http://www.investigate-europe.eu/76-million-to-survey-migration-routes-largest-eu-public-drone-tender-decided/>.
- [13] J.Sobral, L. Ferreira, and P. Gonçalves. Airworthiness Process Applied to the Portuguese Remotely Piloted Aircraft Systems. *NATO STO-MP-AVT-273*, 2017.
- [14] V. Franco. Design of a class i remotely piloted aircraft for maritime surveillance: Performance, aerodynamics and stability. 2018 june. Unpublished Master Thesis.
- [15] T. C. Corke. *Design of AIRCRAFT*. Prentice Hall, 1st edition, 2003. ISBN:0-13-089234-3.
- [16] NATO. Nato Standard Aep83 Light Unmanned Aircraft Systems Airworthiness Requirements (Usar-Light). 2014.
- [17] A. Parsch. *RQ-2 Pioneer*, 2007(Retrieved March 12, 2018). URL <http://www.designation-systems.net/dusrm/app2/q-2.html>.
- [18] I. W. LTD. *Aerostar*, (Retrieved March 12, 2018). URL <http://www.israeli-weapons.com/weapons/aircraft/uav/aerostar/Aerostar.html>.
- [19] A. F. Technology. *Aerostar Tactical Unmanned Aerial Vehicle*, 2012 (Retrieved March 12, 2018). URL <https://www.airforce-technology.com/projects/aerostaruav/>.
- [20] TEKEVER. *AR5 Life Ray Evolution*, (Retrieved March 10, 2018). URL <http://airray.tekever.com/ar5/>.
- [21] M. C. Niu. *Airframe Stress Analysis and Sizing*. Conmilit Press, 2nd edition, 1999. ISBN 978-9627128120.

- [22] M. C.-Y. Niu. *Airframe Structural Design: Practical Design Information and Data on Aircraft Structures*. Conmilit Press, 1st edition, 1988. ISBN 962-7128-04-X.
- [23] P. Widas. *Introduction to Finite Element Analysis*. Number January 2008. 2008. ISBN 9781119993834.
- [24] S. Brandt, R. Stiles, J. Bertin, and R. Withford. *Introduction to Aeronautics: A Design Perspective*. AIAA Educational Series, 2nd edition, 2004.
- [25] T. H. G. Megson. *Aircraft Structures*. Elsevier Butterworth-Heinemann, 3rd edition, 1999. ISBN 0340705884.
- [26] L. C. Dorworth, G. L. Gardiner, and G. M. Mellema. *Essentials of Advanced Composite Fabrication and Repair*. Aviation Supplies and Academics, 1st edition, 2009. ISBN:978-1-56027-752-1.
- [27] J. N. Reddy. *Mechanics of Laminate Composite Plates and Shells: Theory and Analysis*. Boca Raton: CRC Press, 2nd edition, 2004. ISBN:0-8493-1592-1.
- [28] D. Cripps. *Unidirectional Fabric*, (Retrieved February 6, 2018). URL <https://netcomposites.com/guide-tools/guide/reinforcements/unidirectional-fabric/>.
- [29] M. Hollmann. *Composite Aircraft Design*. Aircraft Designs, INC., 5st edition, 2003.
- [30] S. Ekşi and K. Genel. Comparison of Mechanical Properties of Unidirectional and Woven Carbon, Glass and Aramid Fiber Reinforced Epoxy Composites. *Acta Physica Polonica A*, 132(3):879–882, 2017. doi: 10.12693/APhysPolA.132.879.
- [31] M. C.-Y. Niu. *Composite Airframe Structures: Practical Design Information and Data*. Conmilit Press, 3rd edition, 2010. ISBN 987-962-7128-11-3.
- [32] João Silva. *Design and Optimization of a Wing Structure for a UAS Class I 145 kg*. PhD thesis, Academia Da Força Aérea, 2017.
- [33] K. R. J. Tomblin, J. Mckenna, Y. Ng. Advanced General Aviation Transport Experiments: B-Basis Design Allowables for Wet Layup / Field Repair Fiber Reinforced Composite Material Systems: AGATE-WP3.3-033051-115. Technical Report August, 2001.

- [34] J. Gundlach. *Designing Unmanned Aircraft Systems: A Comprehensive Approach*. 2012. ISBN 9781600868436. doi: 10.2514/4.868443.
- [35] D. SYSTEMES. *SolidWorks Manual 2017*, (Retrieved April 7, 2018). URL http://help.solidworks.com/2017/english/SolidWorks/SWHelp_List.html?id=dd61f48c463f46c499c3946503773821#Pg0&ProductType=&ProductName=.
- [36] E. J. Barbero. *Finite Element Analysis of Composite Materials Using Abaqus*. CRC Press, 1st edition, 2013. ISBN:978-1-4665-1663-2.
- [37] *CLOUD CAP TECHNOLOGY - Piccolo II*, (Retrieved October 27 , 2017). URL <http://www.cloudcaptech.com/products/detail/piccolo-ii>.
- [38] E. A. S. Agency. Certification specification for large aeroplanes (cs-25): Structure. Technical Report August, 2010.
- [39] J. Roncz. *Schrenk Approximation*, (Retrieved February 1, 2018). URL <https://www.lightaircraftassociation.co.uk/2010/Engineering/Design/schrenk%20approximation.pdf>.
- [40] Luís Félix. Projeto e Construção do Trem Pricipal da Aeronave ANTEX-X03 nc 17510. Technical report, CIDIFA, Força Aérea Portuguesa, 2016.

Appendix A

Technical Requirements

The requirements here presented were made through a CIAFA analysis, to obtain a UAS capable of fulfilling the EMSA's tender missions. These specifications set the desired path of operations of the future FAP UAS, knowing that it should accomplish similar operations as the ones done by EMSA.

OPERATIONAL REQUIREMENTS	DESCRIPTION	OBSERVATIONS
Area of Operations	Areas of operation can be all sea areas surrounding the European Union with an EU or EFTA country, up to 50 km of the coast. GCS can be located away from shore-line.	Address loss of communication issues due to flights over water.
Endurance	An endurance of 8 hours with the full set of sensors. A longer endurance above 8 hours is a key advantage of the system.	
Time of operations	Day and night operations.	
Environmental conditions	Operation in strong and turbulent weather conditions incl. crosswind (> Bft. 6 or 22-27kts). Operation in light precipitation (1mm) situations and reduced visibility. Operation in icy conditions (heated pitot). Temperature: -25° C to +50° C.	Pitot tube with drain.
Type of mission (do not consider for project)	Monitoring mode: Flying in order to detect vessels, pollution, humans in distress, and other human activity at sea. Loitering: Supporting actions (e.g. pollution response, search and rescue, rendezvous at sea) at different flight levels. Adaptation of the flight track and sensor operation according to last user request upfront and during the flight operation.	
Flight Altitude	Up to 15 000 feet AMSL.	
Range	300km BRLOS 100km RLOS	NAL Research: Iridium Hardware, Model A3LA-RS.
Communication	RLOS and BRLOS with satellite Data Down Link (SATCOM) capabilities for payload data. Live stream of sensors in LOS. Metadata in BROLS (SATCOM).	Octopus: IP-data-link
Take-off and landing	The RPAs shall allow automatic take-off and landing -> needs DGPS hardware. Take-off and land from runway under 150m. Gravel/non-prepared T/O and Landing capability. Max T/O altitude 10 000ft.	
AIRFRAME REQUIREMENTS		
Construction/Manufacture	Fuselage made of flat shapes. Manufacture using wet lay-up. Wing transportation capable within 3 meters. Wires away from fuel tanks. Fuel tank should be close to CG. Fuel tank occupy all the inside of main frame/fuselage (made to fit the frame without dead space).	
Redundancy	All control surfaces should be redundant (excl. engine).	
Electric System / Wiring	Cables and wiring should be capable of being inspected at any point. Not loose cables or wires in frame.	
PERFORMANCE		
Vmax for normal operations (Vno)	100kts	
V cruise with full set of sensors (Vc)	90kts	
Vmax (Vmax)	120kts	
V for max load factor (Va)	75kts	
Vstall (Vs)	< 55kts	
Vstall landing config (Vso)	< 45kts	
Glide Ratio	1:10 or better	
Climb Rate at MTOW	> 750ft/min	
POWERPLANT		
Onboard Generator	Enough to provide power to all subsystems and sensors.	
Onboard Starter		Advantage (not mandatory)

SENSOR REQUIREMENTS		
All sensors	Specification of the sustainable environmental conditions for operations and for storage (e.g. humidity, stable wind and gusts, salt concentrations, etc).	
Gimble, including the following devices:	Forward looking and steerable in all directions (fully stabilised) Including an EO sensor and thermal IR sensor and laser illuminator (if available). All sensors in synchronisation.	
Electro optical (EO), visible	Field of view > 40 degrees. Optical zoom more than 10. At least 1000 pixels in one dimension.	
IR, either SWIR, MWIR or LWIR	Field of view > 30 degree. Optical zoom more than 10 (for LWIR it is an advantage). Noise equivalent temperature resolution better 0.1K (if no thermal IR nadir scanner is available). Temperature range 0 to 2000 degrees C. At least 600 pixels in one dimension.	
Laser illuminator in the IR	Field of view > 60 degree. At least 1000 pixels in one dimension. Noise equivalent temperature resolution better than 0.1K.	
Radar	360° coverage with multimode capabilities with 50km range Maritime modes: <ul style="list-style-type: none"> - Detection and tracking of vessels (up to 100 km). - Detection localization and tracking of small targets in High Sea States. Other modes: <ul style="list-style-type: none"> - Detection and localization of aircraft x Detection and localization of rainy zones x Interrogation/Detection of Search and Rescue beacons With a resolution of up to 50cm depending on the mode. 	
Synthetic aperture radar (SAR)	X or C band. Range > 30km preferably 360 degrees or otherwise each side of the aircraft with the detection capability of oil on water and of vessels. With a resolution of up to 50cm depending on the mode.	SRCinc: radar RASAR
AIS	AIS receiver with capabilities to relay the data.	MillTechMarine: Smart Radio SR161, AIS Receiver.
Distress sensors	Distress signal receiver with capabilities to relay the data (EPIRB).	
Telephone mobile unit detections	Terrestrial mobile frequencies Satellite mobile frequencies.	
Aircraft Data	e.g. position, altitude, aircraft principal axes, viewing geometry of the sensors, health of the system and sensors, communication links. The data provided shall be georeferenced with an accuracy of better 100m within a range of 20 km.	
SUBSYSTEMS		
Autopilot	Piccolo Autopilots.	
Power Supply	Power supply supplied by onboard generator when engine working. Backup battery capable of 2 hours of main systems (Autopilot, servos, transponder). Sensor Backup Batteries enough for 20min of full operation (Radar/SAR and Gimble).	Power distribution box developed at CIDIFA.
Servo-actuators	Capable of CAN data protocol. Monitored independently on system.	
Transponder	Mode S and ADS-B.	https://sagotech.com/mx-transponders/
Onboard Computation	Capable of processing sensor data and broadcasting through selected data link (RF or SATCOM).	Connecttech Nvidia Jetson embedded systems: 1 of Rosie and 1 of Rudi

Appendix B

Material Properties

The material used in this project presents the properties shown in table B.1. The manufactured specimens were obtained through hand lay-up lamination followed by a curing process, using a vacuum bag at minus 0,5 bar during 24 hours at a room temperature of 20°C, in a dry heat condition of low humidity environment. Also, the percentages of resin (100g of Resin Epoxy SR 1500) and hardener (33g of Hardener Sicomin SD 2505) were kept the same for both carbon fibres materials.

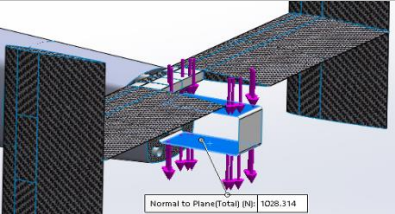
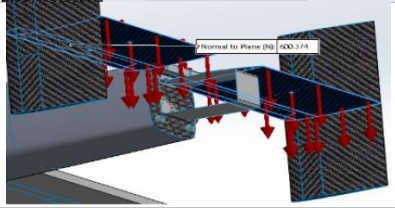
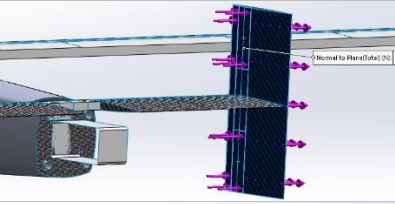
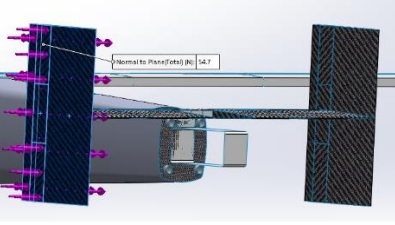
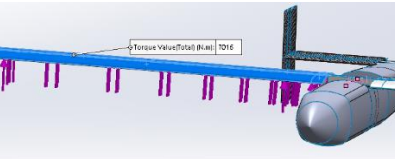
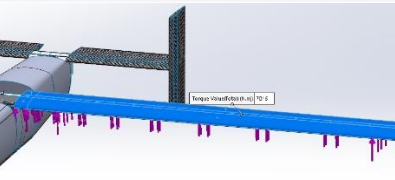
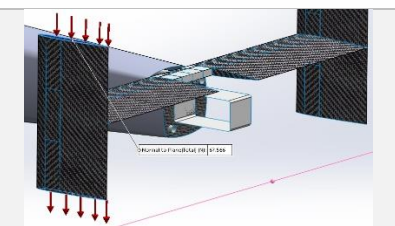
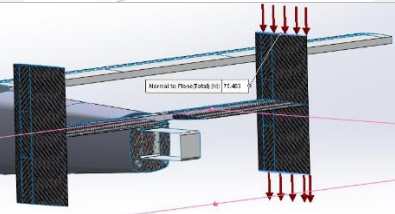
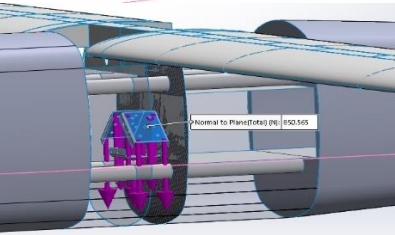
#	<i>Uni. Carbon Fibre</i>	<i>Bi. Carbon Fibre</i>	<i>Airex C70.75</i>
ρ [kg/mm ³]	1450	1300	89
<i>Ply Thickness</i> [mm]	0,222	0,19	3
E_1 [MPa]	95069,96	44792,61	85
E_2 [MPa]	9172,87	53192,65	-
E_3 [MPa]	9172,87	9172,87	-
ν_{12}	0,262	0,06	0,3
ν_{23}	0,396	0,388	-
ν_{13}	0,262	0,388	-
G_{12} [MPa]	5000	5000	30
G_{23} [MPa]	3470	2889	-
G_{13} [MPa]	5000	2889	-
S_{tu_1} [MPa]	1500	622,598	2
S_{tu_2} [MPa]	22,46725	508,568	-
S_{cu_1} [MPa]	1200	570	1,45
S_{cu_2} [MPa]	250	570	-
$\tau_{u_{12}}$ [MPa]	49,4125	90	1,2
<i>yieldstrength</i> [MPa]	1500	450	
CTE_1 [/K]	-0,3	2,1	$4,387e^{-5}$
CTE_2 [/K]	28	2,1	
CTE_3 [/K]	28	28	

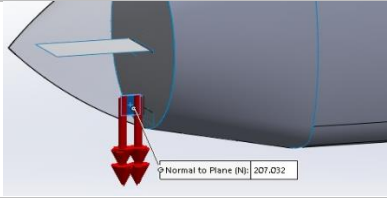
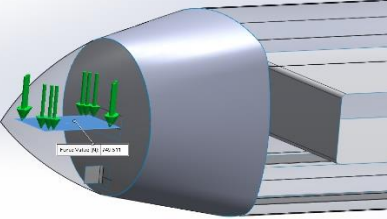
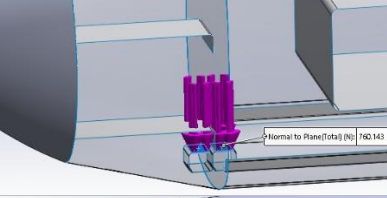
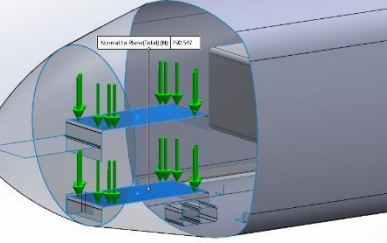
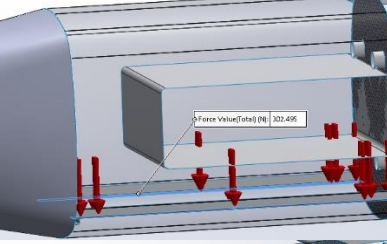
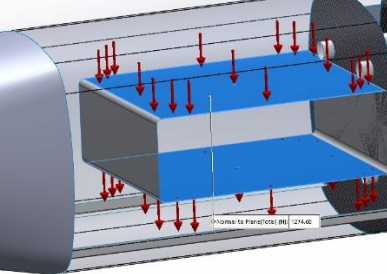
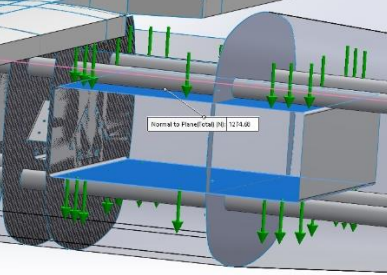
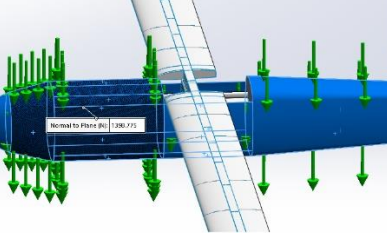
Table B.1: Properties of the CIDIFA's Composite Materials

Appendix C

External Loads

It is presented all the external loads applied to the aircraft within the FEA simulation environment. Each Load is named by its zone of application and it is described with the correspondent intensity and details. Each image shows the load vectors of the applied force or moment, and the correspondent surfaces where the load is applied are blue coloured.

Load name	Load Image	Load Details
1 : Engine Weight		Entities: 2 face(s), 1 plane(s) Reference: Top Plane Type: Apply force Values: -1028.31 N
2: Tail Lift		Entities: 6 face(s), 1 plane(s) Reference: Top Plane Type: Apply force Values: -600.374 N
3: Tail Lateral Gust (Right)		Entities: 5 face(s), 1 plane(s) Reference: Right Plane Type: Apply force Values: -54.7 N
4: Tail Lateral Gust (Left)		Entities: 5 face(s), 1 plane(s) Reference: Right Plane Type: Apply force Values: -54.7 N
5: Wing Lift (Right)		Entities: 13 face(s) Reference: Axis1 Type: Apply torque Value: 7016 N.m
6: Wing Lift (Left)		Entities: 13 face(s) Reference: Axis1 Type: Apply torque Value: -7016 N.m
7: Left Vertical Tail Weight		Entities: 2 face(s), 1 plane(s) Reference: Top Plane Type: Apply force Values: -67.566 N
8: Right Vertical Tail Weight		Entities: 2 face(s), 1 plane(s) Reference: Top Plane Type: Apply force Values: -75.483 N
9: Main Landing Gear Weight		Entities: 2 face(s), 1 plane(s) Reference: Top Plane Type: Apply force Values: -850.565 N

<p>10: Nose Landing Gear Weight</p>		<p>Entities: Reference: Type: Values:</p> <p>1 face(s), 1 plane(s) Top Plane Apply force -207.032 N</p>
<p>11: Batteries, Energy box and Gimble Weight</p>		<p>Entities: Type: Value:</p> <p>1 face(s) Apply normal force -749.511 N</p>
<p>12: Radar SAR Weight</p>		<p>Entities: Reference: Type: Values:</p> <p>2 face(s), 1 plane(s) Top Plane Apply force -760.143 N</p>
<p>13: Fixed Equipment and Other Payload Weight</p>		<p>Entities: Reference: Type: Values:</p> <p>2 face(s), 1 plane(s) Top Plane Apply force -790.547 N</p>
<p>14: Wiring Weight</p>		<p>Entities: Type: Value:</p> <p>2 face(s) Apply normal force -302.495 N</p>
<p>15: Front Fuel Tank Weight</p>		<p>Entities: Reference: Type: Values:</p> <p>2 face(s), 1 plane(s) Top Plane Apply force -1274.68 N</p>
<p>16: Rear Fuel Tank Weight</p>		<p>Entities: Reference: Type: Values:</p> <p>2 face(s), 1 plane(s) Top Plane Apply force -1274.68 N</p>
<p>17: Fuselage and Paint Weight</p>		<p>Entities: Reference: Type: Values:</p> <p>16 face(s), 1 plane(s) Top Plane Apply force -1398.78 N</p>

